University of Insubria
Doctoral School of biological and medical sciences

Ph.D. Programme in Neurobiology

Mitochondrial network fragmentation initiates Purkinje cells degeneration via Ca^{2+} buffering impairment: dissecting the molecular events from AFG3L2 mutation to defective mitochondrial dynamics

Francesco Consolato
Matricola: 718263

Internal tutor: Prof. Riccardo Fesce

External tutors: Prof. Giorgio Casari
Dott.ssa Francesca Maltecca

Coordinatore: Prof.ssa Daniela Parolaro

Ciclo di dottorato: XXVII
Anno Accademico: 2013/2014

Ai miei genitori

Table of Contents

ABSRACT

Spinocerebellar ataxia type 28 (SCA28) is a neurodegenerative disorder characterized by unbalanced standing, gait incoordination, nystagmus, ophthalmoparesis and pyramidal signs. Several disease-causing mutations have been identified in the AFG3L2 gene. The encoded protein, AFG3L2, coassembles with paraplegin into multimeric complexes, called the *m*-AAA proteases, in the inner mitochondrial membrane. These complexes are crucial components of the mitochondrial protein quality control system and regulate mitochondrial morphology.

The haploinsufficient *Afg312* mouse recapitulates the features of SCA28 patients, displaying motor incoordination due to dark degeneration of Purkinje cells (PC-DCD). This is a form of degeneration characterized by toxic levels of intracellular $Ca^{2+}$and activation of calpains. Differently from other forms of SCA, where this phenomenon is associated to excitotoxicity, in the SCA28 mouse is unique since it originates from a mitochondrial dysfunction.

We established, that *Afg312*-depleted mitochondria ineffectively buffer the evoked peaks of Ca^{2+}.This enhances cytoplasmic Ca^{2+} levels in PC, thus triggering PC-DCD. We demonstrated that this defect is caused by the negative synergism between the mitochondrial network fragmentation and the altered trafficking of the organelles to PC dendrites.

To determine the molecular mechanism that induces mitochondrial network fragmentation in the absence of AFG3L2, we studied the regulatory pathway

involved in mitochondrial dynamics. Previous work demonstrated that mitochondrial morphology alteration, in the absence of AFG3L2, is caused by an increased OMA1-mediated OPA1 processing. Studying the regulatory pathway that drives OMA1 activity, we discovered that AFG3L2 is deeply involved in this pathway. Full length OMA1 protein is 60 kD, while the proposed active form is 40kD. We identified AFG3L2 as the most important protease involved in OMA1 60/40 kD processing although, additional unknown protease(s) contribute to alternative pathway during stress conditions.

We found that the absence of the *m*-AAA protease induces a striking accumulation of the 60 kD band and a reduction of the 40kD. To clarify the role of AFG3L2 in OMA1 processing we performed co-immunoprecipitation experiments, which disclosed a physical-interaction between the two proteins. Interestingly, we were able to rescue OMA1 processing in *Afg3l2* ko murine embryonic fibroblasts by overexpression of wild type AFG3L2, but not with the proteolytic inactive mutant (AFG3L2-E575Q).

Moreover, we showed that OMA1 40kD form is a substrate of the the *i*-AAA protease demonstrating that the *m*-AAA proteases and the *i*-AAA proteases work coordinately in the regulation of OMA1.

These data, besides disclosing the pathogenetic mechanism of SCA28, demonstrate for the first time the impact of defective mitochondrial Ca^{2+}uptake on local Ca^{2+} signaling in a physiopathological condition of the nervous system. We demonstrated that the altered Ca^{2+} homeostasis is caused by the mitochondrial network

fragmentation, via OPA1 over processing OMA1-mediated consequent to the absence of AFG3L2.

Moreover, we demonstrated for the first time the fundamental role of the *m*-AAA and the *i*-AAA complexes in the regulation of OMA1 processing and confirming their fundamental role in mitochondrial dynamics.

ABBREVIATIONS

AAA	ATPase associated with a varietyof cellular activities
AFG3L1	ATPase family gene 3 like -1
AFG3L2	ATPase family gene 3 like -2
AD	Alzheimer's disease
ALS	Amyotrophic Lateral Sclerosis
ATP	Adenosine triphosphate
Ca^{2+}	Calcium
CMT	Charcot-Marie-Tooth disease
CNS	central nervous system
CuZn-SOD	copper-zinc superoxide dismutase
DCD	Dark cell degeneration
DMSO	dimethyl sulfoxide
DOA	Autosomal Dominant Optic Atrophy
DRP	dynamin-related protein
EM	electron microscopy
FBS	fetal bovine serum
FCCP	Carbonyl Cyanide p-Trifluoromethoxyphenylhydrazone
HBSS	Hank's Balanced Salt Solution (HBSS)
HD	Huntington's disease
HRP	Hereditary Spastic Paraplegia
HSP 60	heat shock protein 60
H_20_2	hydrogen peroxide
IMM	inner mitochondrial membrane
IMS	intermembrane space
kD	kiloDalton
ko	knockout
LTA	large T antigen
MEFs	mouse embryonic fibroblasts
MEM	minimum essential medium
MFN	mitofusin
mHSP 70	Mitochondrial heat shock protein 70
MrpL32	mitochondrial ribosomal protein L32
MS/ MS	mass spectrometry/ mass spectrometry
mtDNA	mitochondrial DNA
mtYFP	mitochondrial yellow fluorescent protein
MTS	mitochondrial targeting sequence
MW	molecular weight
OMA1	Overlapping m-AAA

OPA1	Optic Atrophy 1
02^-	superoxide radical ion
PARL	presenilin associated, rhomboid-like
PBS	phosphate buffered saline
PCs	Purkinje cell
PCR	polymerase chain reaction
PIC	protease inhibitor cocktail
PD	Parkinson's disease
Phb	prohibitin
PNS	peripheral nervous system
PTP	permeability-transition pore
PTM	Post translational modification
QC	quality control
RC	respiratory chain
ROS	reactive oxygen species
RT	Room temperature
SCA	spinocerebellar ataxia
Scr	Scrambled
SD	standard deviation
SDS-PAGE	sodium dodecyl sulphate-polyacrylamide gel electrophoresis
SPG7	Spastic Paraplegia 7
SV40	Simian Virus 40
TIM	translocase of inner membrane
TM	transmembrane domain
TOM	translocase of outer membrane
VDAC	voltage-dependent anion channel
WA	Walker-A motif
WB	Walker-B motif
Wt	wild type
YME1L1	YME1-Like 1 ATPase
$\Delta\varphi$	mitochondrial membrane potential

INTRODUCTION

Role of mitochondria in neuronal cells

Mitochondria are the central organelles for cell survival in fact, they are the primary generators of cellular energy by OXPHOS but also because in the last decades it has been demonstrated the pivotal role of these organelles in several cellular aspect. They play an important role in regulating calcium (Ca^{2+}) homeostasis, in mediating amino acid biosynthesis, fatty acid oxidation, steroid metabolism, intermediate metabolic pathways and free radical scavenging. Moreover, mitochondria are integrated in a number of signaling pathways, including cell death cascades. Cells of highly metabolic tissues such as muscle, liver and brain, are therefore particularly dependent on mitochondria.

The central nervous system (CNS) has an intense demand for mitochondria, which produce over 95% of ATP utilized by the brain. A cortical neuron in human brain utilizes up to ~ 4.7 billion ATP molecules per second to power various biological functions (Zhu et al., 2012). Constant ATP supply is essential for nerve cell survival and function (Nicholls and Budd, 2000). Mitochondrial ATP production supports synapse assembly (Lee and Peng, 2008), generation of action potentials (Attwell and Laughlin, 2001), and synaptic transmission (Verstreken et al., 2005). Synaptic mitochondria maintain and regulate neurotransmission by buffering Ca^{2+} (David and Barrett, 2003; Medler and Gleason, 2002). In addition, mitochondria sequester presynaptic Ca^{2+} transients elicited by trains of action potentials and release Ca^{2+} after

stimulation, thus inducing certain forms of short-term synaptic plasticity (Kang et al., 2008). Removing mitochondria axon terminals results in aberrant synaptic transmission likely due to insufficient ATP supply or altered Ca^{2+} transients (Stowers et al., 2002) (Ma et al., 2009). Neurons are polarized cells consisting of a relatively small cell body, dendrites with multiple branches and elaborate arbors, and a thin axon that can extend up to a meter long in some peripheral nerves. Due to these extremely varied morphological features, neurons face exceptional challenges to maintain energy homeostasis. Neurons require specialized mechanisms to efficiently distribute mitochondria to far distal areas where energy is in high demand, such as synaptic terminals, active growth cones, and axonal branches (Fig. A) (Ruthel and Hollenbeck, 2003). Axonal branches and synapses undergo dynamic remodeling during neuronal development and in response to synaptic activity, thereby changing mitochondrial trafficking and distribution. Neurons are postmitotic cells surviving for the lifetime of the organism. A mitochondrion needs to be removed when it becomes aged or dysfunctional. Mitochondria also alter their motility and distribution under certain stress conditions or when their integrity is impaired (Cai et al., 2012). Therefore, efficient regulation of mitochondrial trafficking and anchoring is essential to: (1) recruit and redistribute mitochondria to meet altered metabolic requirements; and (2) remove aged and damaged mitochondria and replenish healthy ones at distal terminals.

Compelling evidence is pointing the attention on altered mitochondrial trafficking as a potential contributor to diseases of the nervous system. Mitochondrial biogenesis

primarily takes place close to the nucleus in the cell body and subsequent distribution of mitochondria to regions where their functions are required occurs by organelle transport system. Mitochondrial trafficking is especially important in neurons, where regions with high demands for mitochondrial functions often are localized at a great distance from the cell body in axonal ends and synapses (Hollenbeck, 1996). Mitochondria are also required at active growth cones (Morris and Hollenbeck, 1993), at nodes of Ranvier and at myelination/demyelination interfaces (Bristow et al., 2002). Fast axonal transport requires microtubule networks constructed by parallel microtubule polymers with the (+)-end directed towards the axon terminals. Kinesin motor proteins (KIF5) bind to mitochondria via anchor proteins and drive the anterograde-directed transport (towards axon terminals) whereas motor proteins of the dynein family drive transport of mitochondria in the retrograde direction towards the cell body. Mitochondrial transport can also take place on actin microfilaments using myosin motor proteins in more short-range transport processes (Saxton and Hollenbeck, 2012). Axonal transport involves coordinated frequent start and stop motions and switch between anterograde and retrograde movements, which are regulated by physiological events and intracellular signals (Miller and Sheetz, 2004). The average velocity of mitochondrial transport falls between that of fast-moving small vesicles and slow-moving cytoskeletal proteins (Saxton and Hollenbeck, 2012). Mitochondria with high mitochondrial membrane potential ($\Delta\varphi_m$), indicative of metabolically active mitochondria, preferentially move from the cell body towards the axon ends, whereas 80% of the mitochondria with low potential, indicative of

dysfunctional mitochondria move toward the cell body (Miller and Sheetz, 2004). This suggests that dysfunctional mitochondria are transported back to the cell body where replenishing of mitochondria with new proteins can restore their functionality. Disturbance of axonal transport has been linked to axonal degeneration in spastic paraplegia by the discovery that some of the mutated genes in hereditary forms of the disease encode proteins with known or putative roles in axonal transport (e.g. the kinesin gene ICIF5A) (Ankarcrona et al., 1995).

Figure A: Mitochondrial trafficking and anchoring in neurons.

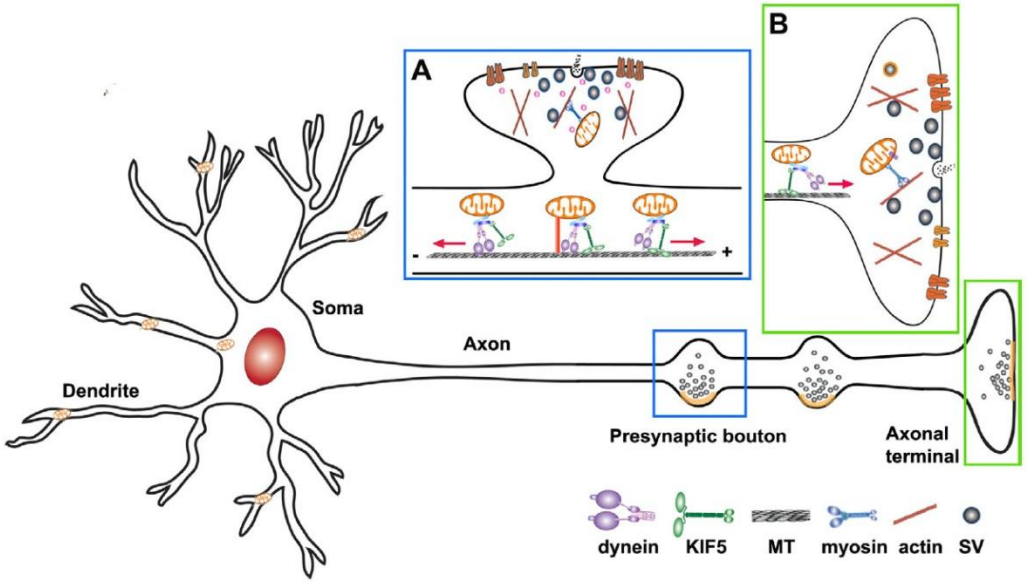

Due to complex structural features, neurons require specialized mechanisms trafficking mitochondria to their distal destinations and anchoring them in regions where metabolic and calcium homeostatic capacity is in a high demand. The figure highlights transporting mitochondria to a presynaptic bouton (A) and an axonal terminal (B). MT-based long-distance mitochondrial transport relies on MT polarity. In axons, the MT's plus ends (+) are oriented toward axonal terminals whereas minus ends (−) are directed toward the soma. Thus, KIF5 motors are responsible for anterograde transport to distal synaptic terminals whereas dynein motors return mitochondria to the soma.
Picure adapted from (Sheng and Cai, 2012)

Mitochondrial dysfunction and neurodegeneration

Mitochondrial function and delivery are critical for neuronal health. It is therefore expected that disturbances of mitochondrial function and trafficking result in severe cellular damage and contribute to pathophysiology of several neurodegenerative disorders. The principal causes of degeneration can be linked to ATP depletion, dysregulation of Ca^{2+} homeostasis or reactive oxygen species (ROS) production.

ATP depletion can induce necrotic cell death when insufficiently compensated by glycolytic ATP synthesis. In fact, ATP levels are an important determinant of whether cells die by apoptosis or necrosis, as ATP is required for events preceding apoptotic cell death such as apoptosome formation and caspase activation. Moreover, Mitochondrial ATP production supports many important functions, including the mobilization of synaptic vesicles for exocytosis and recycling (Gunter et al., 2004), the assembly of the actin cytoskeleton for presynaptic development (Bonior et al., 2006) and the generation of axonal and synaptic membrane potentials (Sheng and Cai, 2012)

In addition, mitochondria have a tremendous capacity to sequester Ca^{2+} transients elicited by brief trains of action potentials (Lin and Beal, 2006). During neuronal stimulation, synaptic mitochondria maintain Ca^{2+} homeostasis by buffering extra intracellular Ca^{2+} and releasing Ca^{2+} after stimulation to prolong the residual Ca^{2+} levels (Kwong et al., 2006). Through this mechanism, synaptic mitochondria are thought to be involved in maintaining and regulating neurotransmission (Baloh et

al., 2007; Chang and Reynolds, 2006) or certain types of short-term synaptic plasticity (Sheng and Cai, 2012). Mitochondria regulate intracellular Ca^{2+} concentrations ($[Ca^{2+}]_i$) in concert with the sarco-endoplasmic reticulum Ca^{2+}-ATPase and the plasma membrane Ca^{2+}-ATPase and Na^+/ Ca^{2+} exchanger (Saris and Carafoli, 2005). In particular, mitochondrial Ca^{2+} uptake becomes important at $[Ca^{2+}]$ above 400-500 nM. Mitochondria are able to buffer $[Ca^{2+}]$ by virtue of their negatively charged mitochondrial membrane potential and low $[Ca^{2+}]_{mito}$ relative to the $[Ca^{2+}]$. Uptake of Ca^{2+} into the mitochondrial matrix is therefore electrochemically favored, and is largely accomplished through the Ca^{2+} -uniporter. Mitochondrial Ca^{2+} sequestration is reversible, with Ca^{2+} efflux back into the cytosol occurring through the mitochondrial Na^+/ Ca^{2+} exchanger or, in case of pathological accumulation, through non-specific channels in the inner mitochondrial membrane, the so-called permeability-transition pores (PTPs) (Gunter et al., 2004); (Pozzan and Rizzuto, 2000). Alteration in mitochondrial Ca^{2+} buffering, cause not only disruption of normal intracellular Ca^{2+} cycling needed to maintain appropriate Ca^{2+}dependent signaling pathways and enzyme activities, but also pathological accumulation. Mitochondria become overloaded at intracellular Ca^{2+} concentration ($[Ca^{2+}]$i) of 1-3 µM, inducing membrane depolarization, impaired ATP synthesis, generation of reactive oxygen species (ROS), permeability transition and cell death (Gunter et al., 2004)

Mitochondria are important normal generators of reactive oxygen species (ROS) for cell signaling, but they can also be important contributors to oxidative

damage. The toxic effect of ROS is normally counteracted by oxygen defense systems consisting of small antioxidant molecules like glutathione, ascorbate, coenzyme Q10 and ROS-scavenging enzymes like Mn- and CuZn superoxide dismutases, and catalase.

However, mitochondrial dysfunction and oxidative damage are often claimed to be joint contributors to neurodegeneration and it is very likely that oxidative damage and ROS production initiates a vicious cycle where ROS mediated damage causes mitochondrial dysfunction, which then increases ROS production and so forth, resulting in cell damage and activation of cell death pathways generation exceeds these protective mechanisms, multiple destructive redox reactions may emerge.

In the last years several neurodegenerative disorders were associated to one (or more) of these mitochondrial dysfunction; it has been published data demonstrating the relationship between mitochondrial ATP depletion, Ca^{2+} buffering alteration and ROS production for the following neuron diseases: Parkinson's disease, Amyotrophic lateral sclerosis, Alzheimer's disease, Hungtinton's disease, Friedreich Ataxia, Hereditary spastic paraplegias and SCA28.

In the following table the mitochondrial proteins involved in human diseases are listed.

Disease	**Gene(s) mutated**	**Mitochondrial functions**	**Mitochondrial alteration**
Parkinson's disease	Parkin	Ubiquitin E3 ligase that has been found to be	ATP depletion ROS production

		associated with the outer mitochondrial membrane.	
	DJ-1	Redox sensor that partially localizes to the matrix and intermembrane space. Neuroprotective at the mitochondria.	
	PINK1	Nuclear-encoded mitochondrial kinase. Overexpression of mutants causes reduced mitochondrial membrane potential and increased death in response to inhibitors.	
	LRRK2	Kinase associated with the outer mitochondrial membrane. It has been found to interact with parkin.	
Amyotrophic lateral sclerosis	SOD I	Cytosolic ROS scavenging enzyme. It partially localizes to the intermembrane space and matrix.	ATP depletion Ca^{2+} buffering ROS production
Alzheimer's disease	Amyloid β-precursor protein	Its product, β-amyloid, is found in the mitochondria where it binds to amyloid β-binding alcohol dehydrogenase and increases ROS production.	ATP depletion ROS production
	Presenilins 1 and 2	Found at the mitochondrial outer membrane where they are part of the c-secretase complex that cleaves amyloid precursor protein.	

Hungtinton's disaease	Huntingtin	Mutant huntingtin binds to the outer membrane and reduces mitochondrial Ca^{2+} uptake. It may affect mitochondrial biogenesis through interference with nuclear transcription factors.	ATP depletion Ca^{2+} buffering
Friedreich Ataxia	Frataxin	Mitochondrial protein involved in heme biosynthesis, formation of iron-sulfur clusters and iron detoxification.	ROS production
Dominant optic atrophy	OPA 1	Inner mitochondrial membrane GTPase that mediates mitochondrial fusion.	ROS production
Charcot-Marie-Tooth type 2A	Mitofusin 2	Outer mitochondrial membrane GTPase that mediates mitochondrial fusion.	Ca^{2+} buffering
Hereditary Spastic Paraplegia	Paraplegin	Subunit of the mitochondrial *m*-AAA metalloproteases complex.	ATP depletion
Spinocerebellar Ataxia Type 28	AFG3L2	Subunit of the mitochondrial *m*-AAA metalloproteases complex.	ATP depletion ROS production

In the last years we have focused our attention to the dissection of the neurological and molecular pathological events occurring in Spinocerebellar Ataxia Type 28 (SCA28).

Spinocerebellar ataxia type 28: genetic and molecular features

SCA28 is a form of dominant cerebellar ataxia characterized by unbalanced standing, gait incoordination, hyperreflexia of the lower limbs, nystagmus and ophthalmoparesis (Cagnoli et al., 2006). These clinical signs are consequent of a cerebellar atrophy caused by Purkinje cells (PCs) degeneration (Fig. B). PCs are some of the largest and most complex neurons of the mammalian central nervous system. They present extremely branched dendritic trees with a large number of active spines, which uniquely receive glutamatergic stimulation of ionotropic α-Amino-3-hydroxy-5-methyl-4-isoxazolepropionic acid (AMPA) receptors and metabotropic receptors (e.g. mGluR1) as afferent input. PCs are therefore exposed to massive and sudden Ca^{2+} influx and are especially vulnerable to glutamate-mediated excitotoxicity (Ito, 2002). To control Ca^{2+} homeostasis, PCs take advantage of several Ca^{2+} clearance systems: the Ca^{2+} ATP-ase and the Ca^{2+}-Na^{+} exchanger at the plasma membrane, the Ca^{2+} ATP-ase at the endoplasmic reticulum (ER) and Ca^{2+} binding proteins (Gruol et al., 2012). Mitochondria accumulate Ca^{2+} into the matrix, via the low affinity mitochondrial Ca^{2+} uniporter (MCU) in a process that depends on the electrical potential across the inner membrane ($\Delta\psi$mito) (Pizzo et al., 2012). While the capability of mitochondria to internalize Ca^{2+} is undisputed, its functional role in living cells, and especially in neurons, is less clear. Compelling evidence indicates that mitochondria can act as local Ca^{2+} buffers in different neuronal types (Colegrove et al., 2000) (David and Barrett, 2000) (Montero et al., 2001), but the effective impact

of this process on neuronal Ca^{2+} homeostasis and physiology remains to be clarified. The efficacy of mitochondrial Ca^{2+} uptake is strictly dependent on the proximity of the organelles to the Ca^{2+} source (e.g. ER, plasma membrane, dendritic spines) (Duchen, 2012) (Pizzo et al., 2012). Neurons are therefore particularly reliant on proper trafficking of mitochondria to these sites and consequently on their dynamic properties.

Several SCA28-causing missense mutations have been identified in the *AFG3L2* gene (Fig. C) (Cagnoli et al., 2006; Cagnoli et al., 2010; Di Bella et al., 2010; Edener et al., 2010). *AFG3L2* encodes for a mitochondrial protein belonging to the AAA^{+}(ATPase Associated to a variety of Activity)-protease superfamily. Moreover, homozygous mutations in AFG3L2 are responsible for a myoclonic epilepsy-ataxia-polyneuropathy syndrome in childhood (Pierson et al., 2011). SCA28 is the first autosomal dominant SCA to be caused by alterations in this mitochondrial protein. Most of the reported SCA28-causing mutations are heterozygous loss of function mutations clustering within the proteolytic domain of AFG3L2. Several pieces of evidence support the hypothesis that haploinsufficiency is the SCA28-causing mechanism. First, functional studies of human mutant AFG3L2 expression in the *m*-AAA-deficient yeast strain indicate that SCA28 mutations alter the proteolytic competence of AFG3L2 and result in impaired respiration. However, the coexpression of wild type and mutant AFG3L2 is able to correct the respiratory defect for most of the mutations, indicating that haploinsufficiency is the disease-causing mechanism (Di Bella et al., 2010). Remarkably, a partial AFG3L2 deletion

(exons 14-16) has been recently identified as the cause of SCA28 in two large Belgian families and functional studies revealed a reduced amount of the *m*-AAA complexes in such patients, demonstrating that SCA28 is due to haploinsufficiency (Smets et al., 2014).

Figure B: Cerebellar atrophy in SCA28 patient

B

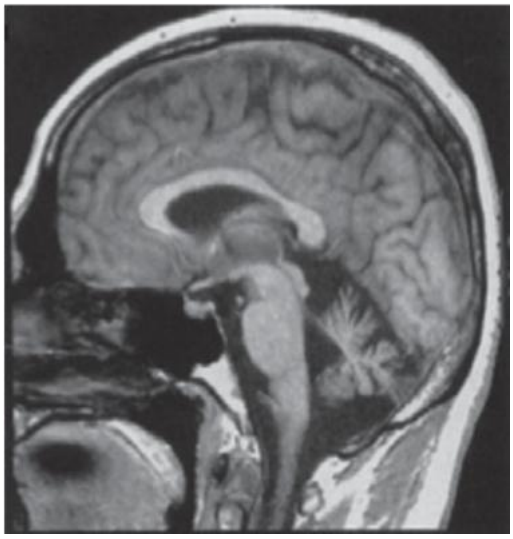

Midline sagittal T1-weighted image showing cerebellar atrophy, particularly evident in the superior vermis. The supratentorial compartment and the brainstem are normal. Picture adapted from Cagnoli et al., 2006)

Figure C: Sca 28-mutations in AFG3L2

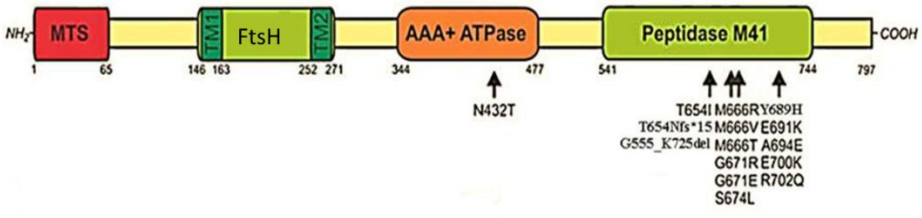

Structure of the AFG3L2 gene and composition of the deduced protein. Mutated codons are marked by asterisks. MT mitochondrialtargeting sequence; TM1 and TM2 transmembrane domains 1 and 2, respectively; FtsH filamentation temperature sensitive H proteolytic domain. Picture adapted from Löbbe et al., 2013

Structure and functions of the *m*-AAA and the *i*-AAA complexes

AFG3L2 is a mitochondrial inner membrane protein belonging to the AAA-protease superfamily (ATPases associated with various cellular activities). Each AAA protease subunit harbors a conserved P-loop ATPase domain of ≈ 230 amino acids, which is characteristic of the AAA^+ superfamily of ATPases (Fig. D) (Hanson and Whiteheart, 2005). AAA^+ proteins convert the energy derived from ATP hydrolysis through the action of two specific regions known as Walker A and Walker B which perform ATP binding and hydrolysis, respectively. AAA+ proteins convert the energy derived from ATP hydrolysis to mechanical work and mediate substrate unfolding and remodeling of macromolecular structures, thereby controlling a variety of cellular processes. A conserved amino acid stretch present within the AAA domain, termed the second region of homology (SRH), defines AAA proteases as members of the classical AAA subclass of this superfamily (Iyer et al., 2004). The AAA domain of AAA protease subunits is followed by an M41 metallopeptidase domain. One or two hydrophobic transmembrane helices within the amino terminal region anchor each subunit to the inner membrane. Crystal structures of eubacterial FtsH proteases suggest that mitochondrial AAA proteases, like other AAA^+ proteins, represent hexameric, barrel-like assemblies, which are formed by identical or closely related subunits and which provide an internal cavity harboring the proteolytic sites (Bieniossek et al., 2006; Suno et al., 2006). Two classes of AAA protease complexes can be distinguished based on their topology in the inner membrane: *i*-AAA proteases

expose their active sites to the intermembrane side, whereas *m*-AAA proteases face the matrix space (Fig. E) (Tatsuta and Langer, 2009).

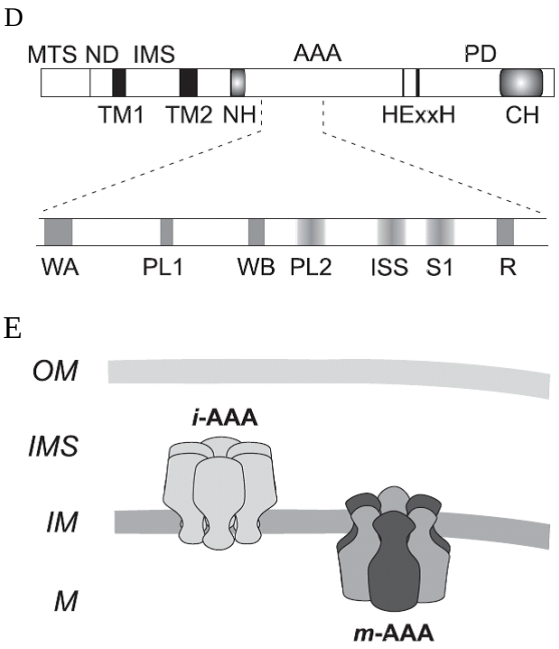

Figure D-E: AAA proteases in mitochondria.

A) Domain structure and conserved elements in subunits of AAA proteases. Yeast Yta10 is depicted. MTS, mitochondrial targeting sequence; ND, N-terminal domain; TM, transmembrane helix; IMS, intermembrane space domain; AAA, AAA domain; PD, protease domain; NH, N-terminal helical substrate binding region; CH, C-terminal helical substrate binding region; WA and WB, Walker A and B motifs of P-loop ATPases; S1 and S2, sensor-1 and 2 motifs; ISS, intersubunit signalling motif; R, arginine finger; PL1 and PL2, pore loops 1 and 2. B) Topology and assembly of two distinct AAA proteases in the inner membrane of mitochondria. OM, outer membrane; IMS, intermembrane space; IM, inner membrane; M, matrix.. Picture adapted from Tatsuta and Langer 2009)

First structural information for the eukaryotic AAA^+ protease was recently obtained for the yeast *m*-AAA protease using single particle electron cryomicroscopy (Lee et al., 2011). The *m*-AAA protease forms a hexamer in solution, resulting in a large, ring like molecular machine, with a central pore for substrates to enter into a proteolytic chamber. In humans, there are two subunits that comprise the *m*-AAA protease, AFG3L2 and paraplegin. Although both assemble into a heteroligomer, it has also been shown that AFG3L2 is capable of assembling into an additional homoligomeric complex (Koppen et al., 2007) . The situation is more complicated in mouse as there is an additional subunit, AFG3L1, which can also form a homoligomeric complex as well as heteroligomeric complexes with AFG3L2 and/ or Paraplegin (Koppen et al. 2007).

The *i*-AAA protease is composed only of a single subunit, YME1L1. The *m*-AAA and the *i*-AAA complexes are crucial component of the quality control system in the inner membrane, where they mediate the selective degradation of non-assembled and damaged proteins (Koppen and Langer, 2007). In addition, they exert chaperone-like activity on respiratory chain complexes (Arlt et al., 1998) (Atorino et al., 2003) (Maltecca et al., 2008), and regulate the processing of the pro-fusion protein OPA1 (Duvezin-Caubet et al., 2007) (Ehses et al., 2009) (Ishihara et al., 2006) (Maltecca et al., 2012). Moreover, it was demonstrated that the *m*-AAA is directly involved in the maturation of mitochondrial ribosomes subunits MrplL32 maturation (Nolden et al., 2005), inducing accumulation the precursor in case of absence of the *m*-AAA. It has been demonstrated that MrpL32 doesn't show a consensus sequence recognized by

AFG3L2, but that the *m*-AAA protease initiates proteolysis from N-terminal amino acids of MrpL32 before a folded domain which halts further degradation resulting in the release of mature MrpL32 (Fig. F) (Bonn et al., 2011).

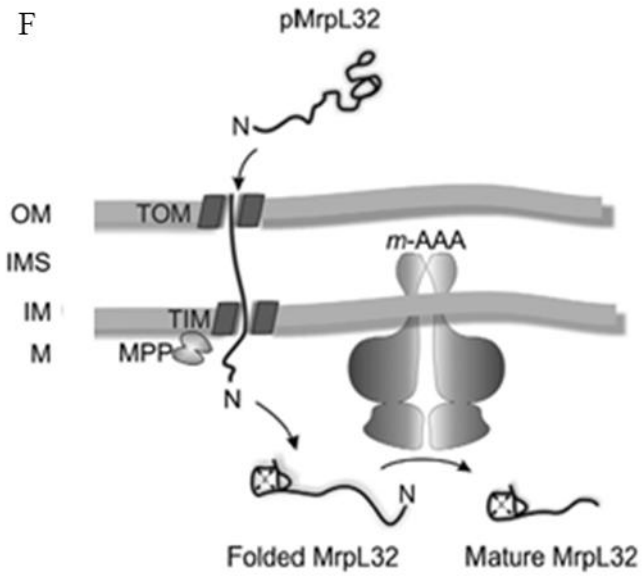

Figure F: MrpL32 maturation by the *m*-AAA complexes

MrpL32 processing by the m-AAA protease after completion of import allows folding of MrpL32 within mitochondria. Mature MrpL32 accumulates in a soluble form, if processing occurs by the m-AAA protease after completion of import, allowing presequence-assisted folding of MrpL32 within mitochondria. Image adapted from Tatsuta and Langer 2007

Molecular features of *Afg3l2* ko and *Afg3l2* haploinsufficient mice models

In our lab it has been previously generated the *Afg3l2* ko animal model. These mice displayed a marked impairment of axonal development with delayed myelination and poor axonal radial growth leading to lethality at P16 (Fig. G). It was demonstrated that the lack of functional AFG3L2 has deep effects on mitochondrial morphology and metabolism. Most mitochondria were morphologically altered in CNS and PNS of *Afg3l2* ko mice where swollen giant mitochondria with damaged cristae could be observed (Fig. H). These aberrant organelles were generally clustered in proximity of the nucleus or the plasma membrane. This phenomenon, together with the presence of several large vacuoles of mitochondrial origin, was primarily observed in neuronal cell bodies of spinal cord anterior horns, in dorsal root ganglia and in PCs, the latter indicating a cerebellar involvement. Mitochondrial morphological alterations correlated with impaired mitochondrial metabolism in the absence of functional AFG3L2. In fact, a dramatic reduction of respiratory complex I and III activities, which correspond to stoichiometric limitation of the enzymatic complexes, were observed. Insufficient assembling, rather than decreased availability of building blocks of respiratory complexes, plays a central role in this deficit of respiratory activities, because neither synthesis of mitochondria-encoded subunits nor import of nuclear-encoded proteins is impaired. All these data demonstrated a role for AFG3L2 in effectively assembling complexes I and III (Maltecca et al., 2008).

G

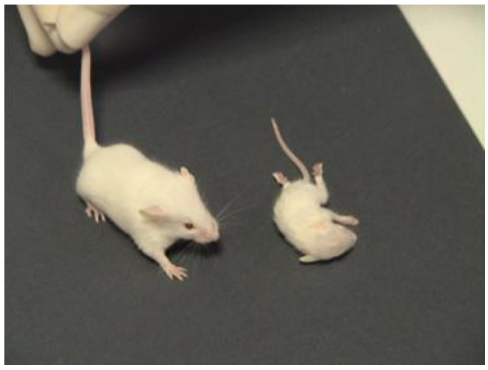

Figure. G: *Afg3l2* ko mice model:

Representative picture of *Afg3l2* ko mice model (on the right) compared to wt littermate. Picture adapted from Maltecca et al., 2008

H

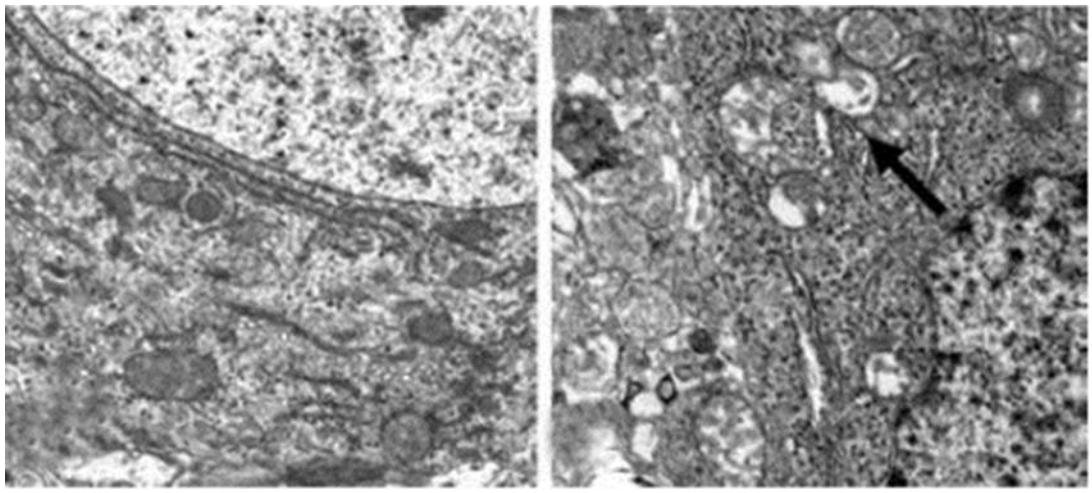

Figure H: The absence of AFG3L2 induces alteration in the mitochondrial structure.

EM analysis of ultrathin sections of cerebellum shows giant mitochondria with swollen, disorganized cristae in the mutants (arrows) compared with controls. Picture adapted from Maltecca et al., 2008.

In our lab was also generated and characterized *Afg3l2* haploinsufficient mouse, which resembles the phenotype of SCA28 patients.

Afg3l2 heterozygous mice develop normally and show normal appearance and fertility. *Afg3l2* heterozygous mice showed alterations in gait coordination, balance, pelvic elevation, and negative-geotaxis reflex; all symptoms correlated to cerebellar dysfunction. These defects appear at 4 months and worsen with age, and mutants older than 12 months present abnormal gait characterized by uncoordinated hind limb movement. These findings demonstrate that the *Afg3l2* haploinsufficient model recapitulates features of SCA28 patients, such as unbalance standing and slowly progressive gait incoordination (Cagnoli et al., 2006).

Maltecca and colleagues (Maltecca et al., 2009) demonstrated that progressive decline in motor performances is caused by PC-DCD. The latter is a specific form of cell degeneration intermediate between necrosis and apoptosis and is characterized by cell shrinkage, cytoplasm darkening and chromatin condensation (Leist and Jaattela, 2001). In the SCA28 mouse this phenomenon is unique since it originates from mitochondrial dysfunction (Maltecca et al., 2009), while in other forms of SCA is associated to excitotoxicity and high levels of intracellular Ca^{2+} (Custer et al., 2006) Ikeda (Ikeda et al., 2006) (Kasumu and Bezprozvanny, 2012). The appearance of morphologically altered mitochondria precedes DCD; swollen mitochondria with damaged cristae were detected already at 4 months, contemporary to the onset of motor coordination defects, while PC-DCD were detected at 6 months (Fig. I). Moreover, it has been detected marked reduction of ATP synthesis associated with a

reduced activity of respiratory complexes I and III. Consistent with what observed in *Afg3l2* homozygous mutants, faulty assembly caused by reduced AFG3L2 chaperone-like activity rather than decreased availability of complex subunits is at the basis of this deficit in respiratory activities. Inhibition of complexes I and III is known to diminish ATP production, to increase leakage of electrons and production of ROS, which attack intracellular biomolecules (Murphy, 2009). Proteins are one of the major targets of oxygen-free radicals and other reactive species. In line with this scenario, in *Afg3l2* haploinsufficient mutants it was reported strikingly increased levels of protein carbonyls in cerebellar mitochondrial enrichments as well as in total lysates. Carbonylation has irreversible and unrepairable consequences modulating biochemical characteristics of proteins such as enzymatic activity susceptibility to proteolytic degradation (Nystrom, 2005). This evidence indicated that dysfunction of the respiratory chain caused by the lack of AFG3L2 cannot be counterbalanced by the mitochondrial antioxidant system, leading to increased reactive oxygen species (ROS) production and oxidative damage (Maltecca et al., 2009).

Nevertheless, what is the molecular link between the mitochondrial alteration and the PCP-DCD is not clarified.

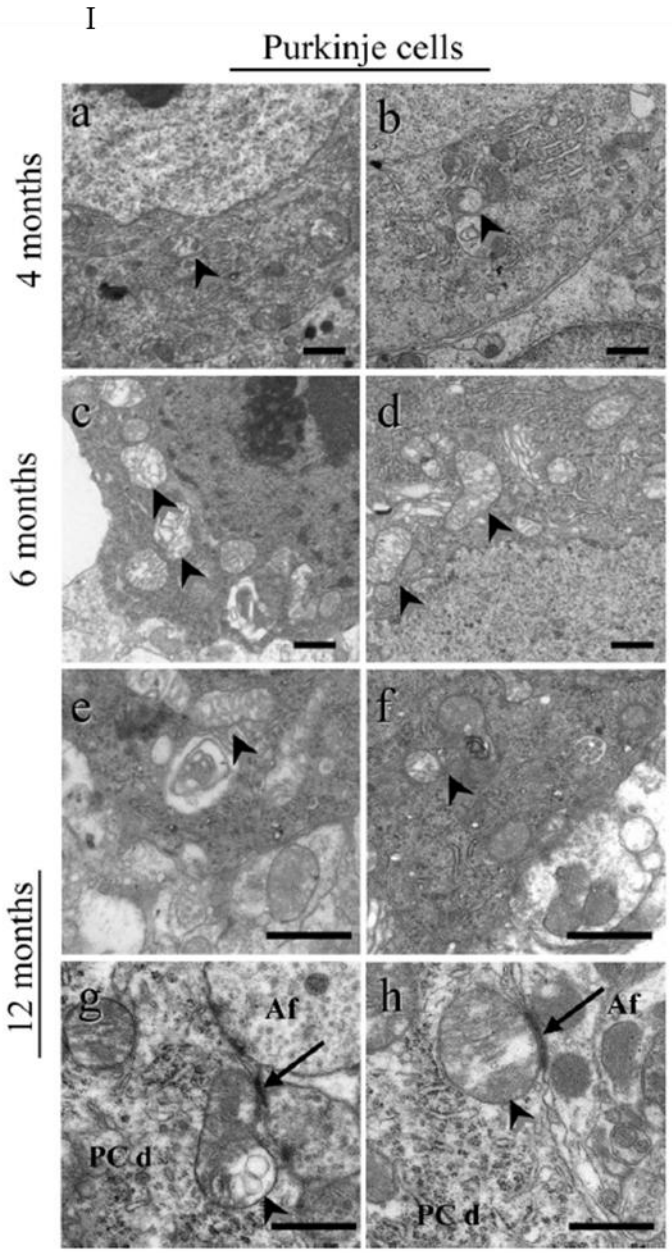

Figure I: Aberrant mitochondria in PCs:

Ultrathin sections of cerebellum from Afg3l2 heterozygous and syngenic control mice at 4, 6, and 12 months are shown .a– h, Mutant PCs show aberrant mitochondria (arrowheads) in the cellular bodies and also in the dendritic synapses. Image adapted from Maltecca et al., 2009

Neurodegeneration and mitochondrial dynamics

Many neurodiseases are associated with changes in mitochondrial function and morphology. Neurons have an especially high demand for mitochondrial metabolism and are particularly sensitive to decreases in mitochondrial function, which lead to energy deprivation and ROS production. By controlling organelle size, mitochondrial fission and fusion also facilitate the efficient microtubule- mediated active transport of mitochondria into the long dendritic and axonal extensions characteristic of highly polarized neurons. As said before, alteration in mitochondrial dynamics, cause by inhibition on mitochondrial fission or fusion, have been suggested to occur as early events during the pathogenesis of many diseases. It was reported that an increase in fission event is reported for AD, PD and HD; while the alteration of fusion event can induce CMT II A or ADOA.

Mitochondrial dynamics.

The antagonistic activities of mitochondrial fission and fusion are required to maintain the form and function of mitochondria. Mitochondrial fusion facilitates communication and sharing of contents between mitochondrial compartments, which can buffer transient defects in mitochondrial function (Chen and Chan, 2010). Mitochondrial division facilitates the transport, distribution, and quality control-mediated degradation of the organelle (Fig. L) (Lackner and Nunnari, 2009). The dynamic processes of mitochondrial division and fusion are mediated by dynamin related proteins (DRPs). DRPs are a family of large GTPases that harness GTP-dependent self-assembly and subsequent GTP hydrolysis-mediated conformational changes to remodel membranes (Faelber et al., 2013; Praefcke and McMahon, 2004). The DRP Dnm1/Drp1 (yeast/mammals) drives the scission of mitochondrial membranes and the DRPs Fzo1/Mfn1/2 and Mgm1/Opa1 mediate fusion of the mitochondrial outer and inner membranes (MOM and MIM), respectively (Hoppins et al., 2007).

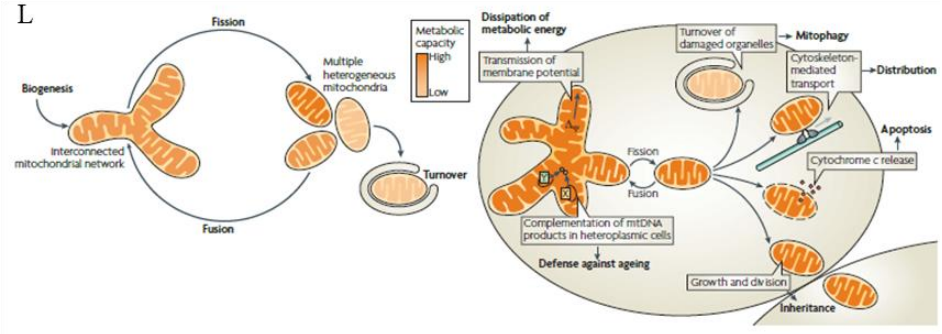

Figure. L: mitochondrial fusion and fission balance

Mitochondrial fission

The dynamin related GTPase Dnm1/Drp1 is a core component of the mitochondrial division machine (Smirnova et al., 2001). Dnm1/Drp1 assembles into helical structures that wrap around mitochondria and mediate the scission of mitochondrial membranes (Smirnova et al., 2001). GTP binding drives Dnm1/Drp1 helix assembly, which in turn triggers GTP hydrolysis via the formation of a catalytic interface between the GTPase domains of molecules in adjacent helical rungs (Frohlich et al., 2013) (Ingerman et al., 2005). Consequent GTP hydrolysis-driven conformational changes in the helix result in further constriction and ultimate scission of the underlying mitochondrial membranes (Mears et al., 2011). Drp1-mediated membrane remodeling is subject to regulation at various points in the division pathway, including targeting of Drp1 to the mitochondrial outer membrane (MOM) and modulation of the GTP-regulated assembly, constriction, and disassembly of the Drp1 helix. Post-translational modification (PTM) of Drp1, which includes phosphorylation, sumoylation, ubiquitination, nitrosylation and O-glycosylation, can positively or negatively impact Drp1 activity, and alternative RNA splicing produces functionally distinct Drp1 isoforms, which themselves are subject to differential PTM (Strack et al., 2013). The activity of the mitochondrial division DRP is also regulated by protein effectors (adaptors): Mdv1 in yeast and Fis1, Mff, MiD49 and MiD51 in mammals (Zhao et al., 2011). These effectors function to target and/or regulate the assembly of the division DRP on the mitochondrial surface, providing

critical spatial and temporal regulation (Koirala et al., 2013). Distinct combinations of Drp1 isoforms, effectors and PTMs provide contextual regulation to Drp1 activity and allow for the integration of mitochondrial division with cellular needs. For example, site-specific phosphorylation activates Drp1 activity during mitosis, which facilitates segregation of mitochondria into daughter cells (Taguchi et al., 2007). During nutrient starvation, the phosphorylation of one site and dephosphorylation of another attenuate Drp1 activity, leading to mitochondrial elongation, which protects mitochondria from autophagic degradation and sustains cell viability (Gomes et al., 2012). Recent studies indicates that mitochondrial division site selection involves communication between unexpected extramitochondrial factors and internal mitochondrial structures. The initial observation that the ER physically wraps around mitochondria and facilitates mitochondrial constriction at nascent division sites added a novel player to the mitochondrial division pathway (Friedman et al., 2011). ER-mediated mitochondrial constriction occurs upstream of Drp1 recruitment and represents an early stage in mitochondrial division (Friedman et al., 2011). In mammalian cells, an ER-associated form, INF2, has been functionally linked to this early stage mitochondrial constriction (Korobova et al., 2013). Evidence indicates that INF2 mediates actin polymerization and subsequent myosin recruitment to sites of ER-mitochondria contact, providing a force-generating mechanism to drive the constriction of mitochondria (Korobova et al., 2014). This initial constriction likely generates a geometric hotspot that is more favorable for Drp1 helix assembly (Friedman et al., 2011). Finally, based on the recent addition of novel and unexpected

players to the mitochondrial division pathway in both yeast and humans, it is clear that our knowledge of the entire complement of proteins that comprise and regulate the division complex is far from complete (Fig. M)

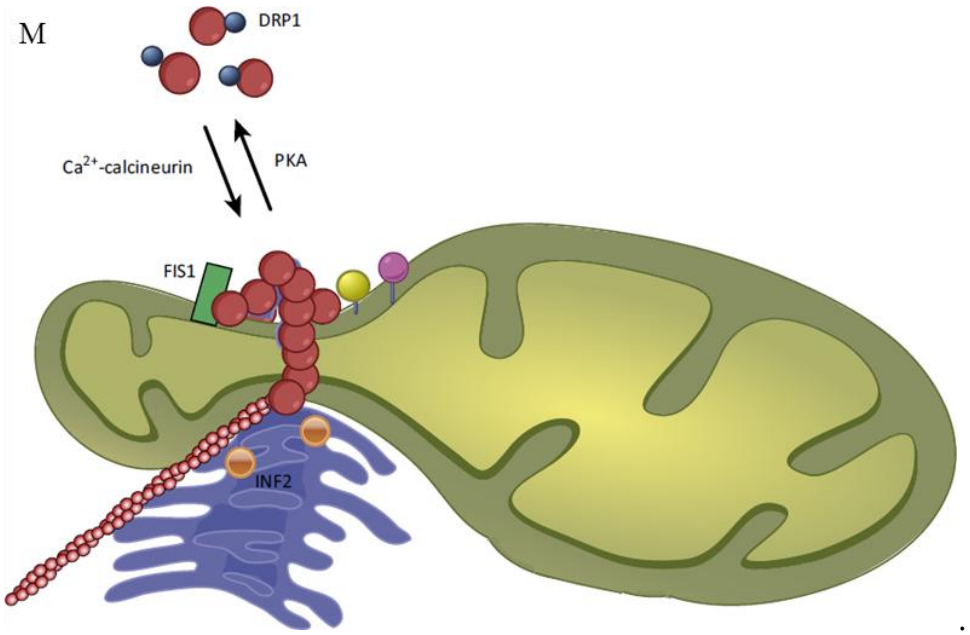

Figure M: Mitochondrial fission DRP1 mediated:

Dynamin-related protein-1 (DRP1) is normally phosphorylated and sequestered in the cytoplasm. At the endoplasmic reticulum (ER)–mitochondria contact site where ER tubules cross over and wrap around mitochondria in presence of F-actin and its ER receptor INF2, dephosphorylated dynamin-related protein 1 (DRP1) is recruited to the OMM where it oligomerizes and interacts with its receptors and mediates mitochondrial constriction. Image adapted from Kasahara et al., 2014 (Kasahara and Scorrano, 2014)

Mitochondrial fusion

Fusion of mitochondrial outer membranes is mediated by a different set of Dynamin family members. The first of these was discovered in Drosophila sperm cells, where it was named fuzzy onions for the onion-like and fuzzy appearance of unfused mitochondria in electron micrographs of these mutants (Hales and Fuller, 1997). A second mitochondrial outer membrane protein, named Marf, was later shown to mediate fusion in other cell types (Dorn et al., 2011). The sequences of Marf and fuzzy onions are similar, but their expression patterns are different so the mutants have different phenotypes: fuzzy onions mutants are sterile whereas Marf mutants are lethal (Dorn et al. 2011). Yeast and Caenorhabditis elegans each have only one fuzzy onions or Marf homolog (Fzo1p and FZO-1, respectively) (Hermann et al., 1998; Rapaport et al., 1998). Mammals do have two homologs (the Mitofusins Mfn1 and Mfn2), but those are often expressed in the same cells (Chen et al., 2003; Santel and Fuller, 2001). Although some functional differences between Mfn1 and Mfn2 have been observed, both of these proteins are also able to support mitochondrial fusion by themselves, suggesting that they fulfill partially redundant functions in this process (Chen et al. 2003). Mitochondrial outer membrane fusion is almost always coordinated with inner membrane fusion (Fig. N). There are, however, some instances in which outer membrane fusion can occur without concomitant inner membrane fusion as, for example, when mutations or loss of membrane potential block inner membrane fusion whereas outer membrane fusion can still occur (Olichon

et al., 2003). Localized loss of membrane potential and its effects on inner membrane fusion may explain why the matrix compartments in larger mitochondrial networks sometimes have breaks, whereas their outer membranes appear to be fully fused. The physiological relevance of these observations has not yet been explored. In comparison to the division DRPs, less is known about the mechanism by which fusion DRPs harness GTP driven self-assembly and GTP hydrolysis-mediated conformational changes to fuse membranes. Current evidence indicates that MOM and MIM fusion proceed via two separable stages, membrane tethering and lipid content mixing, both of which require fusion DRPs (Song et al., 2009). Membrane tethering is mediated by fusion DRP1 self-assembly, and subsequent GTP hydrolysis-induced conformational changes are proposed to destabilize the lipid bilayers of the tethered fusion partners to facilitate lipid mixing and fusion. While assembled structures of the fusion DRPs have been observed by electron microscopy, it is not yet clear if and how these structures correlate to active fusion complexes (Abutbul-Ionita et al., 2012). Like the mitochondrial division DRP, the mitochondrial fusion DRPs are subject to various levels of regulation, including alternative splicing, PTM, proteolytic processing and regulated protein degradation, all of which can link mitochondrial fusion with cellular physiology. For example, one of the peptidases responsible for Opa1 processing, OMA1, has been shown to be activated in response to various cellular stressors (Baker et al., 2014). Under such conditions, enhanced Opa1 processing correlates with attenuated fusion and stress-induced mitochondrial fragmentation. In contrast, OXPHOS-stimulated processing of Opa1 via the peptidase

Yme1L has been shown to stimulate MIM fusion (Mishra et al., 2014). Recent work demonstrates that acetylation can also regulate Opa1 activity. Acetylation of OPA1 reduces its activity, and the acetylated state; thus, function of OPA1 can be modulated by the mitochondrial deacetylase Sirt3 (Samant et al., 2014). As the sirtuin is dependent on NAD+, its activity is highly sensitive to the metabolic state of the cell. Thus, context-specific processing and PTM of Opa1 link MIM fusion to both cellular health and metabolism. Acetylation is also proposed to regulate MOM fusion under certain stress conditions by promoting the ubiquitination and subsequent degradation of Mfn1 (Park et al., 2014). Phosphorylation and ubiquitination can also trigger Mfn1/2 degradation and thus inhibit MOM fusion in response to specific stimuli (Leboucher et al., 2012). In addition to promoting degradation, site-specific ubiquitination can stabilize MOM fusion DRPs, as it has been shown for Fzo1, and promote fusion, perhaps via the stabilization of Fzo1 oligomers (Anton et al., 2013). Regulation of the oligomeric state of Mfn2 via modification by oxidized glutathione has also been proposed to promote mitochondrial fusion (Shutt et al., 2012). Additionally, localization of Mfn2 to both the MOM and ER raises the possibility that differential targeting of the protein can also be used as a means to regulate fusion. As interactions between ER-associated Mfn2 and mitochondrial-associated Mfn1/2 function to tether the two organelles (De Brito and Scorrano, 2008), ER-mitochondrial contacts may also play direct and/or regulatory roles in mitochondrial fusion

N

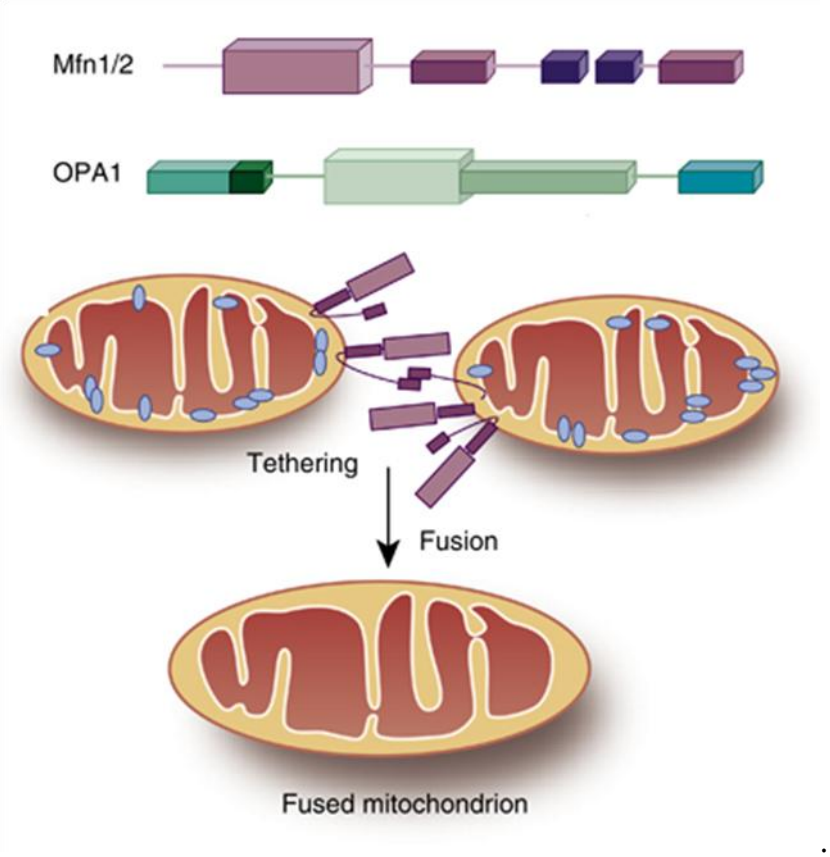

Figure N: mitochondrial outer and inner membrane fusion:

Mfn1 and 2 mediate outer mitochondrial membrane (OMM) tethering through the interaction of adjacent C-terminal regions, which leads to subsequent OMM fusion by GTP hydrolysis through Mfn. OPA1 is required in IMM fusion and the maintenance of cristae structure. Picture adapted from (Zhan et al., 2013)

Dynamin-like 120 kD protein, mitochondrial (OPA1)

In the last years compelling evidence points at the1 Dynamin-like Optic Atrophy 1 GTPase (OPA1) processing a pivotal step in fusion and fission events. OPA1 exists in different splicing isoforms that can be partially or totally proteolytically processed at one or two distinct sites according to the nature of the isoform. Nevertheless, a general OPA1 domain organization can be recognized. OPA1 mitochondrial localization is assured by a bipartite-type mitochondria targeting sequence (MTS) present in the 5' end of the coding region. Downstream this sequence there is the cleavage signal for the mitochondria processing peptidase (MPP) that cleaves off the MTS upon OPA1 import into mitochondria. Mature OPA1 lacks the MTS and includes in its N-terminal portion hydrophobic regions, the more hydrophobic predicted to constitute a membrane-spanning domain that anchors OPA1 to the IMM and projects the bulk of the protein towards the IMS, leaving the N-terminal tail protruding in the matrix space (Ishihara et al., 2006). Downstream this tract, there are the GTPase domain, a middle domain and the GTPase effector domain (GED) (Hoppins et al., 2007). In the first third and in the C-terminal portion of OPA1 there are also regions that assume a coiled-coil conformation that is important for OPA1 self-association (Akepati et al., 2008). In fact, OPA1 can oligomerise forming in mouse 184 kDa dieters and 258 kDa complexes (Akepati et al., 2008). Alternative splicing interests OPA1 N-terminal portion; in particular, in human, exons 4, 4b, and 5b can be present or not in the mature mRNA. All the combinations in which these

exons can arrange give rise to eight different OPA1 isoforms (Song et al., 2007). In mouse, there are only four alternative splicing products since exon 4 is not alternatively spliced (Akepati et al., 2008). Moreover, OPAI can undergo proteolytic cleavage at two sites, S1 and S2. S1 is located in exon 5 and is present in all OPA1 L isoforms; on the contrary, S2 is contained in exon 5b and therefore is present only in isoforms 4, 6, 7, and 8 in human and only in isoforms 7 and 8 in mouse. (Fig. O). (Akepati et al., 2008; Song et al., 2007)

O

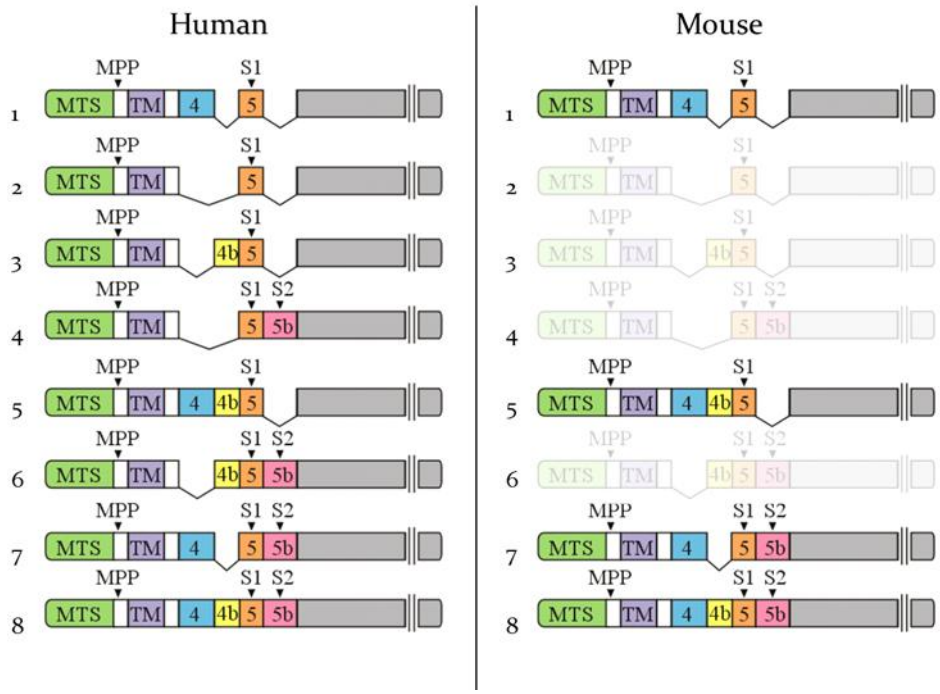

Figure O: OPA1 isoforms

OPA1 isoforms alternative splicing in human and mouse. Cleavage sites are depicted. Picture adapted from Song et al., 2007

The combination of splicing isolorms and proteolytic cleavage results in Western blot analyses in five distinct bands, named from L1-L2-S1-S2-S3. The distribution of OPA1 cleaved and un-cleaved forms in human and mouse is depicted in Fig.P . The assignment of the content of each OPA1 band is based on the work of Song et al., 2007, in which authors expressed single or combinations of tagged OPA1 variants in OPA1- null cells.

P

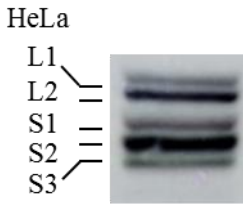

	OPA1 isoform	
	Human	Mouse
L1	7	7
L2	1-2-4	1
S1	4-6-7-8	7-8
S2	4-6-7-8	7-8
S3	1-2-3-5	1-5

Figure P: OPA1 western Blot and cleavage form distribution

OPA1 Processing

The proteolytic processing of OPA1 is a fundamental step in mitochondrial dynamics and a recent work explained in which way this cleavage can induce fusion or fission (Anand et al., 2014). Non-processed forms of Opa1 (long Opa1) are sufficient to mediate mitochondrial fusion, while the accumulation of processed forms (short Opa1) correlate with mitochondrial fragmentation without negatively effecting fusion rates, indicative of a role for short Opa1 in division. Cleavage of OPA1 and its yeast homolog Mgm1 as well as the assembly of long and short isoforms is stimulated by cardiolipin, resulting in the stimulation of the GTPase activity, which promotes mitochondrial fusion (DeVay et al., 2009). It is presently not understood how a balanced formation of long and short isoforms of OPA1 is ensured. The IM rhomboid protease, Pcp1, is responsible for cleavage of Mgm1 in yeast (McQuibban et al., 2003); (Sesaki et al., 2003); (Herlan et al., 2004).The mammalian homolog of Pcp1, PARL, has been linked to the release of short OPA1 isoforms from mitochondria during apoptosis and suggested to play a role in OPA1 processing (Cipolat et al., 2006). However, studies in cell lines lacking PARL revealed that it is dispensable for OPA1 cleavage (Cipolat et al., 2006); (Duvezin-Caubet et al., 2007) (Ehses et al., 2009). Rather, the *i*-AAA protease Yme1 has been implicated in generation of at least one short form of OPA1 by constitutive cleavage at the processing site S2 (Song et al., 2007). Loss of Yme1 results in loss of a particular short isoform of OPA1 and is accompanied by a highly fragmented mitochondrial morphology (Griparic et al.,

2007) (Song et al., 2007). Components of the *m*-AAA protease have also been shown to influence OPA1 processing. In a heterologous system, subunits of the mammalian *m*-AAA protease were able to cleave OPA1 when coexpressed in yeast (Duvezin-Caubet et al., 2007). Loss of the *m*-AAA protease in mammalian cells results in enhanced processing of the long OPA1 isoforms, accompanied by fragmentation of the mitochondrial network and loss of cristae structures (Ehses et al., 2009). Stress-induced degradation of long OPA1 isoforms was found to be mediated by OMA1 (Ehses et al., 2009) (Head et al., 2009). The increased cleavage of OPA1 by OMA1 occurs rapidly in response to different mitochondrial insults, ensuring that a damaged mitochondrion can be efficiently segregated from the network and removed through mitophagy in a rapid fashion (Fig. Q)

Figure Q: OPA1 processing and mitochondrial dynamics

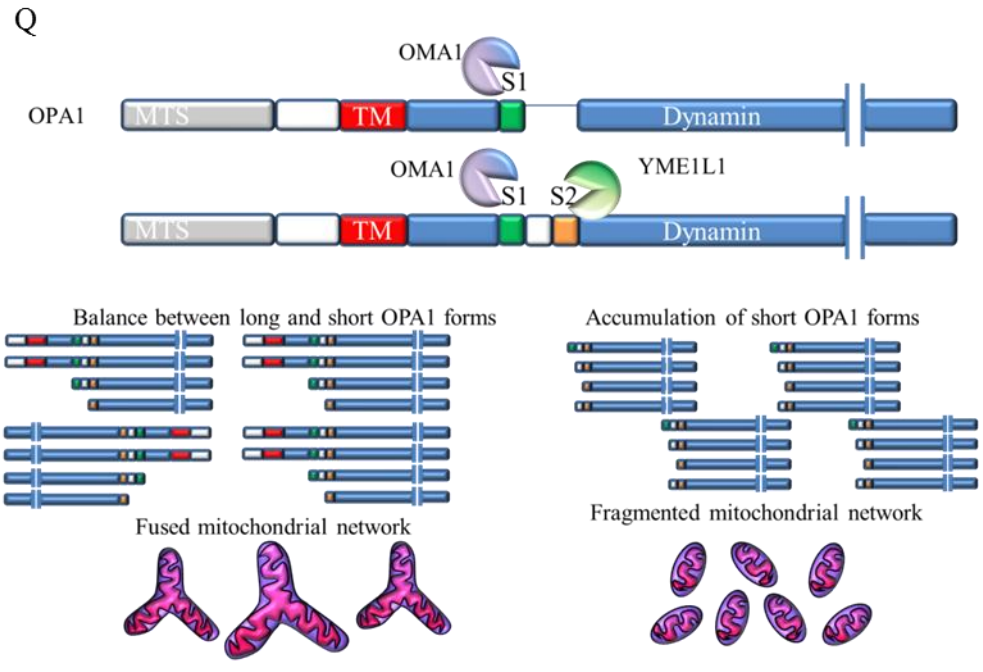

.

The stress activated OMA1 protein

In the last years our lab has focused its attention on the role of OMA1 in mitochondrial dynamics, a new member of a conserved and widespread family of membrane-bound M48 metallopeptidases. Oma1 was identified in yeast mitochondrial inner membrane as a peptidase that can substitute for the function of the *m*-AAA pro-tease during degradation of a misfolded membrane protein (Kaser et al., 2003). Similarly, synthetic growth defects have been observed when mutations in the bacterial AAA protease FtsH were combined with mutations in HtpX, which is a distant homologue of OMA1, indicating overlapping proteolytic activities (Shimohata et al., 2002). It was demonstrated that OMA1 can cleave OPA1 in S1 site (Ehses et al., 2009; Head et al., 2009). The substrate specificity of OMA1 is distinct from yeast Oma1, which cleaves neither OPA1 when expressed in yeast nor the yeast OPA1 homologue Mgm1 (Duvezin-Caubet et al., 2007). It was demonstrated that OMA1 promotes OPA1 processing if mitochondrial activities are impaired. The loss of mtDNA, dissipation of $\Delta\psi_m$, decrease of mitochondrial ATP levels, heat shock, ROS production induces OPA1 processing by OMA1 (Baker et al., 2014); Ehses et al., 2009; Head et al., 2009). The characterization of the OMA1 null mice model demonstrated that OMA1 performs OPA1 processing even in physiological condition; in fact, *Oma1* ko MEFs lack OPA1 form S1 and form S3 clearly indicate that OMA1 is responsible for the in vivo proteolytic processing of L-OPA1 forms (Quiros et al., 2012). Notably, even under stress conditions, *Oma1* ko cells display

the same pattern of OPA1 isoforms characterized by the lack of processing of L-OPA1, which finally results in the shift of mitochondrial dynamics towards fusion events.

Interestingly OMA1 null mice model doesn't show significant neurological alterations in adult mice differently from what observed in the absence of paraplegin or AFG3L2, other two regulators of same mitochondrial pathway. Nevertheless deficiency in OMA1 induces the obesity phenotype, which leads us to suppose a new and unexpected role for this mitochondrial protease in metabolic control. Quirós and colleagues demonstrate that *Oma1* deficiency causes reduced energy expenditure, which agrees with previous results, indicating that a reduction in energy expenditure causes obesity in animal models (Lowell et al., 1993); (Feldmann et al., 2009). Accordingly, the reduced energy expenditure in *Oma1*-deficient mice may account for their increased adipose mass. In addition, *Oma1* deficiency causes a reduced expression of nuclear genes encoding for mitochondrial proteins and key metabolic transcription co-activators, so this may be instrumental in the reduced energy expenditure shown in *Oma1*-null mice. Moreover, deregulation in lipid metabolism due to defects in β-oxidation genes observed in *Oma1*-deficient mice contributes to the obesity and thermoregulation defects.

The authors speculated that altered OPA1 processing induces changes in mitochondrial dynamics, modifying expression levels of dynamic proteins to compensate or counteract this deficiency. Thus, under physiological conditions and in the absence of any relevant stressor, the lack of OMA1 induces changes in

mitochondrial dynamics without seriously affecting any physiological function. In this situation, *Oma1*-deficient mice display a modest increase in body weight, improvement in glucose metabolism, hepatic steatosis, decrement in energy expenditure and low body temperature. However, under stress conditions such as a high-fat diet, the lack of OMA1 induces obesity, loss of glucose metabolism improvement and decrease in β-oxidation that induce the marked increase in the expression of genes of the lipogenic pathway and manifests as the significant hepatic steatosis observed in *Oma1*-deficient mice. Finally, and in relation to the putative implications of these findings for human metabolic control, several genome-wide linkage studies have found evidence of a quantitative trait locus for human obesity phenotypes in the region harbouring OMA1 (Choquette et al., 2008); (Saar et al., 2003).

OMA1 structure and activation

OMA1 predicted molecular weight is 60 kD but recent data support the idea that the cleaved OMA1 40 kD form performs OPA1 processing, which is in turn processed by an auto-catalytic mechanism that involves the C-term part of the protein generating a smaller form (Baker et al., 2014). OMA1 40 kD form oligomerises into a complex of 200–300 kD and it was proposed that its proteolytic activity is regulated by intermolecular interactions of C-terminal helices within the oligomer (Baker et al., 2014). It is known that the 60 kD form is imported inside the mitochondria where it will be processed and that stress condition induces the 60 kD form accumulation. Head and colleagues demonstrated by carbonate extraction, that OMA1 full length is an integral membrane protein and not only an associated mitochondrial outer membrane protein (Head et al., 2009). Nevertheless, nothing is known about the generation of OMA1 40 kD band and which is/are the protease(s) involved in this mechanism.

OMA1 is constitutively active on OPA1 but it was demonstrated that there is an overactivation during cellular stress conditions (i.e. ATP depletion, ROS production, $\Delta\varphi$ depletion). Activation of OMA1 critically depends on positively charged amino acids within the N-terminal domain of OMA1 and is accompanied by its autocatalytic degradation, which is initiated from C-terminal ends and results in the complete turnover of OMA1. It was demonstrated that OMA1 activity under stress critically depends on an N-terminal domain outside the conserved M48 metallopeptidase

domain, which is composed of a hydrophobic region and a cluster of positively charged amino acids. While the proteolysis by OMA1 depends on hydrophobic amino acids within this domain, the following cluster of positively charged amino acids was found to be critical for OMA1 activation in depolarized mitochondria. Authors proposed that this domain is a sensor domain, perhaps stabilized by ionic interactions with negatively charged phospholipid head groups, which induces conformational changes in OMA1 upon membrane depolarization leading to its activation and autocatalytic turnover (Fig. R-S) (Baker et al.,2014). Clearly, structural information on OMA1 is required to substantiate this hypothesis. It is noteworthy, however, that the structural characterization of distantly related metallopeptidases from thermophilic prokaryotes suggests novel intra- and intermolecular latency mechanisms (Lopez-Pelegrin et al., 2013). These include intermolecular interactions of C-terminal helices within an oligomer that impair proteolytic activity. Such a scenario may explain the accelerated processing of OPA1 upon deletion of C-terminal amino acid residues in OMA1. This regulatory mechanism ensures the reversibility of the response and allows restoration of the mitochondrial network upon alleviation of stress stimuli or repair of mitochondrial damage.

R

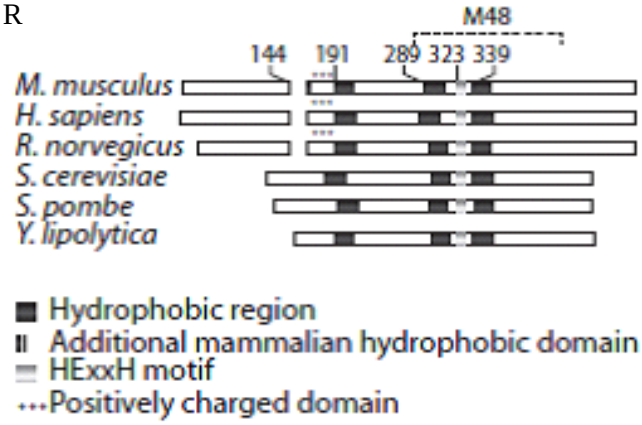

S

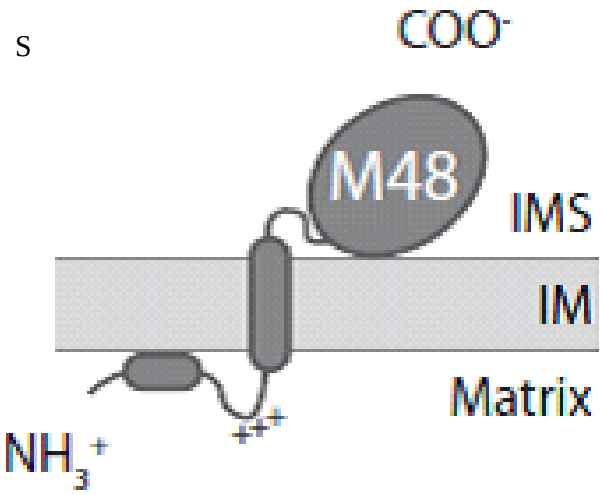

Figure Q and R: OMA1 structure

Picture adapted from Baker et al., 2014

AIM OF THE WORK

SCA 28 is a form of autosomal dominant cerebellar ataxia, characterized by gait difficulties, nystagmus, ophtalmoparesis and hyperreflexia. Many SCA28-causing mutations were discovered in the last years in the *AFG3L2* gene. This gene codifies for a mitochondrial protease of the inner membrane belonging to the AAA-protein family that can assemble into homo-oligomers and hetero-oligomers with paraplegin forming the *m*-AAA complex. The role of this complex is not totally clarified but different evidence shows that it is involved in protein quality control of the inner membrane and mediates chaperone-like activity on respiratory chain complexes. Moreover, it controls mitochondrial morphology by regulating the processing of the pro-fusion protein OPA1. The *Afg3l2* haploinsufficient mouse recapitulates most features of SCA28 patients. It displays defects in motor coordination and balance due to PCs degeneration. Mutant PCs show increased electron density and condensed cytoplasm and nucleus but no signs of nuclear blebbing or apoptotic bodies. These features are peculiar of dark cell degeneration (DCD) that is characteristic of excitotoxic injury. Intriguingly, in the SCA28 model this type of degeneration originates for the first time from mitochondrial dysfunction. Indeed, histological studies on *Afg3l2* heterozygous cerebellum show dramatic defects in mitochondrial morphology and cristae organization, in fact biochemical investigations revealed reduced activity of the respiratory chain. Mitochondrial phenotypes precede PC-DCD, demonstrating the mitochondrial origin of the degeneration.

We hypothesized that the pathological mechanism at the basis of PC-DCD in SCA28 mice involves defective Ca^{2+} internalization in mitochondria as a triggering event. This can in turn cause alteration of Ca^{2+} homeostasis and pathological accumulation of Ca^{2+} in *Afg3l2* heterozygous PCs in condition of normal glutamate stimulation, thus mimicking exitotoxic-mediated DCD. Indeed, it is well known that mitochondrial Ca^{2+} buffering has a key role in the regulation of cellular Ca^{2+} homeostasis, especially in neurons.

The project is aimed at dissecting the molecular pathogenesis of SCA28 at the mitochondrial level and at clarifying the missing molecular link between loss of AFG3L2 and mitochondrial dysfunction.

One direction of the research was focused on the link between loss/haploinsufficiency of *Afg3l2*, altered mitochondrial metabolism and DCD. Considering that DCD is characterized by excitotoxic injury, we wanted to verify if the absence of AFG3L2 induces an alteration in the mitochondrial Ca^{2+} buffering and if the hypothetical Ca^{2+} deregulation could be linked to altered mitochondrial morphology.

The second part of my research work was centered on the mitochondrial morphological defects due to the absence of AFG3L2. In particular, I focused on the link between AFG3L2 and mitochondrial dynamics studying the regulatory mechanism the pro-fusion protein OPA1 and its regulator OMA1.

MATERIAL AND METHODS

Chemicals and suppliers

Chemicals

All chemicals were obtained from Sigma-Aldrich, if not otherwise indicated. Cell culture media and reagents purchased from GIBCO Cell Culture Systems (Invitrogen).

Antibodies

Anti-HA antibody was from Sigma-Aldrich (St. Louis, MO, USA) Anti-OPA1 antibody was from BD Transduction Laboratories (Franklin Lakes, NJ, USA), anti-Hsp60 and Hsp70 antibodies were from Stressgen (San Diego, CA, USA), anti-GAPDH was from Santa Cruz Biotechnology,INC. (Europe), anti-c-Myc antibody was from Novus biologicals (Cambrige, UK), anti-YME1L1 antibody was from ProteinTech Group (Chicago, USA) anti-AFG3L2 and anti paraplegin were previously generated in our lab(Atorino et al., 2003), anti beta –tublin was from DSHB (university of Colorado, Colorado;USA); anti beta-actina was from Sigma Aldrich(St. Louis, MO, USA), TIM44 and TIM23 were from BD transduction laboratories (Qume DriveSan Jose, CA,USA), anti –porin was from Calbiochem (EMD biosciences, INc. la Jolla, CA,USA), anti MFN2 was from Abcam (Cambridge, UK).

ECL anti mouse and anti rabbit IgG, horseradish peroxidase (HRP)-linked species specific whole antibodyes were purchased from Amersham Biosciences (UK).

Polycolonal rabbit anti-goaqt immunoglobulins/HRP were obtained from DakoCytomation (Denmark)

DNA oligonucleotides

DNA oligonucleotides were purchased from Primm srl (Milan, Italy).

Cell line cultures

Mouse embryonic fibroblast (MEFs)

All cell lines were cultured at 37°C in 95% humidified air and 5% CO_2

Primary MEFs were established from embryonic day E16.5 from *Afg3l2* knockout, heterozygous and wild type embryos (Maltecca et al., 2008) and immortalized by SV40 (Schuermann, 1990), using 300 μg/ml geneticin for selection. MEFS were cultured in D-MEM medium supplemented with 5% FBS, 2 mM L-glutamine and Sodium Pyruvate 1 mM.

Human cell lines

HeLa cells were maintained in Dulbecco's Modified Eagle's Medium containing penicillin/streptomycin, 10% fetal bovine serum, 1 mM L-glutamine and Sodium Pyruvate 1M.

Human immortalize fibroblasts from a control and the patiens belonging to *SPG7* family (De Michele et al., 1998) were obtained from Istituto Neurologico Besta (Milan, Italy). Cells were cultured in D-MEM medium supplemented with 10% FBS, 2 mM L-glutamine and Sodium Pyruvate 1 mM.

Primary Purkinje cells

For primary PC cultures, a modified version of previously described protocols (Tabata et al., 2000) was used. Cerebella from newborn mice were incubated in Hanks' balanced salt solution 1X (HBSS, Gibco, Paisley, UK) containing 5 U/mL papain (Sigma), 50 mg/mL cystein-HCl, 0.1 mM EDTA and 1 mg/mL DNase I (Millipore) for 30 min at 37°C. Tissues were then dissociated by mechanical

trituration. The reaction was blocked with 10% horse serum and samples were centrifuged at 1200 rpm for 10 min. The cellular pellet was washed twice in HBSS 1X and resuspended in a cultured medium containing: Neurobasal (Gibco), B27 supplement (Invitrogen), 200 mg/mL D-glucose, 2 mM GlutaMax (Gibco), 100 U/mL PenStrep (Gibco), 1% horse serum (Invitrogen), 3 mM KCl, 50 ng/mL 2.5 S NGF (Millipore). Cells were plated at a density of 1.5 x $10^4/cm^2$ on coverslips (14 mm or 24 mm in diameter) or bottomglasses (Mattek, Ashland, MA, USA) coated with Poly-L-lysine (Sigma).

Imaging

Imaging analysis on MEFs cells

Analysis of mitochondrial network morphology was performed as described (Cipolat et al., 2004) by expressing a mitochondrial targeted enhanced yellow fluorescent protein (mtYFP, Clontech, Mountain View, CA, USA) and live imaging confocal microscopy. An average of 150 cells were analyzed for each experimental condition. Cells were divided into three classes accordingly to mitochondria shape: tubular mitochondrial network, intermediate or fragmented mitochondrial structures. Experiments were repeated at least three times, and three operators analysed the images, independently. Chi squared test on row data was applied for significance calculation (degrees of freedom=2).

For the analysis of mitochondrial and ER volumes, cells were transfected with mitochondrial targeted red fluorescent protein mt-RFP (Clontech, Mountain View, CA, USA) and ER- targeted green fluorescent protein (ER-GFP, kindly provided by R. Sitia) and stacks of consecutive confocal images taken at 0.1-μm intervals were acquired. 3D reconstruction and volume rendering were performed using Volocity 3D Image Analysis Software vers. 5.5.1, Perkin Elmer, Norwalk, MA, USA.

Manders' coefficient was applied for the quantitative analysis of mitochondria-ER colocalization. In all the experiments, confocal microscopy was performed using Perkin Elmer UltraVIEW Spinning Disk Confocal Microscope and EMCCD Hamamatsu C9100 imaging camera. The system is equipped with a stage incubator

from OkoLab (www.okolab.com), allowing to work with live cells maintained under stable conditions of temperature, CO_2 and humidity.

For each cell, the total number of objects mitochondria was identified using the IN Cell Developer Toolbox 1.8 (GE Healthcare, Little Chalfont, UK). After the optimisation of segmentation parameters, a mask was created to cover the mitochondrial network. This mask was projected on the ER. At this point a threshold was set in order to classify mitochondria using the green (ER) intensity. Mitochondria with a green signal intensity greater than or equal to the threshold were classified as in contact with the ER, whereas mitochondria with a green signal intensity less than threshold were classified as free of contacts.

Morphometric analyses of primary PCs

IF were performed on primary PCs at 14 DIV. Stacks of consecutive confocal images were taken at 0.3 μm intervals using Perkin Elmer UltraVIEW Spinning Disk Confocal Microscope (Norwalk, MA, USA). The analyses of soma/dendrites area and total mitochondria volume were performed using Volocity 3D Image Analysis Software version 5.5.1 (Perkin Elmer). For the mitochondrial volume evaluation, a ROI was drawn to cover the profile of each PC (or dendrites only). A threshold for the red signal (mitochondria) and green signal (PCs) was set in order to exclude background. Mitochondria with red signal intensity greater than or equal to the green threshold were identified as belonging to PC. This analysis was extended to the whole cell volume.

Electron microscopy

The semithin and ultrathin sections from mouse tissues and on primary PCs at 14 DIV were prepared as previously described (Maltecca et al., 2009).

Ca^{2+} measurement

Ca^{2+} measurement in MEFs cells

MEFs grown on 13 mM round glass cover slips at 50% confluence were transfected with the cytosolic (cytAEQ) or mitochondrial aequorin probes (mtAEQmut or mtAEQ). Cells were reconstituted with 5 mM coelenterazine for 90 min in DMEM supplemented with 1% fetal bovine serum, incubated in KRB (Krebs–Ring modified buffer: 125 mM NaCl, 5 mM KCl, 1 mM Na3PO4,1 mM MgSO4, 5.5 mM glucose, 20 mM 4-(2-hydroxyethyl)-1-piperazineethanesulfonic acid (HEPES), pH 7.4, 378C) supplemented with 1 mM CaCl2 and then transferred to the perfusion chamber. When indicated, 100 nM bradykinin was added. The experiments were concluded by lysing MEFs with 100 mM digitonin in a hypotonic Ca^{2+}-rich solution (10 mM CaCl2 in H2O), thus discharging the remaining aequorin pool. The light signal was collected in a purpose-built luminometer as previously described (Chiesa et al., 2001).

Mitochondrial Ca^{2+} measurement in PCs

To measure $[Ca^{2+}]_{mito}$ in PCs in primary cerebellar cultures, we created an adeno-associated viral vector expressing a mitochondria-targeted version of the GFP-based Ca^{2+} probe, 4mtD1cpv (Palmer et al., 2006), under the synapsin promoter.

4mtD1cpv pcDNA3 was used as a template in a PCR with the following primers:

Primer Forward:

5’-TTATCGAAATTAATACGACTCACGTGGAATTCGCCACCATGTCCGTCC-3’

Primer Reverse:

5'- CCGCCAGTGTGATGGATATCTGCAGAATTCTTA-3'

The forward primer was designed to introduce an EcoRI restriction site at the 5' of 4mtD1cpv and a Kozak sequence to improve translation efficiency. The PCR product was then cloned in the EcoRI site of the pDC511 syn BGH-polyA vector (Montesinos et al., 2011). This shuttle plasmid carries the 470 bp human synapsin promoter to guaranty neuron specific expression of the cameleon probe.

Second generation rAd was produced by transfecting E2T cells (Zhou and Beaudet, 2000) with the genomic helper plasmid (Microbix Biosystems inc., Mississauga, Ontario, Canada) that had been modified to contain the E2a deletion and the pDC511 syn 4mtD1cpv-BGH PolyA vector as previously described (Montesinos et al., 2011). Preparation of a high titer viral stock from crude lysate was performed as described in Ng and Graham (Ng and Graham, 2002). The titer was determined by limiting dilution to have a plaque-forming unit (pfu) of $3.1*10^7$ pfu/ml.

PCs were transduced at 5 DIV with multiplicity of infection (M.O.I.) of 60 and imaged for Ca^{2+} measurement 72 hours after infection. The FRET data were acquired on a Leica TCS SP-5 DS confocal microscope equipped with a 63x NA 1.4 objective. (Leica Microsystems GmbH, Wetzlar Germany). The light of a 405 nm solid-state laser was used to excite CFP, and the fluorescence emission from both CFP and YFP was collected simultaneously using two separate detection channels (CFP 470-505

nm and YFP 525-600 respectively). PCs were easily distinguished from granule cells and neurons, being markedly bigger and more ramified. Time series of 100 frames were collected using an imaging time of 1.314 s/image. After approximately 20 images 30 mM KCl was added to the imaging medium as described above to quantify the mitochondrial calcium response. The FRET signal was quantified by measuring the background-subtracted ratio between the YFP and the CFP channels on pixels corresponding to mitochondria.

Cytosolic Ca^{2+} measurement in PCs

$[Ca^{2+}]_{cyto}$ measurements was performed as previously described (Codazzi et al., 2006). Fura-2 acetoxymethyl ester (Calbiochem, Merck KGaA, Darmstadt, Germany) loading was performed at 37°C (4 μM, 40 min) in Krebs Ringer Hepes buffer (KRH, containing 5 mM KCl, 125 mM NaCl, 2 mM $CaCl_2$, 1.2 mM $MgSO_4$, 1.2 mM KH_2PO_4 and 6 mM glucose, 20 mM HEPES, pH 7.4). When K^+ concentration was increased in the solution, the concentration of Na^+ was adjusted to maintain isotonicity. Excitation wavelengths of 340 and 380 nm were used with an emission wavelength of 510 nm. The 340/380 fura-2 ratio was calculated as mean values within regions of interest drawn in neuronal soma. The time course of the intensity ratio was analyzed by custom-written routines in MATLAB (The MathWorks Inc., Natick, MA, USA).

Expression vectors:

- **pcDNA3.1**
- **pcDNA3.1-*MrpL32*-HA**
- **pcDNA3.1-*Oma1*-HA:**

OMA1 mouse cDNA clone image was bought from Thermo Scientific (Waltham, MA, USA).To introduce an HA tag into c-terminus before the stop codon and the XhoI restriction sequence after the stop codon of the purified product, I performed a PCR with the following primers:

FWD: 5'-cacaggaaacagctatgacca-3';

REV: 5'- tccgctcgagtcaagcgtaatctggaacatcgtatgggtagcctgcagttctcttctctag-3'

PCR product was purified using "QIAEX II Gel Extraction Kit" (Qiagen) and digested with EcoRI and XhoI. The digested product was cloned into pcDNA3.1 using T4-ligase (Promega) according to the manufacturer's instruction.

- **pcDNA3.1-*Oma1*- (deleted mutants) -HA**

To generate the following constructs I used "QuikChange Site-Directed Mutagenesis Kit" by Agilent Technologies (Stratagene Products Division, La Jolla, CA) with the appropriate primers.

construct	**Primers**
pcDNA3.1-*Oma1*-E324Q-HA	5'-ttcctcctgggccatcagatcgcacacg-3' 5'-cgtgtgcgatctgatggcccaggaggaa-3'
pcDNA3.1-*Oma1*-Δ147-149-HA	5'-cccagtccctctcttgctgaagccagtgcaaa-3' 5'-tttgcactggcttcagcaagagagggactggg-3'
pcDNA3.1-*Oma1*-Δ150-152-HA	5'-cctctcttgctgctcattgtgcaaaagctccttg-3' 5'-caaggagcttttgcacaatgagcagcaagagagg-3'
pcDNA3.1-*Oma1*-Δ153-155-HA	5'-ctgctcattctgaagccactccttgctatcatcgtg-3' 5'-cacgatgatagcaaggagtggcttcagaatgagcag-3'
pcDNA3.1-*Oma1*-Δ170-HA	5'-gcataaggaaatggtgggcacttccccctaacaa-3' 5'-ttgttagggggaagtgcccaccatttccttatgc-3'
pcDNA3.1-*Oma1*-Δ171-HA	5'-ataaggaaatggtggcaacttccccctaacaagaag-3' 5'-cttcttgttagggggaagttgccaccatttccttat-3'
pcDNA3.1-*Oma1*-Δ172-HA	5'-gcataaggaaatggtggcaagcacccccctaacaag-3' 5'-cttgttagggggtgcttgccaccatttccttatgc-3'
pcDNA3.1-*Oma1*-Δ169-172-HA	5'-ggggcataaggaaatggcccccctaacaagaagg-3' 5'-ccttcttgttagggggccatttccttatgcccc-3'
pcDNA3.1-*Oma1*-Δ173-176-HA	5'-gggcataaggaaatggtggcaagcacttaaggagctatttaaa-3' 5'-tttaaatagctccttaagtgcttgccaccatttccttatgccc-3'

pcDNA3.1-*Oma1*-Δ175-178-HA	5'-ggcaagcacttccccctctatttaaagacagcgt-3' 5'-acgctgtctttaaatagaggggaagtgcttgcc-3'
pcDNA3.1-*Oma1*-Δ177-180-HA	5'-cacttccccctaacaagaaagacagcgtgaggaa-3' 5'-ttcctcacgctgtctttcttgttagggggaagtg-3'

- **pcDNA3.1-*Oma1*-Δ92-144-HA**

To generate the construct pcDNA3.1-*Oma*1-Δ92-155-HA we used this clone strategy:

1) pcDNA3.1-OMA1-HA was digested by EcoRI and XhoI and purified using the appropriate Qiagene kit. Two different PCR were performed to obtain two OMA1 fragments.
2) I used the universal primer T7 forward and 5'AATGAGCAGCAAGAGGGTAAGCACCCCCAATTCC-3' to clone OMA1 amino acid region from the first to the 91th amino acid. Then, I performed a PCR with 5'-TTGGGGGTGCTTACCCTCTTGCTGCTCATTCTGAAG-3' and the universal primer BGHrev to clone the amino acid region from 145 to 521.
3) The two pcr products were purified using "QIAquick PCR Purification Kit" by Quiagen. The two purified products were ligated using T4 ligase (promega) according to the manufacturer's instruction.
4) This products were digested using EcoRI and XhoI and cloned in pcDNA3.1

- **PcDNA3.1-*AFG3L2*-myc**
- **PcDNA3.1-*AFG3L2*-E575Q-myc**
- **PcDNA3.1-*AFG3L2*-E408Q-myc**

These three constructs were already present and used in our laboratory(Koppen et al., 2007), but to overexpress them in the presence of the specific Stealth RNAi against *AFG3L2* we needed to mutagenize them to generate insensitive Stealth RNAi constructs. For this reason we modified the last base of 4 codons in the region recognized by the Stealth RNAi. To perform this mutation we used the QuikChange Site-Directed Mutagenesis Kit" by Agilent Technologies with this specific primers:

FWD: 5'-ctatctttcaaaaggagtagtagaccgcctagaagtcgtcaacaagcgttttgttc-3'

REV: 5'-gaacaaaacgcttgttgacgacttctaggcggtctactactccttttgaaagatag-3.

- **pMT21-*YME1L1*-E543Q-myc (isoform 3)**

  pMT21-YME1L1-MYC was mutagenized to generate the proteolytic inactive form. To do this I used "QuikChange Site-Directed Mutagenesis Kit" by Agilent Technologies with this specific primers:

  5'-ataatggcatgaccagactgatgatatgctgtgatggttttgtttttgttat-3'

  5'-ataacaaaaacaaaaccatcacagcatatcatcagtctggtcatgccattat-3'

  To overexpress them in the presence of the specific Stealth RNAi against *YME1L1* we needed to mutagenize them to generate insensitive Stealth RNAi constructs. We used the same strategy describe above with these primers:

5'-agaaggattcttatttcttgttcgattgcggactgagtttctggacttagtttccctgtatc-3'

5'-gatacagggaaactaagtccagaaactcagtccgcaatcgaacaagaaataagaatccttct-3'

The fidelity of all constructs was confirmed by automated DNA sequencing.

Biochemical assay

Protease inhibitors experiment

HeLa cells were transfected overnight with pcDNA3.1 OMA1-HA and 14 h after transfection they were incubated for 10 h with the following protease inhibitors: 0.5 mM o-phe, 100 µM E-64d and 400 µM PMSF (Sigma-Aldrich)

Uncoupler treatment

HeLa cells were treated with Carbonyl cyanide-4-(trifluoromethoxy)phenylhydrazone (FCCP)(Sigma Aldrich) 10 µM for the indicated time points.

Western blot analysis

Western blot was performed using standard protocols. Briefly, total cell lysate was prepared by protein extraction using a Triton-containing buffer (50 mM Tris-HCl pH 8, 150 mM NaCl, 2% Triton, 0.5 mM EDTA pH 8, 1X Protease Inhibitor Cocktail, Roche Applied Science). The protein concentration was evaluated using Quick Start™ Bradford Protein Assay.(Hercules, CA, United States of America). 25 µg of protein extracts were dissolved in Sample buffer (60 mM Tris-HCl pH 6.8, 5% glycerol, 1,7% SDS, 0,1 M DTT, 0,002% bromophenol blue), were separated on SDS-PAGE and analyzed by standard immunoblotting procedures.

Co-immunoprecipitation

Co-transfected HeLa cells were lysate after 24h from transfection with buffer A (50 mM Tris HCl ph 8.00, 150mM NaCl, 0.5mM EDTA ph8, 1X Protease Inhibitor

Cocktail, 0.15% Sarkozyl- 30'- 4°C). At the end of the incubation the lysate was sonicated. The soluble fraction was recovered after centrifugation (13.000 rpm - 10' at 4°C). Supernatant represent the soluble fraction and it is quantified by Quick Start™ Bradford Protein Assay (Bio-Rad, city and country). 1000 µg of lysate underwent to pre-clearing step to reduce nonspecific binding of proteins to sepharose. For this reason recombinant Protein G Sepharose beads were incubated in buffer B (50 mM Tris HCl ph 8.00, 150mM NaCl, 0.5mM EDTA ph8, 1X Protease Inhibitor Cocktail, 0.03% Sarkozyl) for 30 at 4°C and then incubated 1h with the lysate. After this step, beads were precipitated by centrifugation (1200 rpm- 5'- 4°C) and discarded. Supernatant was incubated with the anti-Myc antibody for an hour in constant gentle agitation. Before adding protein G Agarose beads to the lysate, they have to be incubated in buffer B (50 mM Tris HCl ph 8.00, 150mM NaCl, 0.5mM EDTA ph8, 1X Protease Inhibitor Cocktail, 0.03% Sarkozyl) within gentle agitation for 30'- 4°C. Then beads were added to the lysate for 1h at 4°C in constant suspension. In the end, beads were precipitated by centrifugation (1200 rpm- 5'-4°C) and washed three time with the buffer C (50 mM Tris HCl ph 8.00, 150mM NaCl, 0.5mM EDTA ph8, 1X Protease Inhibitor Cocktail, 0.015% Sarkozyl). Precipitates were used for Western blot analysis.

For the reverse Co-Ip (immunoprecipitation OMA1-HA and detection AFG3L2) 1000 µg of lysate underwent to pre-clearing step, then the supernatant was incubated with HA.11 Clone 16B12 Monoclonal Antibody, Affinity Matrix beads (Covance, Princeton, New Jersey, USA) that have been previously incubated in buffer B for 30'

at 4°C. The incubation between lysate and conjugated HA sepharose beads occurred for 1 h at 4°C in constant gentle agitation. At the end of the incubation, beads were treated as before.

Mitochondrial isolation

Mitochondria were isolated from HeLa cells according to manufacturer's protocol (Pierce) with minor modifications. Briefly, the cells were trypsinized and harvested. A Dounce homogenizer was used to lyse the cells by 40 strokes. After removing the nuclear fraction (centrifugation of total lysate at 2500 rpm for 10 minutes at 4°C) , the crude supernatant was spun at 13,000 rpm for 25 minutes to pellet the intact mitochondria. The mitochondrial pellet was resuspended in Mitochondrial buffer (0.25M sucrose, 20 mM MOPS, 1mM EDTA, and 1X protease inhibitor cocktail (Sigma) to collect mitochondrial proteins. For each fractionation, equal amounts of soluble cytosolic protein and mitochondrial protein were determined by BCA assay (Pierce).

Proteinase proteolysis assay

Mitochondria were isolated by the mitochondrial isolation protocol described above. The mitochondrial pellet was resuspended in Mitochondrial buffer (0.25M sucrose, 20 mM MOPS, 1mM EDTA) and aliquoted into equal fractions. Final concentration of 50/100 μg/mL of trypsin was added to the appropriate sample tube with or without a final concentration of 1% Triton X-100. Samples were incubated on ice for 30 minutes and the proteolysis was inhibited by the addition of PMSF and protease

inhibitor cocktail. Then the samples were centrifuged at max speed for 5 minutes and the pellet was resuspended in Sample Buffer. Proteins were resolved on SDS-PAGE.

Mitochondrial import inhibition

Hela cells were transfected with the indicated plasmids. After 10 hours from the transfection, the cells were treated with valinomycin 1μM or valinomycin + Mg 132 (2.5 μM) for 16 hours. Subsequently, the mitochondrial isolation described above was performed.

Transient transfection

Transient transfection for the overexpression or for the silencing was performed using LIPOFECTAMINE 2000 (Invitrogen, Carlsbad, CA, USA) according to the manufacturer's instructions.

Down-regulation

Down-regulation of AF3GL2, OMA1 and YME1L1 was performed using specific Stealth RNAi and the non-targeting Stealth RNAi negative control (Invitrogen).

The sequences are 5'-ACGACUUCCAAUCUGUCUACUACUC-3' for human AFG3L2, 5'-UGGACUACUGCUUGCUGCAAAGGCU-3' for human OMA1, 5'-UCCAGAAACCCAAUCUGCCAUCGAA-3' for human YME1L1.

100 pmoles of each siRNA were transfected using Lipofectamine (Invitrogen). Down-regulation of the target gene was monitored by Immunoblot analysis on cell lysates after 48h/72 h from transfection.

Densitometry analysis

To perform densitometry a of Western Blot bands I used the specific plug in of ImageJ.

Statistical analyses

Results are reported as the mean ± SEM. Most of the experiments were evaluated by Student's *t* test. Chi squared test with 2 degrees of freedom was applied for analysis of ultrastructure of mitochondria.

RESULTS

Part I: AFG3L2 deficiency impairs mitochondrial Ca^{2+} buffering, causes organellar network fragmentation and Purkinje Cells degeneration.

***Afg3l2* ko cells show increased mitochondrial fragmentation**

It was previously demonstrated in the lab that the absence of AFG3L2 induces severe alterations of the mitochondrial structure and function: in particular the disorganization of cristae structure, the alteration of respiratory chain complex I and complex III assembly, the increase in the amount of reactive oxygen species and the decrease in ATP production (Maltecca et al., 2008; Maltecca et al., 2009). Starting from these findings, we evaluated if the absence of AFG3L2 could cause an alteration in the mitochondrial network morphology. To achieve this goal we performed live imaging in MEF cells overexpressing a mitochondria-targeted yellow fluorescent protein (mt-YFP). Cells were divided into three classes accordingly to mitochondria shape: tubular mitochondrial network, intermediate or fragmented mitochondrial structures (Ishihara et al., 2006). We observed an evident alteration in mitochondrial network morphology in *Afg3l2* ko cells. Indeed, morphometric analysis demonstrated that wild-type and heterozygous MEFs have fused mitochondria. In contrast, *Afg3l2* ko cells showed more than 50% of cells with fragmented mitochondria and only 5% of cells with a tubular mitochondrial network (Fig. 1) (Maltecca et al., 2012).

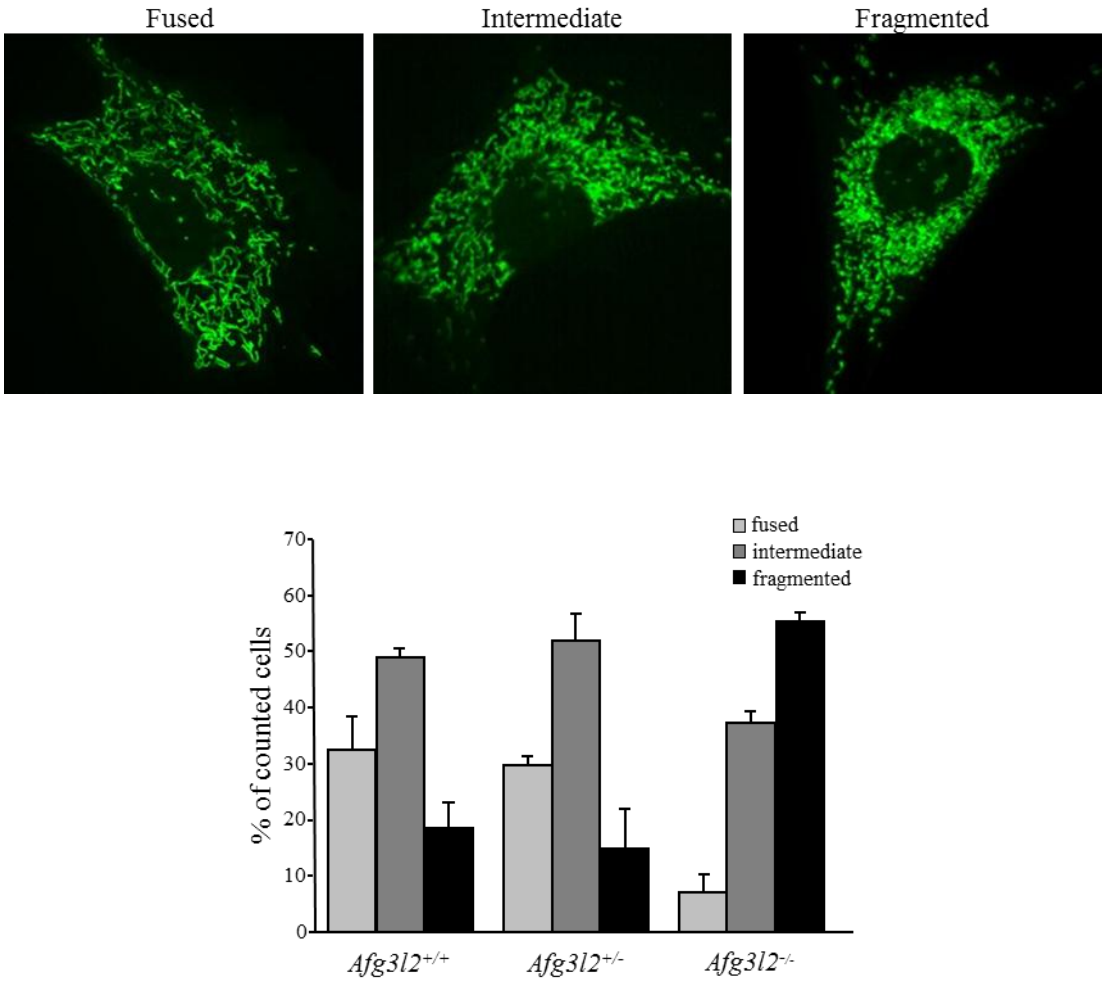

Figure 1:**the absence of AFG3L2 induces mitochondrial network fragmentation.**

A) Representative pictures of mitochondrial morphology in *Afg3l2* MEFs transfected with mt-YFP and visualized by confocal microscopy. (B) Morphometric analysis of mitochondrial morphology in Afg3l2 MEFs. One hundred and fifty randomly selected cells were analyzed in each experiment. Bars represent means+SD of three independent experiments. The Chi-squared test (2 degrees of freedom): *Afg3l2* ko versus either heterozygous or wild-type MEFs = P ,0.001. (C)

Fission of the mitochondrial network in *Afg3l2* ko MEFs reduces organellar matrix continuity and leaves a fraction of mitochondria devoid of connection to the ER

The *Afg3l2* haploinsufficient mouse resembles the phenotype of SCA28 patients, showing a progressive decline in motor performances caused by PC-DCD (Maltecca et al., 2012). We hypothesize that AFG3L2-depleted mitochondria have defective Ca^{2+} buffering capacity, leading to dysregulation of cytosolic Ca^{2+} homeostasis and finally to PC-DCD. We evaluated whether the mitochondrial fragmentation observed in *Afg3l2* ko cells could impact on mitochondrial Ca^{2+} buffering. In particular we wondered whether mitochondrial altered morphology could influence the number of mitochondria/ER contacts, specialized sites where IP3R/RyR mediated Ca^{2+}oscillations are propagated locally to the mitochondria. The close vicinity of mitochondria to Ca^{2+} release sites on the ER is crucial for the activation of the MCU and thus for the rapid and efficient accumulation of Ca^{2+} inside the organelles (Csordas et al., 2010; Rizzuto et al., 1998). To measure the total number of contacts in the whole cell volume, we analyzed the colocalization between mitochondria and ER with three-dimensional (3D) reconstruction and volume rendering of confocal stacks of ER-targeted green fluorescent protein (ER-GFP) and mitochondrial-targeted red fluorescent protein (mt-RFP) in the three genotypes, as previously reported (Nicholls, 1974) (De Brito and Scorrano, 2008) (Fig. 2A) . In this analysis, we considered the overlapping mitochondrial and ER spots as the sites where most-efficient Ca^{2+} transfer between the two organelles occurs, thus satisfying the high

Ca^{2+} concentration demand for the opening of the MCU. As measured by Manders' colocalization coefficient (Manders, 1993), we found that the evident fragmentation of the mitochondrial network does not affect the average number of mitochondria-ER contact sites in *Afg3l2* ko cells (Fig. 2B) Similarly, the overall volume of the organellar network of both mitochondria and ER is unaffected by the loss of AFG3L2, as demonstrated by quantitative morphological imaging of the mitochondrial and ER networks by transfecting cells with mt-RFP or ER-GFP, respectively. After 3D reconstruction of confocal stacks, the images were analyzed evaluating the total volume of the organellar network. ER architecture was unaffected by the loss of AFG3L2, appearing as an interconnected network of cisternae spanning the whole cellular volume. We also observed that fragmentation of the mitochondrial network does not alter either the mitochondrial or the ER total volume, the ratio of the two organellar volumes being comparable in the three genotypes (Fig. 2C). According to the observed fragmentation, we found a significant reduction in the average size of individual mitochondrial particle in *Afg3l2* ko cells compared with controls (6.94+2.3 versus 12.68+3.35 mm^3 in wild-type and 12.3+1.91 mm^3 in heterozygous cells, P , 0.001) (Fig. 2D). Having the cell lines the same mitochondrial total volume, these data indicate that *Afg3l2* ko cells have an increased number of individual mitochondria compared to wild-type and heterozygous cells (Fig. 2E). This hypothesis was verified by counting the total number of RFP-positive objects per cell, which is almost doubled in *Afg3l2* ko cells compared with control cells, while the percentage of objects that are in contact with the ER is reduced (Fig. 2F).

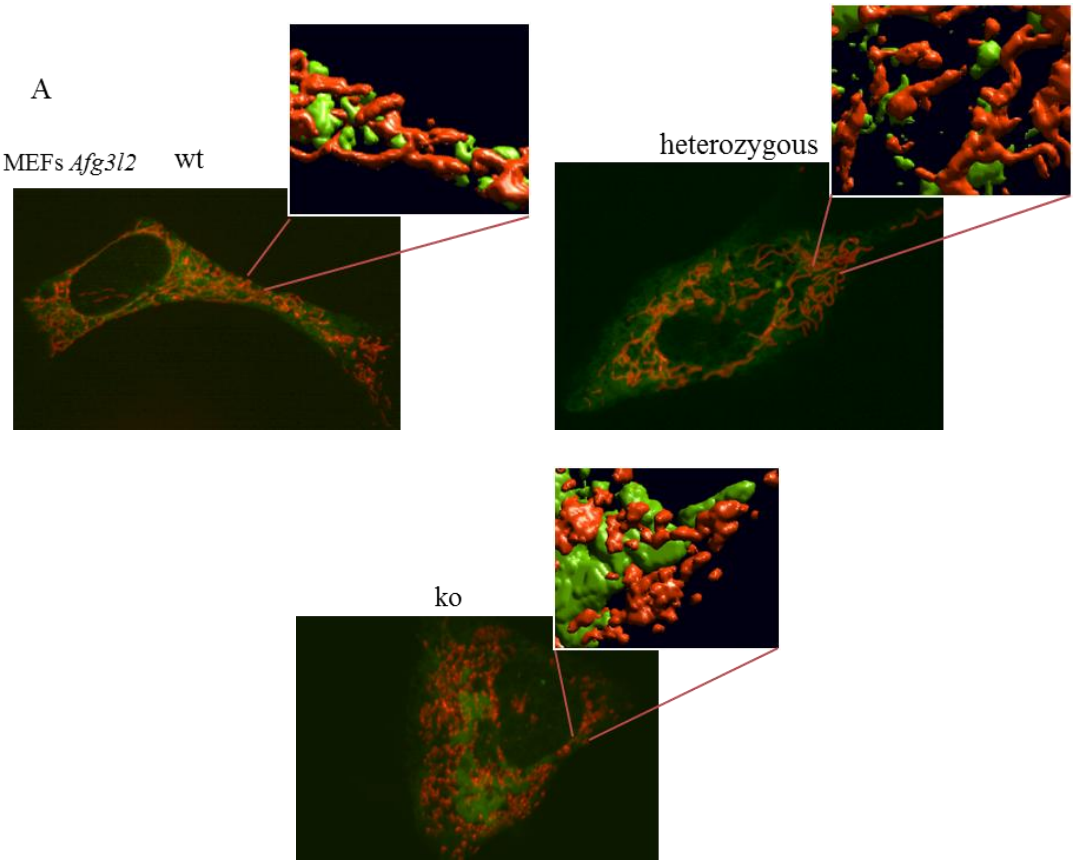
A
MEFs *Afg3l2*
wt
heterozygous
ko

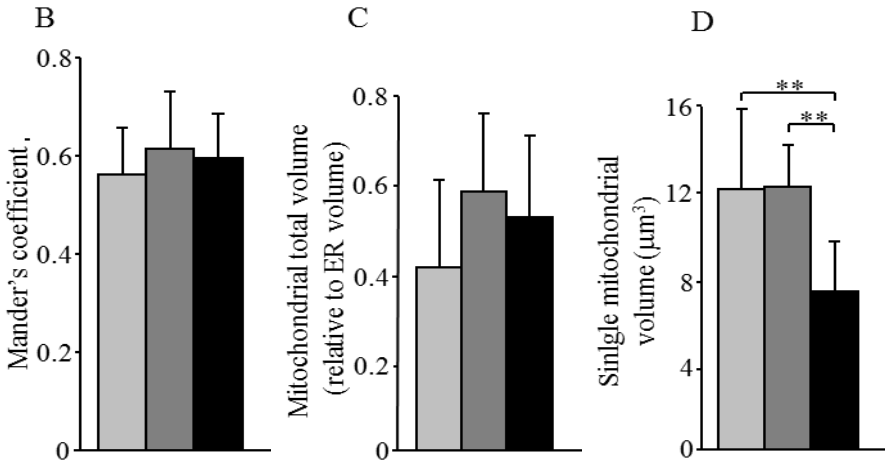
B
Mander's coefficient
0.8
0.6
0.4
0.2
0
C
Mitochondrial total volume (relative to ER volume)
0.8
0.6
0.4
0.2
0
D
Sinlgle mitochondrial volume (μm³)
16
12
8
4
0
**
**

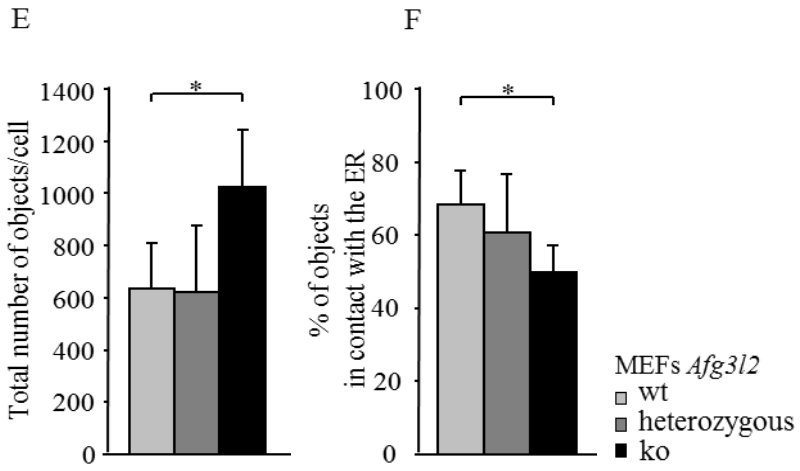

Figure 2: Mitochondrial fragmentation leaves a fraction of organelles free of connections to the ER.

Mitochondrial fragmentation leaves a fraction of organelles free of connections to the ER. (A) Representative images of *Afg3l2* knockout, heterozygous and wild-type MEFs cotransfected with ER-GFP and mt-RFP. Insets show 3D reconstructed confocal stacks. (B) Quantitative analysis of ER-mitochondria colocalization estimated by Manders' coefficient. (C-D) Effect of *Afg3l2* depletion on total mitochondrial volume and on individual mitochondrial particles, respectively. (E-F) Quantification of the total number of RFP-positive objects and quantification of the percentage of RFP-positive objects in contact with the ER in the three genotypes. Data were obtained from an average of 60 randomly selected cells per genotype. Bars represent means+SD of three independent experiments. Student's t-test: $*P < 0.05$,

Loss of AFG3L2 causes reduced mitochondrial Ca^{2+} uptake

To examine the effect of the loss or haploinsufficiency of *Afg3l2* on mitochondrial Ca^{2+} buffering, we performed Ca^{2+} measurements on MEFs by employing aequorin chimeras targeted to mitochondria and cytosol compartments (mtAEQmut and cytAEQ) (Chiesa et al., 2001). Cells were challenged with bradykinin, which leads to an inositol (1,4,5)triphosphate-triggered release of Ca^{2+} from the ER stores and its accumulation in the mitochondrial matrix. In *Afg3l2* ko cells, the mitochondrial Ca^{2+} peak response ($[Ca^{2+}]_m$) elicited by bradykinin stimulation was strongly reduced compared with *Afg3l2* heterozygous and wild-type cells, as measured by the low-affinity mtAEQmut probe (Fig. 3A). The decreased mitochondrial Ca^{2+} response in *Afg3l2* ko cells was specific of mitochondria and not secondary to global cellular Ca^{2+} signaling. In fact, cytosolic Ca^{2+} response ($[Ca^{2+}]_c$) measured by the cytAEQ probe after bradykinin stimulation revealed no alterations in *Afg3l2* ko cells compared with wild-type cells (Fig. 3B). These experiments demonstrate that *Afg3l2* null mitochondria show decreased average $[Ca^{2+}]_m$ elevations in the presence of a maximal Ca^{2+}stimulation demonstrating that the mitochondrial network induces strong defect in Ca^{2+} homeostasis.

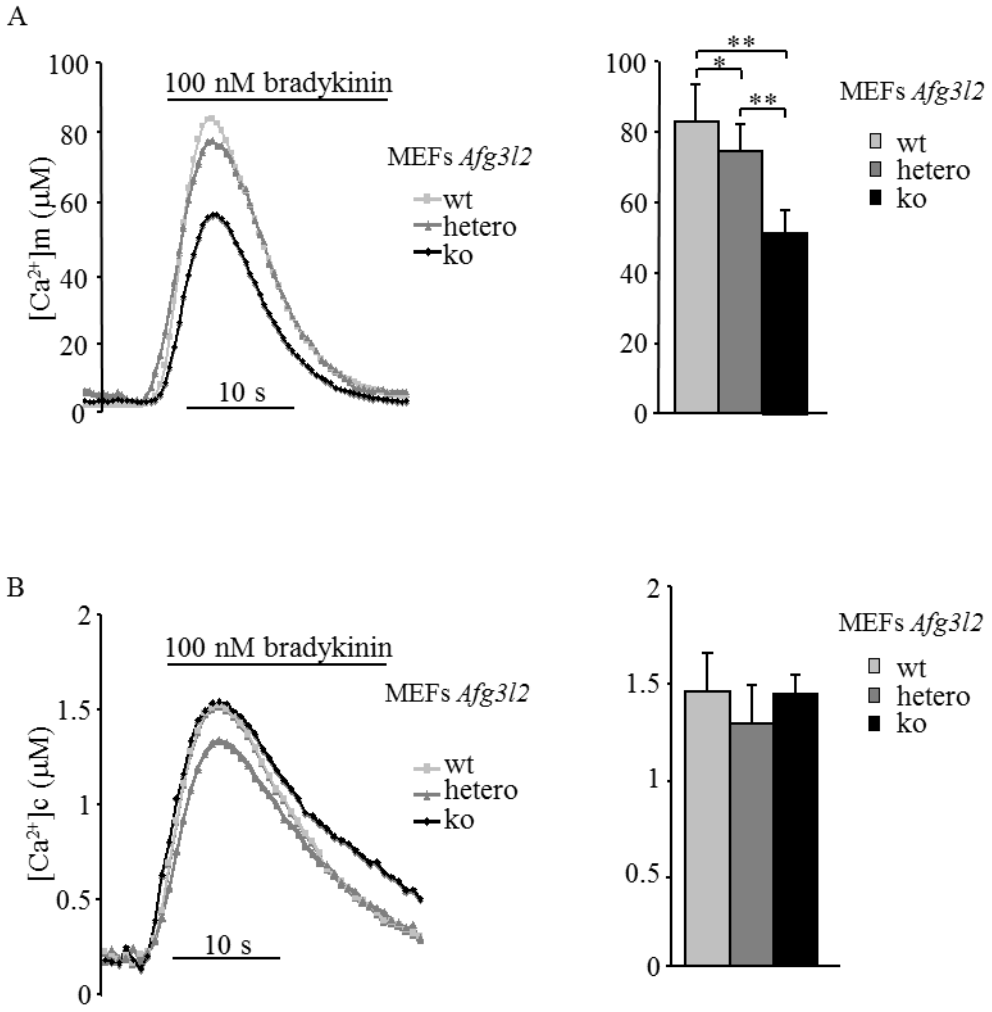

Figure 3: Loss of *Afg3l2* reduces mitochondrial Ca^{2+} uptake.

(A and B) $[Ca^{2+}]_m$ and $[Ca^{2+}]_c$ in *Afg3l2* MEFs of the indicated genotypes measured by aequorin probes (mtAEQmut and cytAEQ). On the left: representative graphs; on the right: means+SD of $[Ca^{2+}]_m$ and $[Ca^{2+}]_c$ peak responses after bradykinin stimulation, respectively (16 traces obtained from four independent experiments). Student's t-test: $**P < 0.001$, $*P < 0.05$.

Loss of AFG3L2 in primary Purkinje cells induces mitochondrial morphological alterations and depletion of dendritic mitochondria

Considering the limitation represented by non-excitable and non-polarized cells such as fibroblasts, we decided to test mechanism of pathogenesis for SCA28 in cultured primary PCs. In fact, these are the neurons primary affected in SCA28 patients. We first performed a quantitative evaluation of PC morphology by IF using anti-calbindin antibody at 14 days in vitro (DIV). *Afg3l2* heterozygpus PCs appeared comparable to wt, while in *Afg3l2* ko PCs dendrites were slightly decreased in number and in length but considerably reduced in terms of area, appearing thinner with shorter side branches (Fig.4 A-B). Then, we examined the morphology, the distribution and the metabolic status of mitochondria in primary PCs. We first performed IF and confocal microscopy using an antibody against COX1 (mitochondrial marker) and against calbindin (PC marker). In *Afg3l2* ko PCs, mitochondria were mostly round shaped as we previously observed in MEFs (Maltecca et al., 2012), in contrast with the tubular shaped organelles observed in syngenic controls (Fig. 4A). We also investigated whether alterations of mitochondrial morphology may alter the trafficking of the organelles to the distal dendritic branches of PCs. By three-dimensional (3D) reconstruction of confocal stacks of PCs stained with anti-calbindin and anti-COX1 antibodies, we analyzed the mitochondrial volume in the whole PC volume and in dendrites. We observed that the total volume of mitochondria is not changed in *Afg3l2* ko PCs, though these cells contain fewer mitochondria in their dendrites (Fig. 4C-D).

To further address a defective trafficking of mitochondria, we assayed mitochondria ultrastructure by electron microscopy (EM). In wt PCs, mitochondria are evenly distributed in the cell soma and in dendrites, have structurally intact inner and outer membranes with well-defined cristae and show tubular shape. On the contrary, in *Afg3l2* heterozygous PCs we observed a remodeling of the inner membrane conformation ranging from widening to vesiculation of the cristae, which worsens dramatically in *Afg3l2* ko PCs, where most of the organelles appear swollen (Fig. 4E). Quantification of these alterations is reported in (Fig. 4F). Consistent with confocal microscopy observations, in *Afg3l2* ko PCs mitochondria aggregated in the soma leaving dendrites depleted of organelles. No differences in mitochondrial distribution were apparently detected in *Afg3l2* heterozygous PC-dendrite compared to wt, indicating that organellar morphological alterations may be not so severe to hamper the entry of the organelles into the dendritic tree, at least in culture conditions.

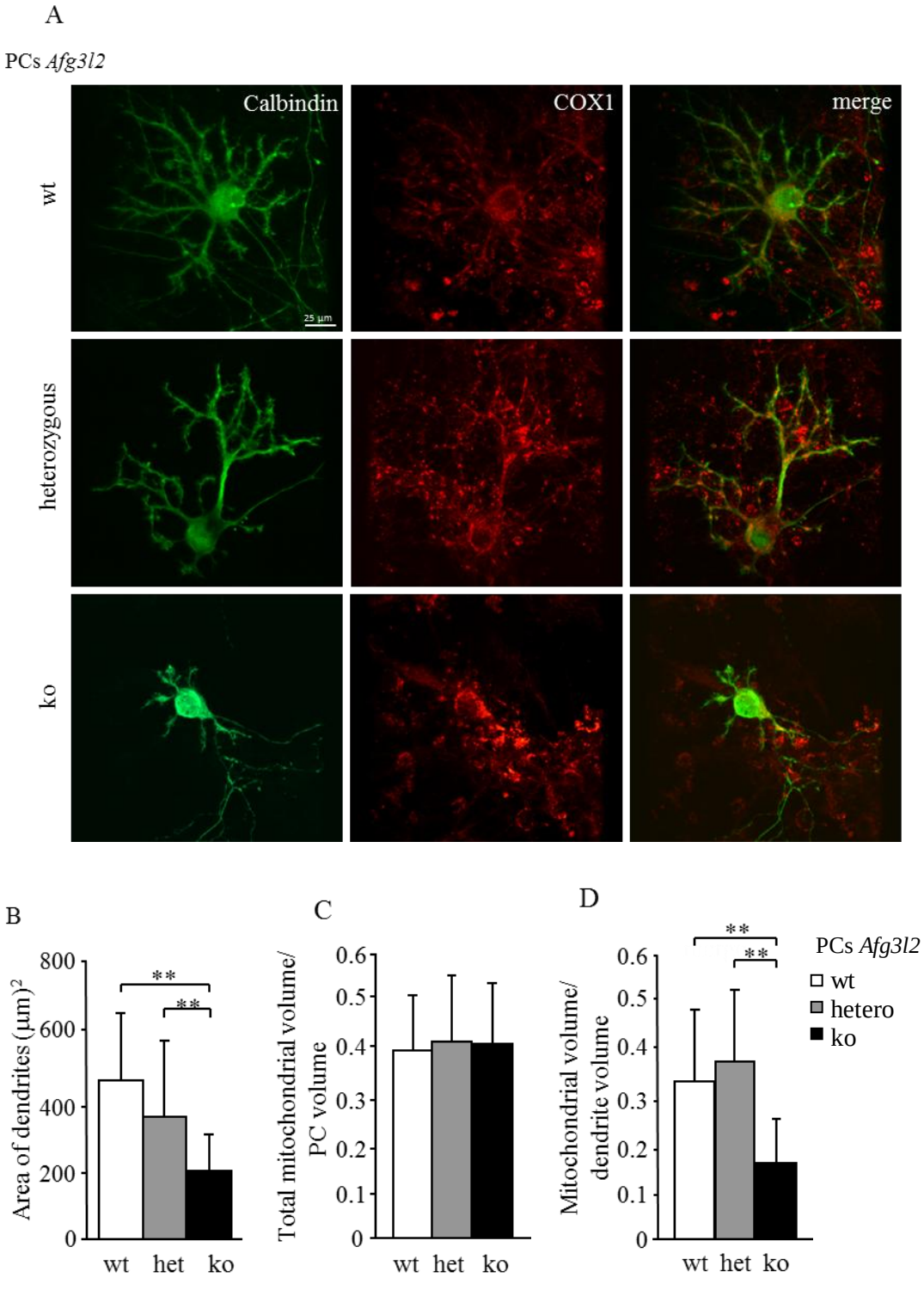
A
PCs *Afg3l2*
Calbindin
COX1
merge
wt
heterozygous
ko
25 µm
B
Area of dendrites (µm)²
800
600
400
200
0
**
**
wt het ko
C
Total mitochondrial volume/ PC volume
0.6
0.5
0.4
0.3
0.2
0.1
0
wt het ko
D
Mitochondrial volume/ dendrite volume
0.6
0.5
0.4
0.3
0.2
0.1
0
**
**
wt het ko
PCs *Afg3l2*
wt
hetero
ko

E

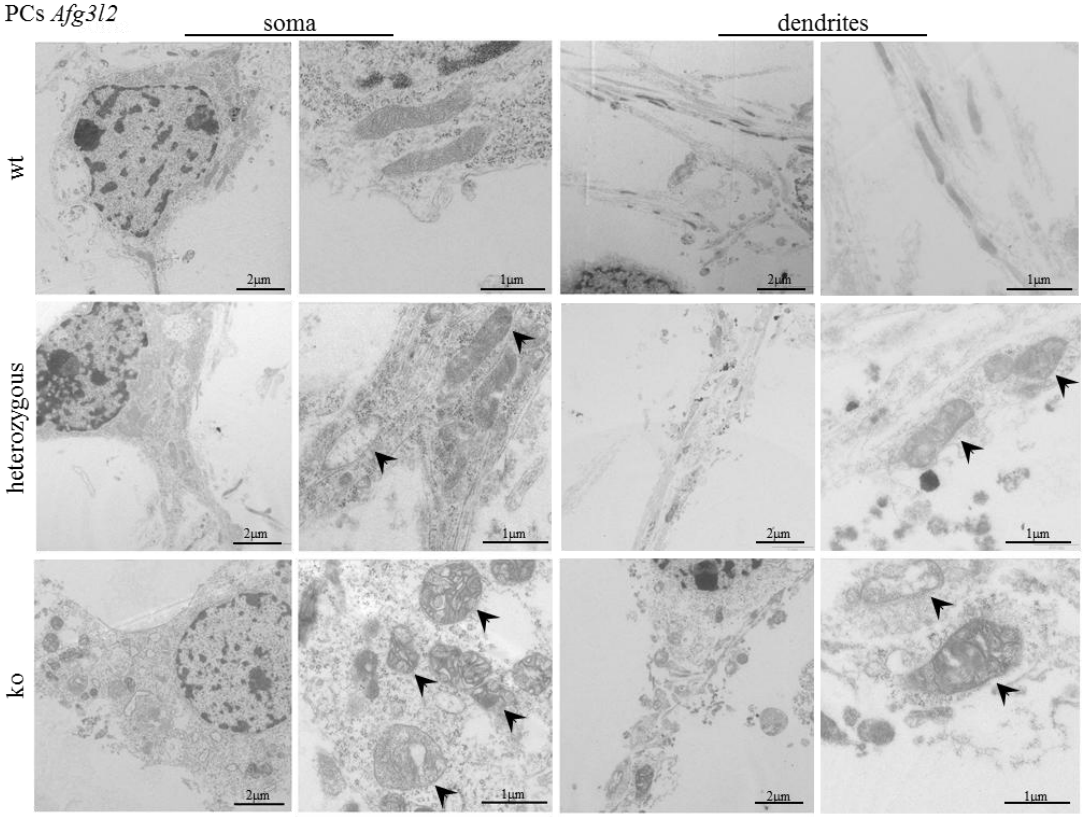
PCs *Afg3l2*
soma
dendrites
wt
heterozygous
ko
2µm
1µm

F

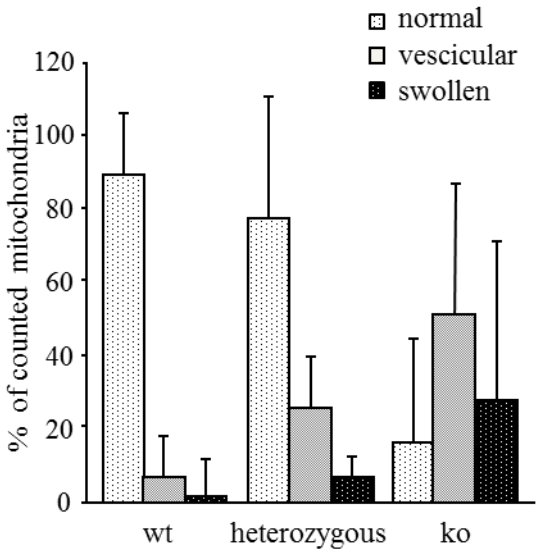
normal
vescicular
swollen
% of counted mitochondria
120
100
80
60
40
20
0
wt
heterozygous
ko

Figure 4: Loss of Afg3l2 in PCs alters dendritic mitochondrial content and the mitochondrial shape.

(A)IF on primary PCs of the indicated genotypes at 14 DIV using antibodies against the PC marker calbindin and the mitochondrial marker COX1 analyzed by confocal imaging. (B) Quantification of the area of dendrites [means +/- SD, n=6, +/-20 neurons analyzed/experiment; student's t test: **p< 0.001]. (C and D) Quantification of the total mitochondrial volume relative to the total PC volume (C) or relative to PC dendrite volume (D) analyzed by 3D reconstructon of consecutive confocal stacks taken at 0.3 μm (n=15 PCs analyzed per genotype). Student's *t* test: **p< 0.001. EM on primary PCs at 14 DIV. Arrowheads indicate aberrant mitochondria. (B) Quantification of mitochondrial ultrastructural alterations. The organelles were classified as normal, vesicular and swollen on the basis of inner membrane remodeling. The graph indicates means ± SD of an average of 200 mitochondria from 5 cells in 3 independent experiments. Chi squared test (2 degrees of freedom): *Afg3l2* ko versus either *Afg3l2* heterozygous or wild-type PCs p< 0.001, wt versus *Afg3l2*$^{+/-}$ p< 0.05.

Loss of AFG3L2 in Purkinje cells results in reduced mitochondrial Ca^{2+} uptake and increased cytosolic Ca^{2+} concentration

In the SCA28 mouse, PC-DCD originates from mitochondrial dysfunction (Maltecca et al., 2009). Since PCs are exposed to massive Ca^{2+} influx (Ito, 2002) and mitochondria can transiently store large amount of Ca^{2+}(Duchen, 2012; Pizzo et al., 2012), we reasoned that a defective Ca^{2+} buffering operated by *Afg3l2*-mutant mitochondria in PCs could increase $[Ca^{2+}]_{cyto}$ and cause DCD, thus mimicking excitotoxicity.

To measure $[Ca^{2+}]_{mito}$ in PCs in primary cerebellar cultures, we created an adeno-associated viral vector expressing a mitochondria-targeted version of the GFP-based Ca2+ probe, 4mtD1cpv (Palmer et al., 2006), under the synapsin promoter. Transduction of this probe in primary cerebellar cultures gave neuron-specific signal. Among the various neuronal types, PCs were easily distinguished in bright field, being markedly bigger and more ramified compared to granule cells. Upon challenge with 30 mM KCl, which depolarizes the plasma membrane in neurons by opening potential-sensitive Ca^{2+} channels, mitochondrial Ca^{2+}-rises of transduced neurons were significantly smaller in *Afg3l2* ko PCs compared to *Afg3l2* heterozygous and wt cells (Fig. 5 A-B).

In parallel, we performed ratiometric measurement of $[Ca^{2+}]_{cyto}$ in PCs employing the high affinity Ca^{2+} indicator fura-2. The basal levels of $[Ca^{2+}]_{cyto}$ were identical in the three genotypes. On the contrary, we observed that in *Afg3l2* ko PCs, the peak of Ca^{2+}

response elicited by acute exposure to 30 mM KCl was significantly higher compared to *Afg3l2* heterozygous and wt PCs (Fig. 5C).This result demonstrates that the inefficient mitochondrial Ca^{2+} buffering in *Afg3l2*ko PCs causes an abnormal cytosolic Ca^{2+} elevation

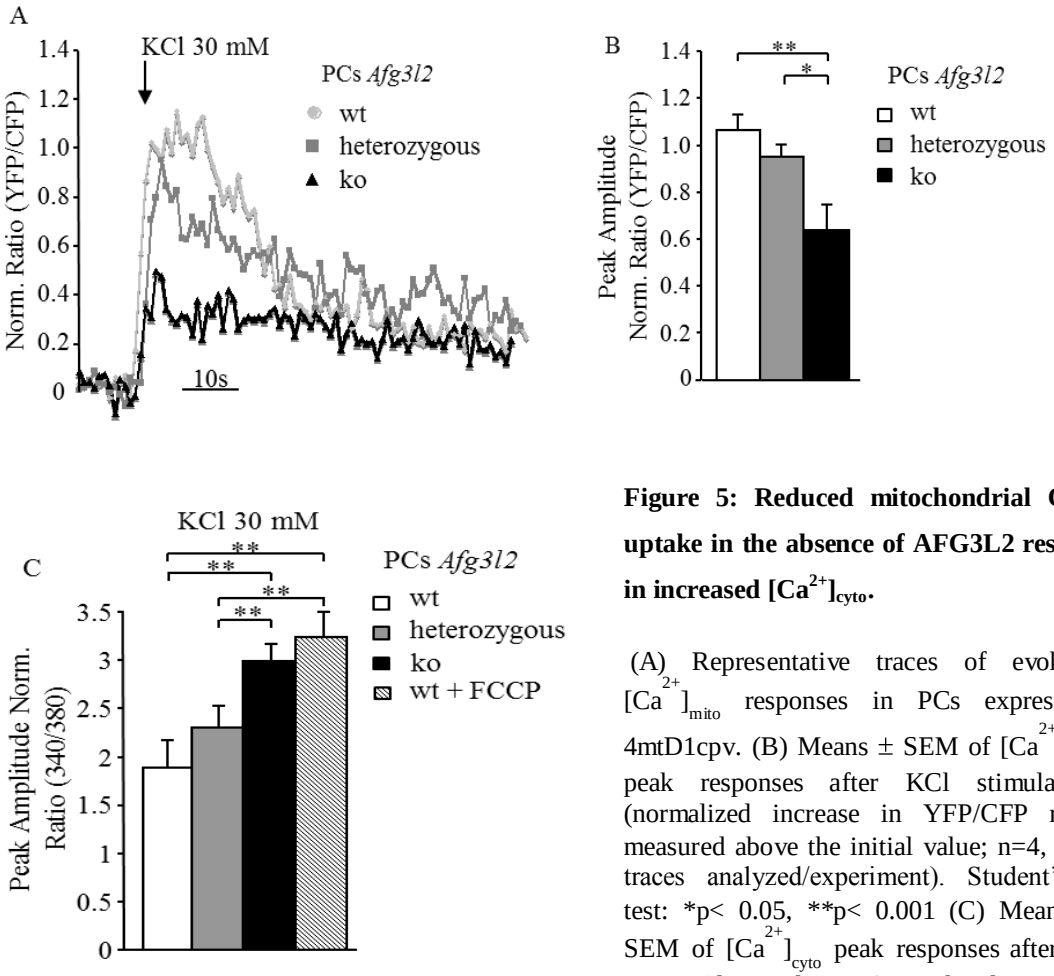

Figure 5: Reduced mitochondrial Ca^{2+} uptake in the absence of AFG3L2 results in increased $[Ca^{2+}]_{cyto}$.

(A) Representative traces of evoked-$[Ca^{2+}]_{mito}$ responses in PCs expressing 4mtD1cpv. (B) Means ± SEM of $[Ca^{2+}]_{mito}$ peak responses after KCl stimulation (normalized increase in YFP/CFP ratio measured above the initial value; n=4, ~20 traces analyzed/experiment). Student's *t* test: *p< 0.05, **p< 0.001 (C) Means ± SEM of $[Ca^{2+}]_{cyto}$ peak responses after 30 mM KCl stimulation (normalized increase measured above the initial value, n=5, ~15 traces analyzed/experiment). Student's *t* test: ** p< 0.001.

Part II: A protease chain reaction functionally links AFG3L2 to OMA1, OPA1 and finally to mitochondrial fragmentation.

The absence of AFG3L2 induces fragmentation through OMA1-mediated OPA1 processing

Demonstrated the importance of mitochondrial morphology in SCA28 pathogenesis, we wanted to understand which molecular pathway is involved in mitochondrial fragmentation in the absence of AFG3L2. To discriminate if mitochondrial network fragmentation was caused by an increase in fission or a decrease in fusion, we decided to analyze DRP1 localization and OPA1 processing. As described in the introduction, DRP1 is a cytosolic protein that can interact with its receptor Fis1 on mitochondria, inducing fragmentation. To verify if the absence of AFG3L2 could activate DRP1 re-localization we performed sub-cellular fractionation of *Afg3l2* wt and ko MEF; we didn't observe any difference among the genotypes (Fig. 6A). This allows us to conclude that the mitochondrial fragmentation observed in the absence of AFG3L2 does not involve DRP1 activation and therefore is not due to increased mitochondrial fission. We thus focused our investigations on the mitochondrial fusion process and, in particular, we analyzed OPA1 processing. OPA1 is a pro-fusion protein that exists in several isoform deriving from alternative splicing. These isoforms are processed in accordance to their proteolytic cleavage sites. By Western blot analysis, OPA1 is detected as 5 different bands: two long bands called L1 and L2 and three short bands called S1-S2-S3. In healthy conditions there is a balance between OPA1 long and short forms, whereas in stress conditions, an increase in short forms is observed parallel to mitochondrial fragmentation.

The analysis of OPA1 band pattern in wild-type, *Afg3l2* heterozygous and *Afg3l2* ko cells by Western blot revealed that the loss of AFG3L2 results in alteration of OPA1 processing: in the absence of AFG3L2 we detected an increased amount of cleaved OPA1 forms and the almost-complete disappearance of the long bands (Fig. 6B). No apparent differences were observed between *Afg3l2* wild- type and heterozygous cells, indicating that *Afg3l2* haploinsufficiency does not affect OPA1 processing and mitochondrial morphology in this cellular system. We observed the alteration of OPA1 processing even in tissues coming from the CNS of *Afg3l2* ko mouse (Fig. 6C). The increased OPA1 processing in absence of AFG3L2 was demonstrated to be correlated to the activation of OMA1, a protease of the IMM (Ehses et al., 2009). However, the relationship between the absence of AFG3L2 and the overactivation of OMA1 has not been identified yet.

We decided to study OMA1 regulatory pathway to clarify if AFG3L2 has a role in OMA1 activation. It has been published that OMA1full length is 60 kD while the identified active form of the protein has a molecular weight of 40 kD, but nothing is known about the protease involved in this cleavage. Moreover, it has been demonstrated that OMA1 is activated during stress condition as ATP depletion or increased ROS production. So, we wanted to clarify if AFG3L2 could be directly involved in OMA1 processing mediating OMA1 cleavage from 60 to 40 kD or indirectly, since the absence of AFG3L2 induces the environmental stress (ATP depletion or increased ROS production) that acts OMA1.

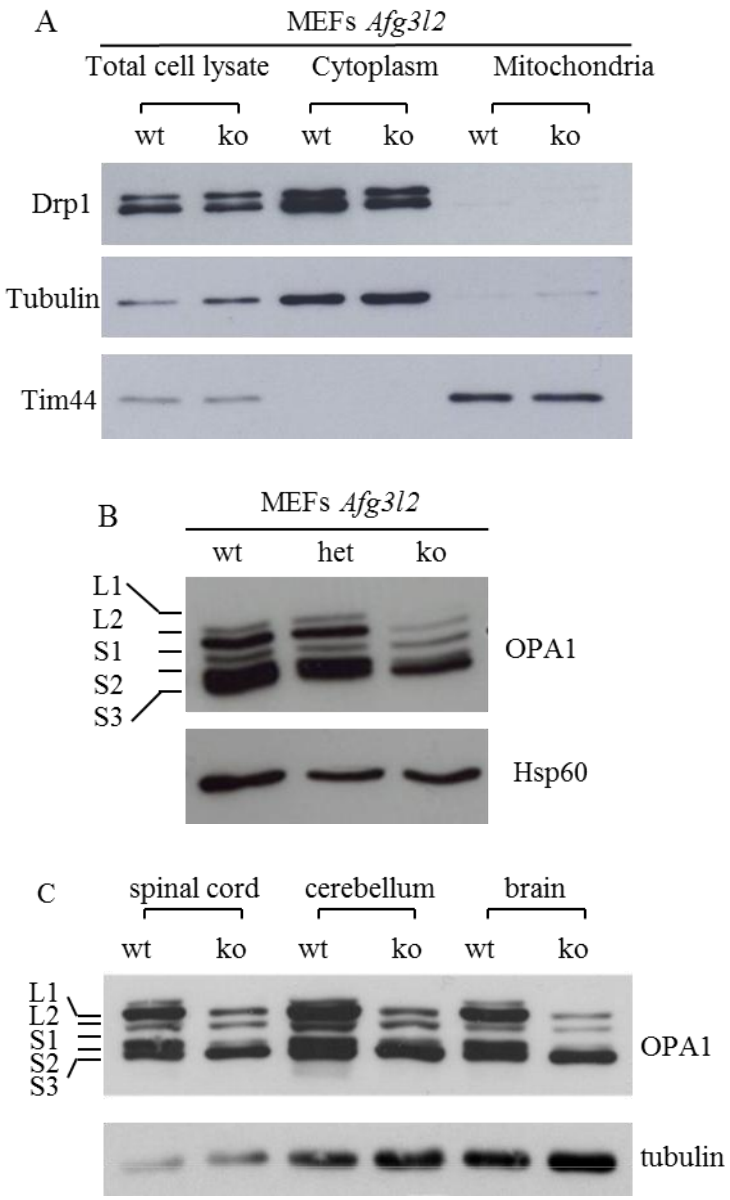

Figure 6: Mitochondrial fragmentation in the absence of AFG3L2 is caused by OPA1 overprocessing:

A) Immunoblot analysis of total cell extracts, cytosolic fraction and mitochondrial fraction from *Afg3l2* wt and ko MEFs detected with antidodies agains Drp1, TIM44 and Tubulin. TIM44 antibody was used as mitochondrial marcker, while tubulin as cytosolic marker

(B-C) Immunoblot analysis of total cell extracts from *Afg3l2* MEFs or neuronal tissues of the indicated genotypes . The five OPA1 bands are indicated as long (L1 and L2) and short isoforms (S1, S2 and S3) (30). Hsp60 and tubulin were used to verify equal loading, respectively.

OMA1 processing occurs inside the inner mitochondrial membrane

To perform our studies deals with OMA1 regulation, we transfected an OMA1-HA form in HeLa or MEFs. We needed to use the overexpression condition since the commercial antibodies against OMA1didn't work in biochemistry. OMA1-HA in Western blot appeared in three major bands; a first band at 60 kD representing the full length protein, a band at 40 kD proposed to be the active one and a doublet around 25 kD generated by autocatalytic process. These three bands were previously described in literature (Baker et al., 2014; Head et al., 2009); but we were the first group able to detect the three major OMA1 bands contemporary. This is an important point since we wanted to clarify the regulatory pathway of OMA1.

To clarify the mechanism involved in OMA1 40 kD generation we started individuating the cellular localization of this process. To understand whether OMA1 40 kD generation occurs in the cytosol or in the mitochondrion we transfected HeLa cells with an HA tag form of OMA1 and treated them with a mitochondrial import inhibitor (Valinomycin) alone or in combination with the proteasome inhibitors MG132. Western blot analysis on mitochondrial and cytosolic enrichments demonstrated that OMA1 40 kD form is present only in the mitochondrial fraction; this band disappears when mitochondrial import is inhibited (Fig. 7A). To determine in which sub-mitochondrial compartment OMA1 40 kD is generated, we combined digitonin extractions with protease digestions. Digitonin disorganizes the outer membrane, making intermembrane space proteins accessible to cleavage by exogenously added proteases such as trypsin. As a control, protease sensitivity of the

integral protein TIM23 of the inner mitochondrial membrane was assessed. OMA1 40 kD was digested in the presence of digitonin, at the same manner of TIM23 indicating that OMA1 40 kD form, is exposed to the intermembrane space. On the other hand the soluble matrix protein HSP60 was less affected by trypsin in this condition (Fig. 7B). We concluded that the processing of OMA1 from 60 to 40 kD is mediated by an inner membrane protease.

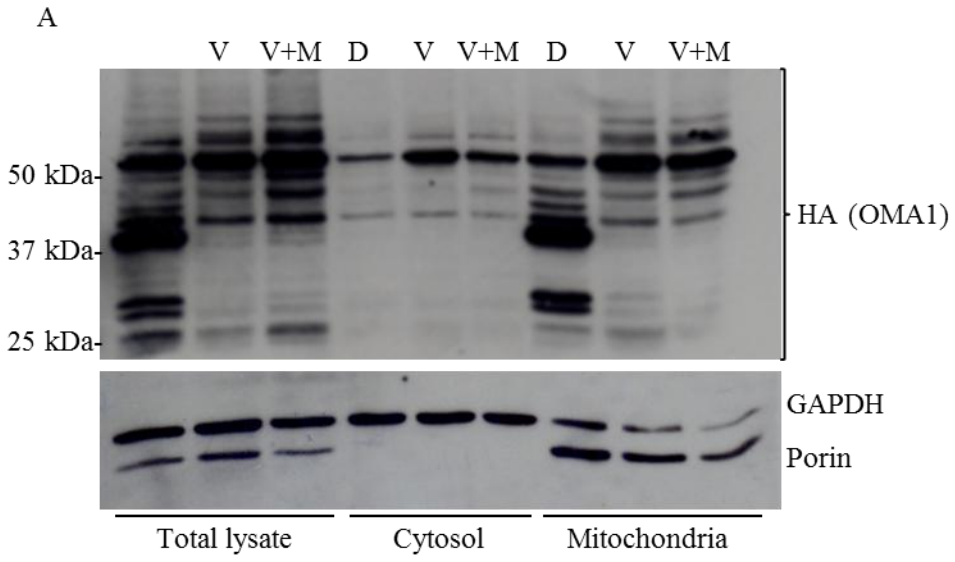

O/N Treatment:
D: DMSO
V= Valinomycin 1 uM
V+M= Valinomycin 1 uM+ MG132 2,5 uM

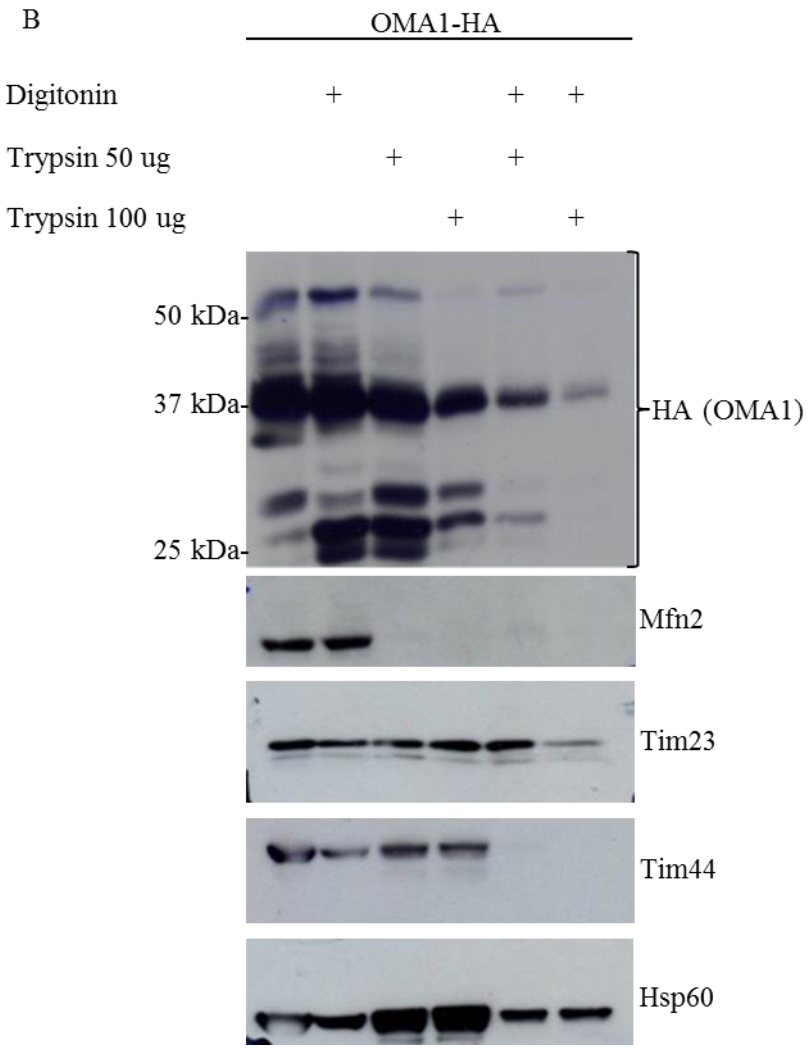

Figure 7: OMA1 60/40 kD process occurs in the inner mitochondrial membrane .

(A)Immunoblot analysis of total cell extracts, cytosolic fraction and mitochondrial fraction from HeLa cells transfected with OMA1-HA. Cells were treated over-night with Valinomycin 1 µM (V) or Valinomycin 1 uM+ MG132 2,5 µM (V+M). The membrane was immunodecorated with antibodies against HA, GAPDH and Porin. Porin antibody was used as mitochondrial marcker, while tubulin as cytosolic marker. (B) Immunoblot analysis of mitochondrial fraction from HeLa cells transfected with OMA1-HA. Or empty vector (E.V.) isolated mitochondria were treated with the indicate concentration of digitonin or/and trypsin. The membrane was immunodecorated with antibodies against HA, (MFN2), TIM 23, TIM44 and HSP60. MFN2 was used as OM protein marker, TIM23 as IMM integrated protein marker, TIM44 as MM associated protein markerand Hsp60 as matrix protein marker.

A metallopeptidase is responsible for the 60/40 kD processing of OMA1

To discover the peptidase(s) involved in OMA1 40 kD generation we transfected HeLa cells with OMA1-HA, incubated them with several peptidase inhibitors and monitored the accumulation of the 60 kD band. We used PMSF to inhibit serine proteases, E64 for cysteine proteases and O-phenantroline (O-phe) to block metallopeptidases. By this approach, we observed that O-phe was able to induce the accumulation of the 60 kD form, indicating metallopeptidase as the class of proteins involved in this mechanism (Fig. 8). Using bioinformatics approach we selected 380 putative mitochondrial proteases coming from four different protein databases: UniProt (UniProtConsortium), MitoCarta (Pagliarini et al., 2008) , MitoMiner (Smith and Robinson, 2009) and Gene Onltology (Ashburner et al., 2000). We selected all the metallopeptidase, or other proteins working using metallo-ions and then we screened them using MEROPS database (Rawlings et al.). This last database helped us to individuate all the proteases inhibited by O-phe and we identified 72 proteases. Nevertheless, a high percentage of these 72 proteins didn't show any experimental data supporting their mitochondrial localization but only an in-silico prediction. To avoid false positive results, we decided to take in consideration only those proteins for which mitochondrial localization was reported in at least two databases; with this criterion we determined 27 proteins. Among them we excluded all the proteins inhibited by metallo-ions, acting in a consensus sequence not present in OMA1 or showing deacetylase/hydrolase features still present in the list. Finally we selected 4

proteins localized in the IMM since this is OMA1 localization and proteolytic site (scheme A) (Tab. 1). These four proteins are: OMA1, paraplegin, AFG3L2 and YME1L1.

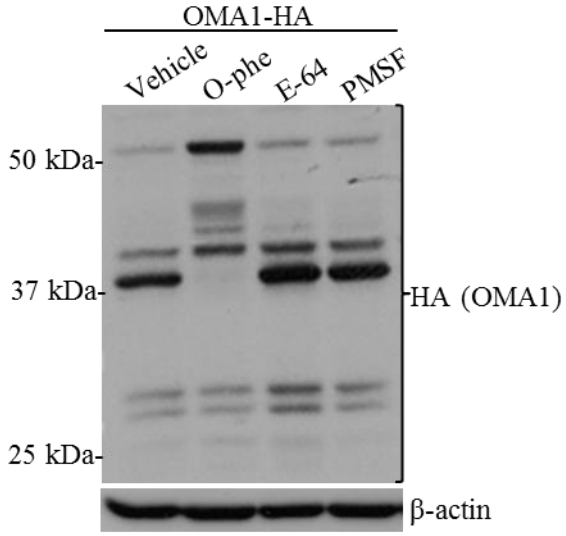

Figure 8: A metallopeptidase cleaves OMA1 from 60 to 40 kD.

Immunoblot analysis of total extracts from HeLa cells treated for 5 hours with DMSO, O-phe, E-64, PMSF detected with the indicated antibodies.

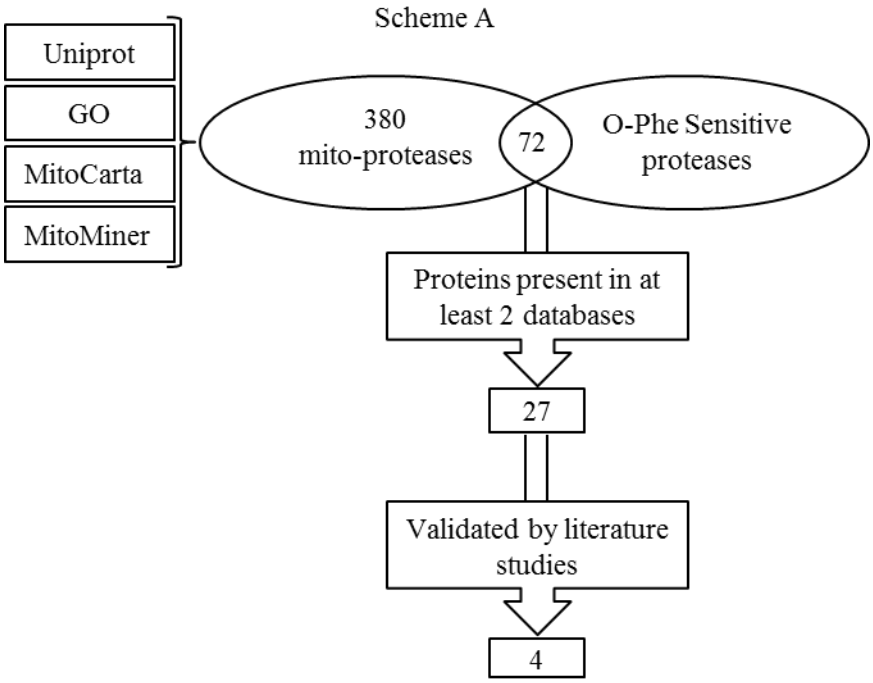

Tab. 1

1	Metallopeptidase OMA1, mitochondrial
2	Paraplegin
3	AFG3-like protein 2
4	ATP-dependent zinc metalloprotease YME1L1

OMA1 60 kD form accumulates in the absence of AFG3L2

Among the four selected proteins OMA1 itself is present in the list. OMA1 is a metallopeptidase belonging to the M48 subclass (Kaser et al., 2003). In agreement to what reported by Head and colleagues (Head et al., 2009), we observed that the overexpression of the proteolytic inactive mutant of OMA1 (OMA1 E324Q-HA) doesn't induce an accumulation of the 60 kD band, thus excluding a direct role of OMA1 in the generation of the 40 kD. On the other hand the bands around 25 kD totally disappeared (Fig. 9A) confirming the auto-processing described by Baker at al. (Baker et al., 2014). Interestingly, the overexpression of OMA1-E324Q-HA was able to affect the autocatalytic process but not OMA1-mediated OPA1 processing (Fig. 9B). We conclude that the endogenous OMA1 is able to perform its activity on OPA1. This indicates that OMA1-mediated OPA1 processing is extremely well regulated.

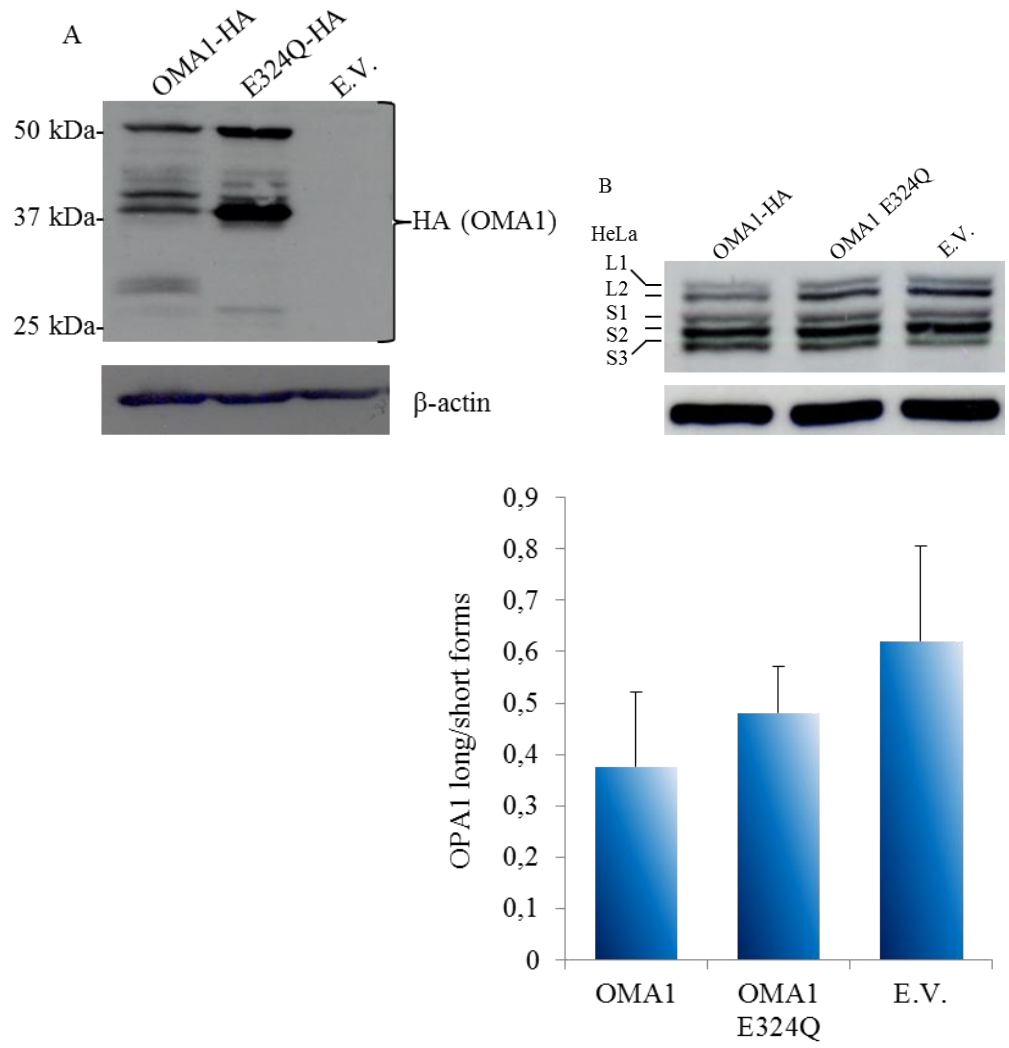

Figure 9: OMA1 performs an autocatalytic cleavage on the C-Term.

(A-B) Immunoblot analysis of total extracts from HeLa transfected with OMA1-HA, OMA1-E324Q-HA or Empty Vector (E.V) detected with the indicated antibodies.
(C): Quantification of ratio between OPA1 long and short forms after over-expression of OMA1-HA, OMA1-E324Q-HA or E. V.

We then analyzed the possible role of paraplegin in the generation of OMA1 40 kD form. Transfecting OMA1-HA in *SPG7*$^{-/-}$ human immortalized fibroblasts we didn't find any alteration in OMA1 processing compared to wt (Fig. 10). This result excludes paraplegin as the protease involved in OMA1 40 kD generation and it is in line with unaltered OPA1 processing in the absence of paraplegin (Ehses et al., 2009).

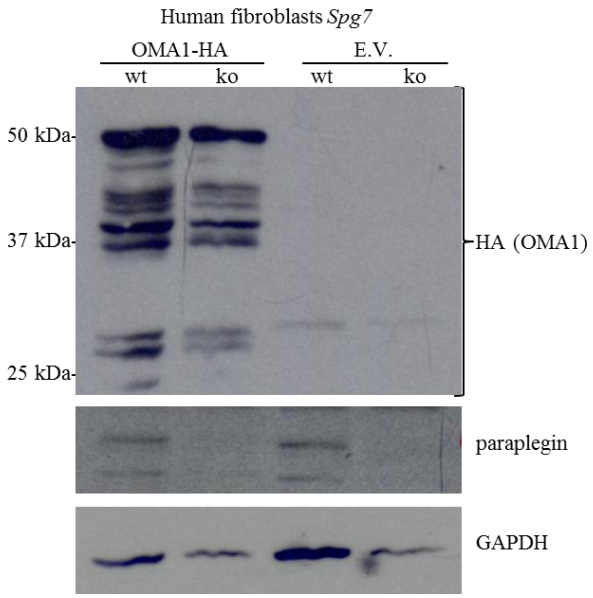

Figure 10: Paraplegin is not involved in OMA1 60/40 kD processing.

Immunoblot analysis of total extracts from immortalized human fibroblast SPG7 wt and ko transfected with OMA1-HA and detected with the indicated antibodies.

We then evaluated OMA1 processing in *Afg3l2* ko MEFs; we found that the absence of AFG3L2 induces a marked accumulation of the 60 kD band and a reduction of the 40 kD (Fig. 11A). To have a further evidence of the role of AFG3L2 in OMA1 processing, we tested the accumulation of the 60 kD band also in HeLa cells silenced for *AFG3L2* (Fig. 11B). HeLa cells, which differently from murine cells do not express the AFG3L2 homologus AFG3L1, behave similarly to *Afg3l2* ko MEFs when *AFG3L2* is knocked down showing the accumulation of the 60 kD band (Fig. 11).

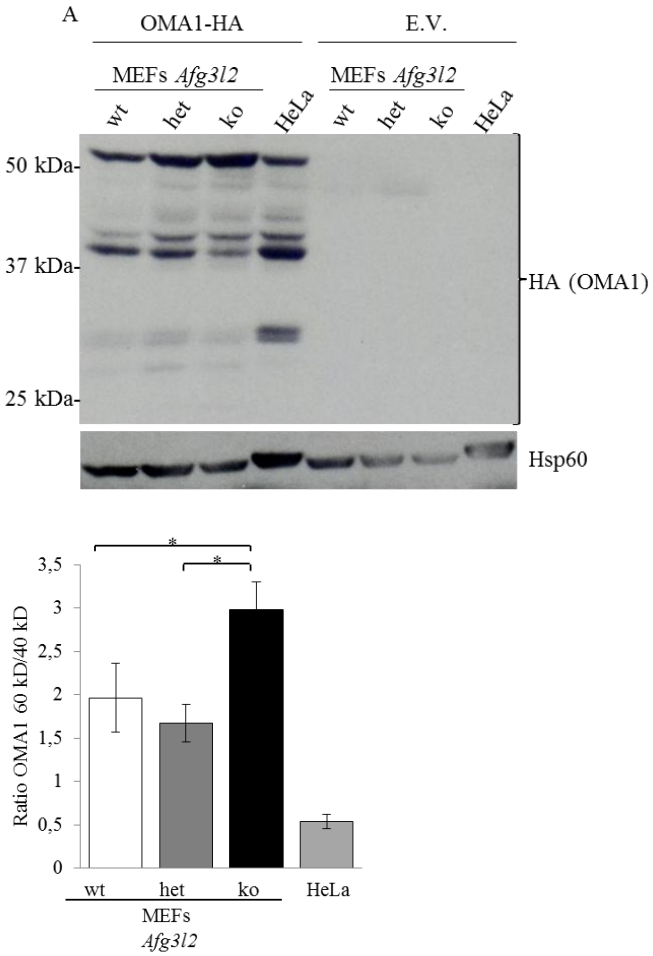

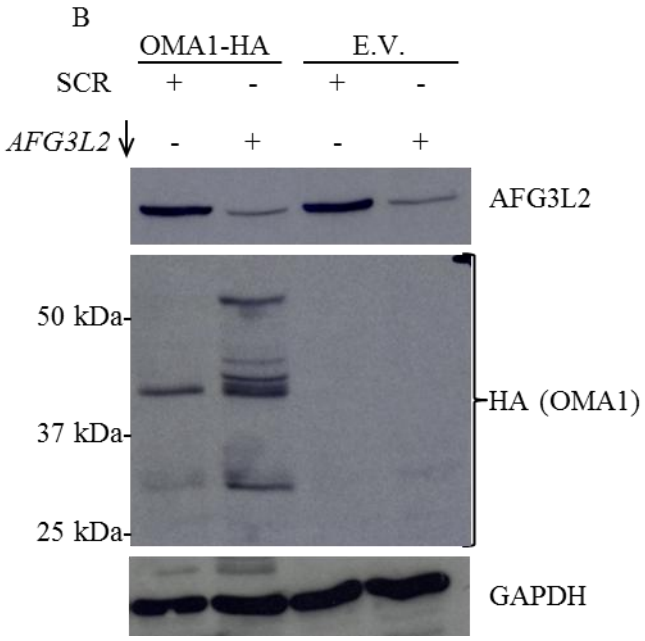

Figure 11: AFG3L2 performs 60/40 kD OMA1 cleavage.

(A) Immunoblot analysis of total extracts, from Afg3l2 MEFs and HeLa cells transfected with OMA1-HA or E.V. and detected with the indicated antibodies. Quantification of ratio between OMA1 60/40 kD band
(B) Immunoblot analysis of total extracts, from HeLa cells knocking down for *AFG3L2* and transfected with OMA1-HA or E.V. Membrane was immunodecorated with the indicated antibodies.

AFG3L2 physically interacts with of OMA1

The inefficient conversion from 60 kD to 40 kD in the absence of AFG3L2 can be explained by a direct or an indirect cleavage. In fact, or AFG3L2 is the directly the protease that mediates OMA1 cleavage or AFG3L2 regulates another protease that cleaves OMA1.

To individuate the right hypothesis we co-transfected *Afg3l2* ko MEFs with OMA1-HA and AFG3L2-myc or its proteolytic inactive mutant AFG3L2-E575Q-Myc and we evaluated both OPA1 and OMA1 processing. The absence of AFG3L2 induces the processing of OPA1 towards the short forms as previously shown (Ehses et al., 2009; Maltecca et al., 2012) and the accumulation of OMA1 60 kD band. The overexpression of AFG3L2 induces a slight increase in the amount of OPA1 L1 band indicating that the overexpression of AFG3L2 is able to restore the physiological processing of OPA1 and, at the same, to induce an increase in the amount of the 40 kD OMA1 band. The overexpression of the proteolytic inactive form of AFG3L2 is not able to restore OMA1 processing, showing that AFG3L2 is involved in OMA1 initial processing (Fig. 12A). To verify if AFG3L2 directly cleaves OMA1 or it activates other proteases, we explored a possible physical interaction between the two proteins by co-immunoprecipation (CoIp) studies. To stabilize the interaction we decided to use AFG3L2-E575Q-Myc, which is still capable of substrate binding but lacks proteolytic activity (Atorino et al., 2003) and, therefore, can be used as a trap to identify short-lived substrate proteins . With this approach we immunoprecipitated

AFG3L2 and identified OMA1 in the CoIp lane and the same result was obtained with the reverse approach (Fig. 12B). This result suggests that AFG3L2 directly performs its action on OMA1 and not through the involvement of other proteases.

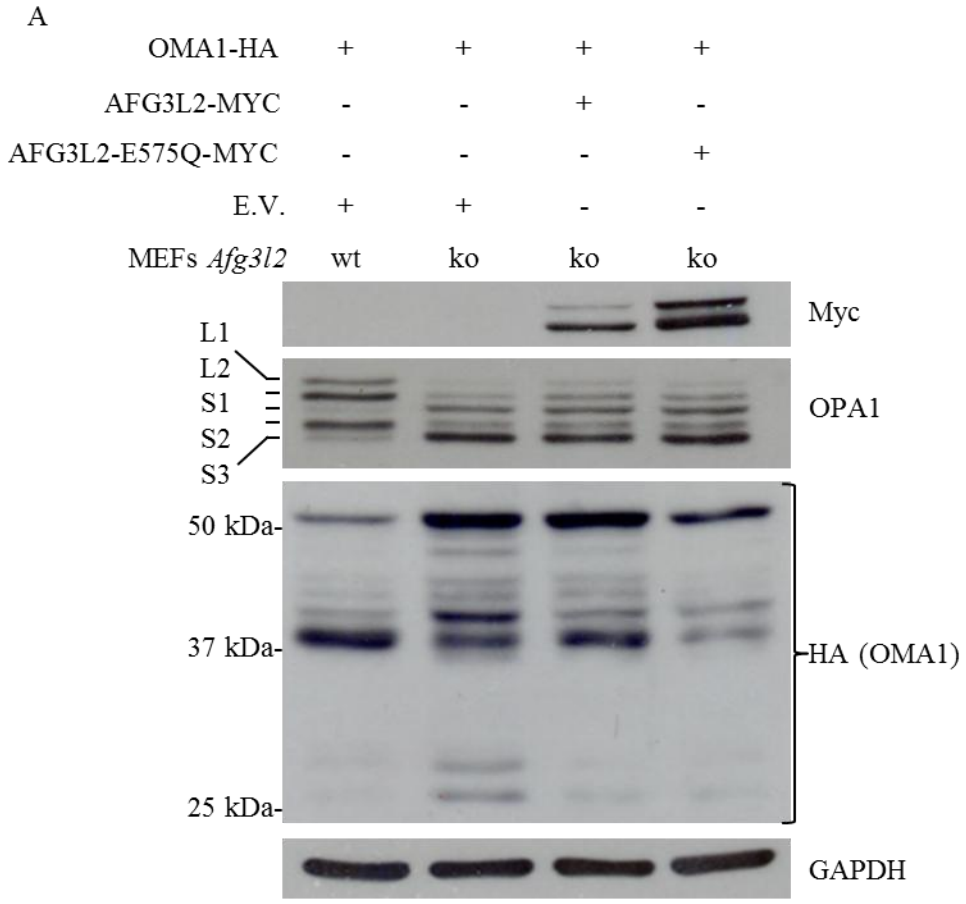

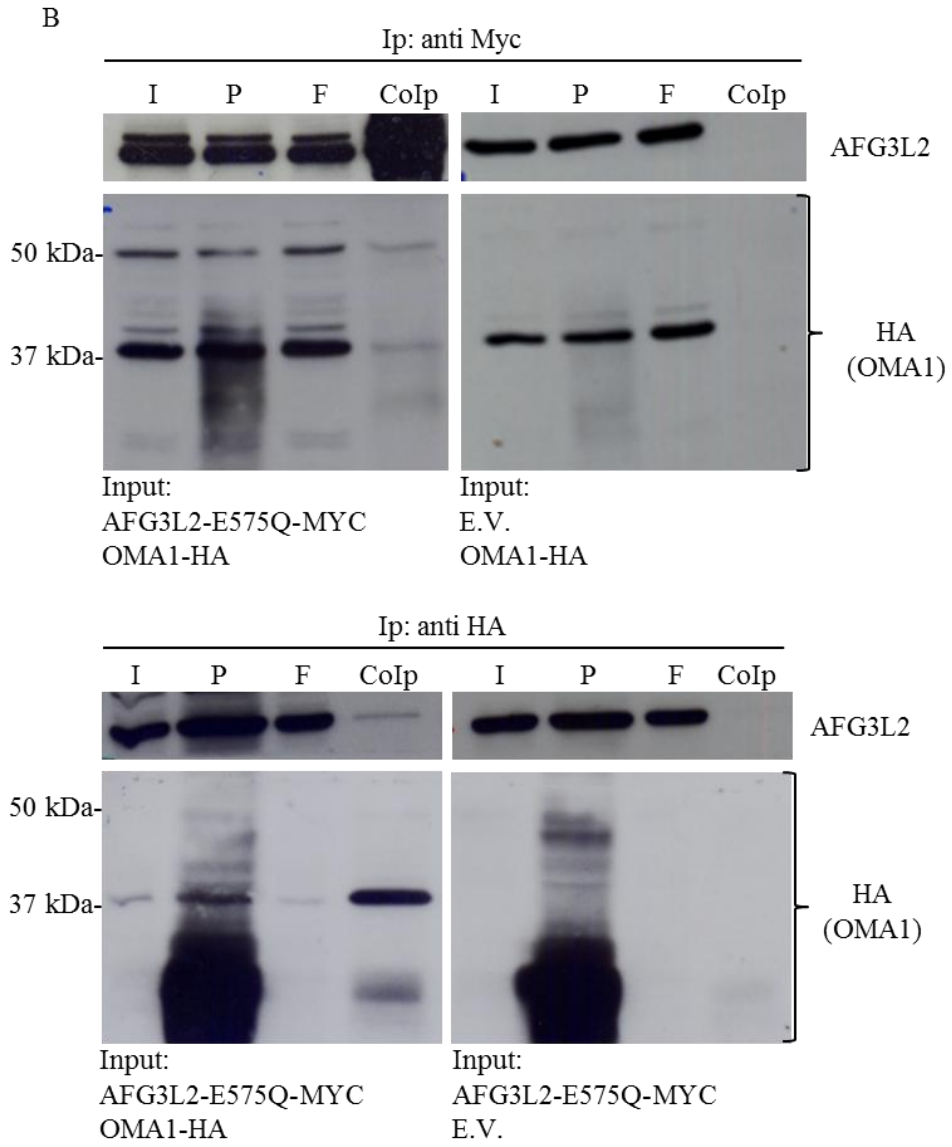

Figure 12: AFG3L2 directly interacts with OMA1

(A): Immunoblot analysis of total extracts, from *Afg3l2* MEFs co-transfected with OMA1-HA, E.V. and AFG3L2-MYC or AFG3L2-E575Q-MYC detected with the indicated antibodies.(B): Co-immunoprecipitation of AFG3L2 with OMA1in HeLa cells after over-expression of OMA1-HA, AFG3L2-E575Q-MYC or E.V. detected with the indicated antibodies. I= input; P= pre-clearing; F=flow-through

OMA1 processing from 60 kD to 40 kD occurs by a trimming mechanism

Clarified the interaction between OMA1 and AFG3L2 we wanted to identify the hypothetical proteolytic consensus sequence recognized by the *m*-AAA to better characterize its general processing activity. To achieve this result we followed four parallel approaches.

1. We performed a BLAST analysis between OMA1 murine amino acids sequence and MrpL32 sequence. MrpL32 (the only known substrate of the *m*-AAA in mammals) is processed by the *m*-AAA protease in position 78 (Alanine) (Nolden et al., 2005). OMA1 alanine in position 171 aligned with MrpL32 alanine in position 78. We hypothesised that this could represent a consensus sequence for the *m*-AAA proteases. To verify it, we decided to remove only the amino acid 171 and or the proximal ones. We generated deleted mutants: OMA1-Δ169-HA // OMA1-Δ170-HA// OMA1-Δ171-HA// OMA1-Δ169-172-HA (Fig. 13A);
2. Using I-TASSER platform (Roy et al., 2012) we generated a 3-D protein prediction structure of OMA1 to individuate a predicted hydrophilic region theoretically more accessible for AFG3L2. With this strategy we detected a hydrophilic loop of eight amino acids from 173 to 180. We removed them generating the following mutants: OMA1-Δ173-176-HA// OMA1-Δ175-178-HA// OMA1-Δ177-180-HA (Fig. 13B);

3. Using second structure prediction toll (PredictProtein Platform) (Yachdav et al., 2014) we individuated the first alpha helix domain (amino acid 144-157) to verify whether the *m*-AAA complexes activity could be influenced by this first hydrophobic region. We removed these amino acids generating: OMA1-Δ147-149-HA// OMA1-Δ150-152-HA// OMA1-Δ153-155-HA// (Fig. 13C);
4. We immunoprecipitated OMA1-HA to detect by MS/MS analysis the first amino acid of the N- terminus of OMA1 40 kD.

A

Range 1: 76 to 93 Graphics

Score	Expect	Method	Identities	Positives	Gaps
15.8 bits(29)	1.3	Compositional matrix adjust.	5/18(28%)	10/18(55%)	0/18(0%)

```
Query  169  WQALPPNKKELFKDSVRK  186
            W A P N++ +  +  R+
Sbjct  76   WMAAPKNRRTIEVNRCRR  93
```

B

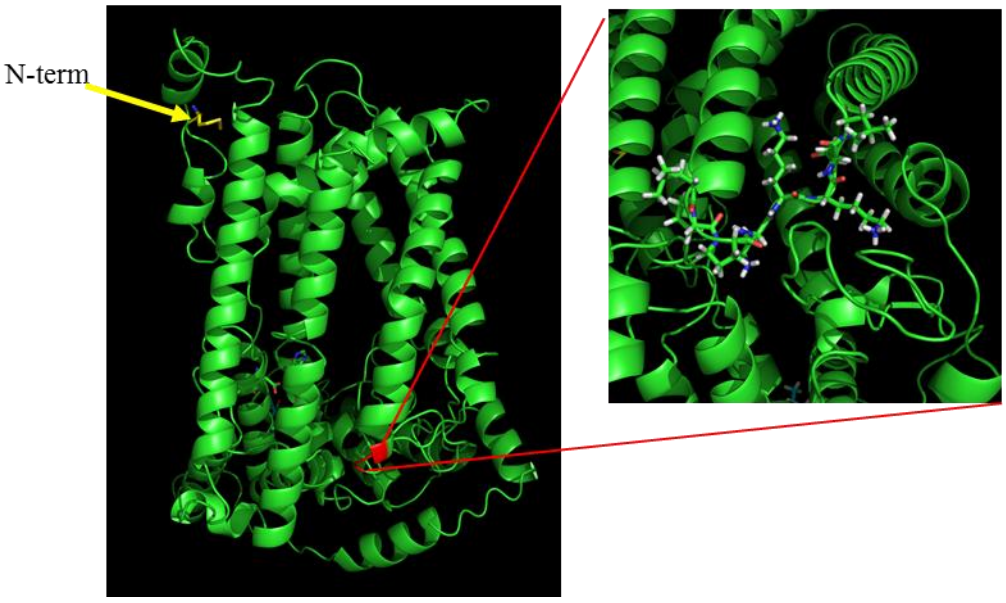

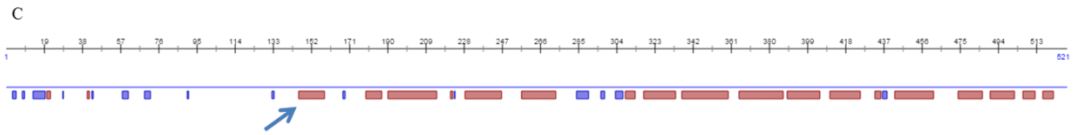

Figure 13: identification of putative OMA1 40kD cleavage sites.

(A) Blast alignment between OMA1 and MrpL32 amino acid sequences. (B) OMA1 third structure prediction. In the insert is represented the hydrophilic region identified as possible cleavage site. (C) OMA1 second structure prediction; arrow indicate the first α-helix hypothetical involved in OMA1 40 generation. red squares indicate α-helix, while purple squares indicate β-sheet.

Sites detected with the first three approaches was mutagenized by deletion of 1, 3 or 4 amino acids to remove the possible *m*-AAA consensus sequence and induce the accumulation of the 60 kD form. We generated 10 deleted mutants but they were correctly processed to generate the 40 kD form (Fig. 14 A-B). We concluded that the *m*-AAA proteases do not recognize a proteolytic consensus sequence.

MS/MS analysis of immunoprecipitated OMA1 40 kD revealed that the N-term amino acid is the alanine in position 140, confirming recently published results by Baker and colleagues (Baker et al., 2014). From this information we decided to remove 53 amino acids between the predicted mitochondrial leader sequence and the first amino acids of OMA1 40 kD sequence. We generated OMA1 Δ92-144-HA; this mutant encodes for a protein of 50 kD and it is processed as the wild type to generate the 40kD form (Fig.14C). We concluded that the m-AAA proteases do not recognize a proteolytic consensus sequence.

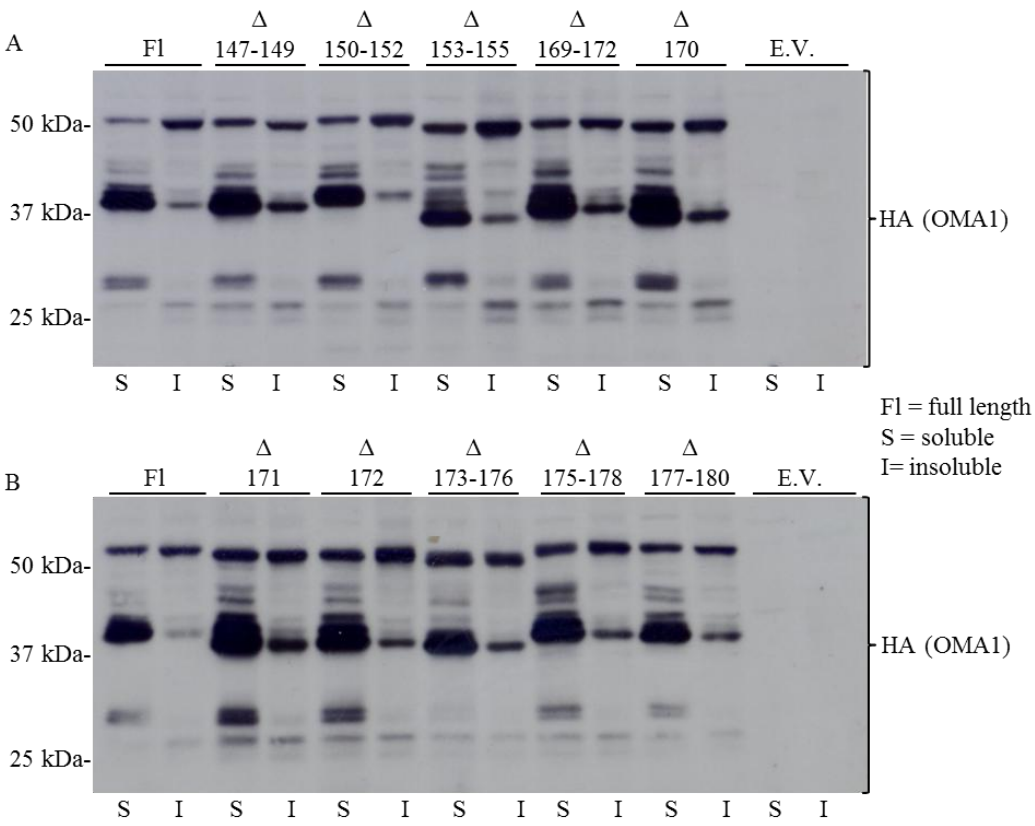

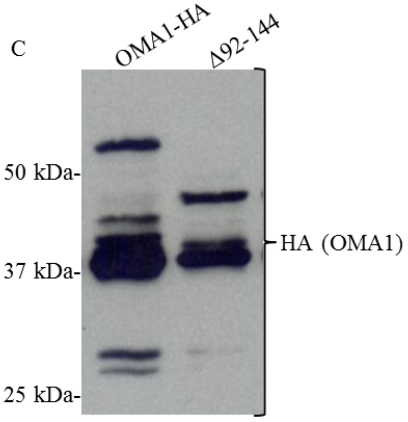

Figure 14: the *m*-AAA proteases do not recognize a proteolytic consensus sequence.

(A-B) Immunoblot analysis of total extracts from HeLa cells transfected with OMA1-HA, with several deleted mutants and. E.V. Soluble (S) and insoluble (I) fractions were loaded and then proteins were detected with the indicated antibodies. FL= full length.
(C) Immunoblot analysis of total extracts from HeLa cells transfected with OMA1-HA, OMA1 Δ92-144-HA and detected with the indicated antibodies.

Interestingly, we always detected the presence of several intermediate specific bands between the major OMA1 60 kD and the 40 kD. These bands are OMA1 degradation products suggestive of a progressive trimming mechanism. This kind of degradative process was previously demonstrated for another *m*-AAA substrate, MrpL32 (Bonn et al., 2011). In fact, it was published that MrpL32 processing occurs immediately after its mitochondrial import; the m-AAA interacts with the N-term part of the protein and performs the processing which is stopped by the folding of a cysteine-containing domain of MrpL32 (Bonn et al., 2011). To verify if these intermediate bands are degradative products generated by a clipping mechanism mediated by the *m*-AAA complexes, we silenced *AFG3L2* in HeLa cells and then we overexpressed a Stealth-RNAi-insensitive AFG3L2-MYC construct or two proteolytic inactive AFG3L2 mutants. These two mutants are respectively: AFG3L2-E575Q-MYC and AFG3L2-E408Q-MYC. The first mutant is proteolytically inactive since the amino acid substitution E/Q prevents the Zn^{+}-ion coordination that is fundamental for AFG3L2 activity. The second mutant carries a mutation inside the Walker B domain, which is important since it hydrolyzes ATP to ADP to ensure the energy necessary for the *m*-AAA complex activity. The ectopic expression of AFG3L2 induced the disappearing of the intermediate bands, which remained stable upon overexpression of the proteolytic inactive mutants (Fig. 15).

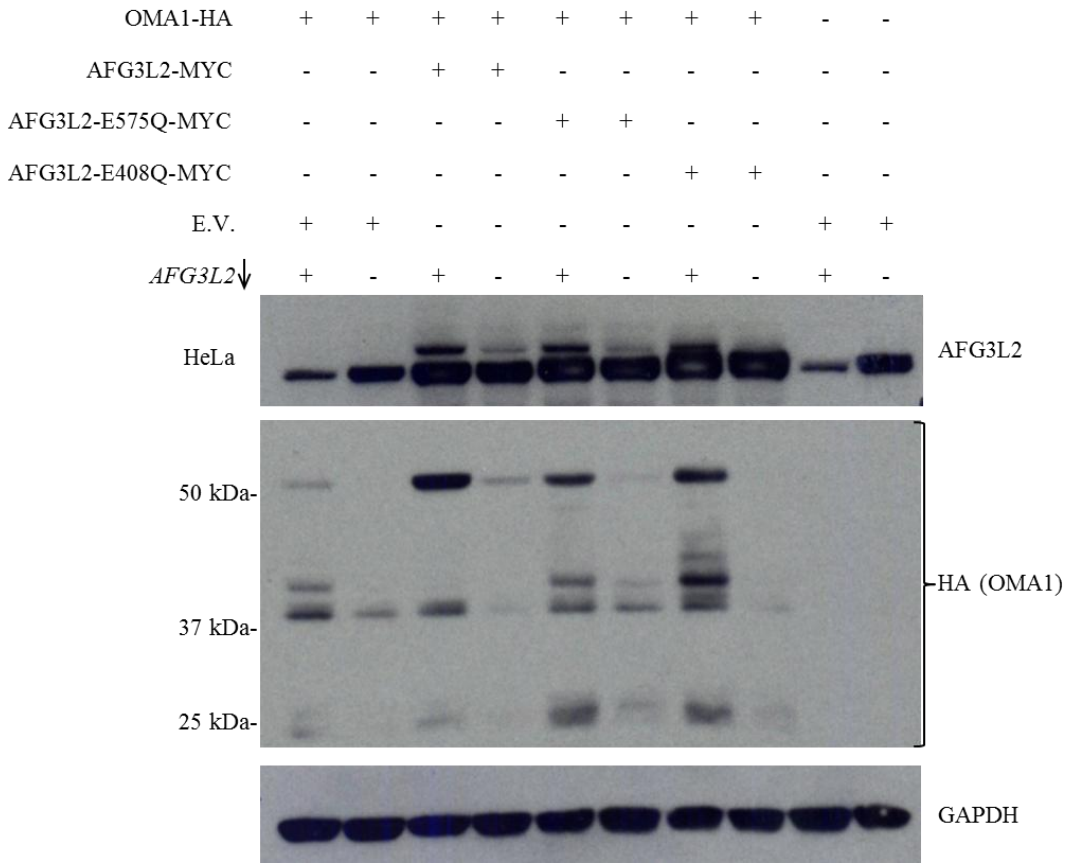

Figure 15: The *m*-AAA complexes process OMA1 by a trimming mechanism.

Immunoblot analysis of total extracts, from HeLa cells silenced for AFG3L2 and co-transfected with OMA1-HA or E.V plus, AFG3L2-MYC, AFG3L2-E575Q-MYC, AFG3L2-E408Q-HA RNAi stealth insensitive and detected with the indicated antibodies

60 kD OMA1 is dispensable for OMA1 processing

Verified the mechanism that generates the OMA1 40 kD, we focused on understanding whether the 60 kD form could have an active role in OPA1 processing. Indeed, it was classified as a pre-pro-protein but without any experiment that excludes any role in OPA1 processing (Baker et al., 2014). Since the impossibility in the generation of an OMA1 uncleavable form, we decided to verify if the absence of the 60 kD could affect OPA1 processing. For this reason we transfected HeLa cells silenced for *OMA1* with OMA1 Δ92-144-HA construct. OMA1 silencing was evaluated following OPA1 processing; in fact, in the absence of OMA1, it was demonstrated that S1 and S3 OPA1 processed bands disappear (Quiros et al., 2012) and we obtained the same result using Stealth RNAi against OMA1 (Fig.16B). In this KD condition, OMA1 Δ92-144-HA shows normal auto-proteolytic activity generating the 25 kD forms as the wild type protein (Fig. 16A). Moreover, it is able to restore OPA1 processing (Fig. 16B) and it is able to be efficiently activated when the mitochondrial membrane potential is altered (Fig. 16D). This deleted mutant, seems to be less prone towards the autocatalytic process (Fig. 16C), as another mutant described in previous paper (Baker et al., 2014), but nevertheless it is proteolytically active towards OPA1.

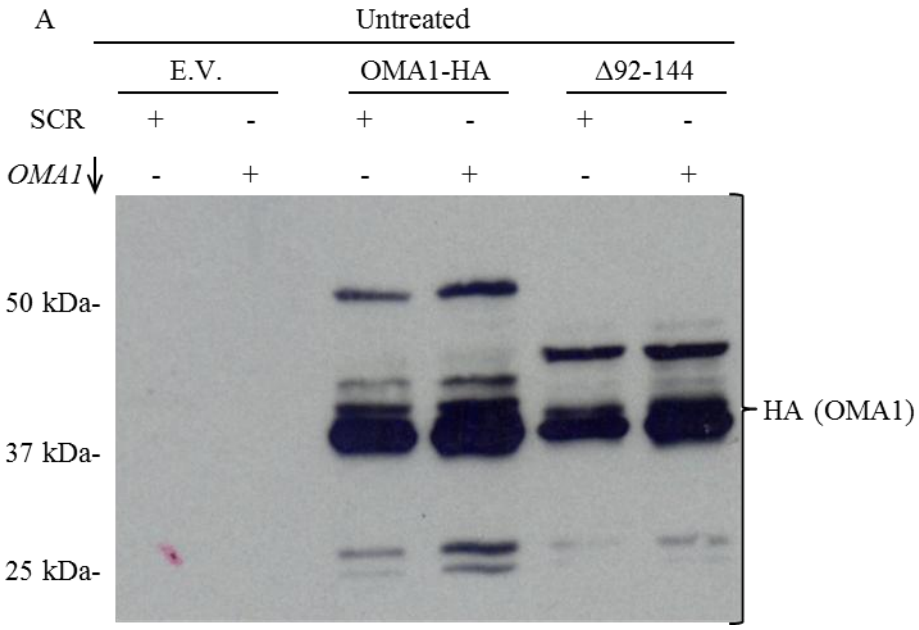
A
Untreated
E.V.
OMA1-HA
Δ92-144
SCR
+ - + - + -
OMA1
- + - + - +
50 kDa-
37 kDa-
25 kDa-
HA (OMA1)

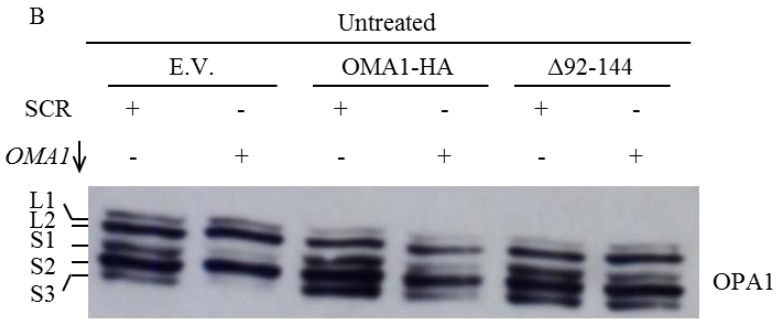
B
Untreated
E.V.
OMA1-HA
Δ92-144
SCR
+ - + - + -
OMA1
- + - + - +
L1
L2
S1
S2
S3
OPA1

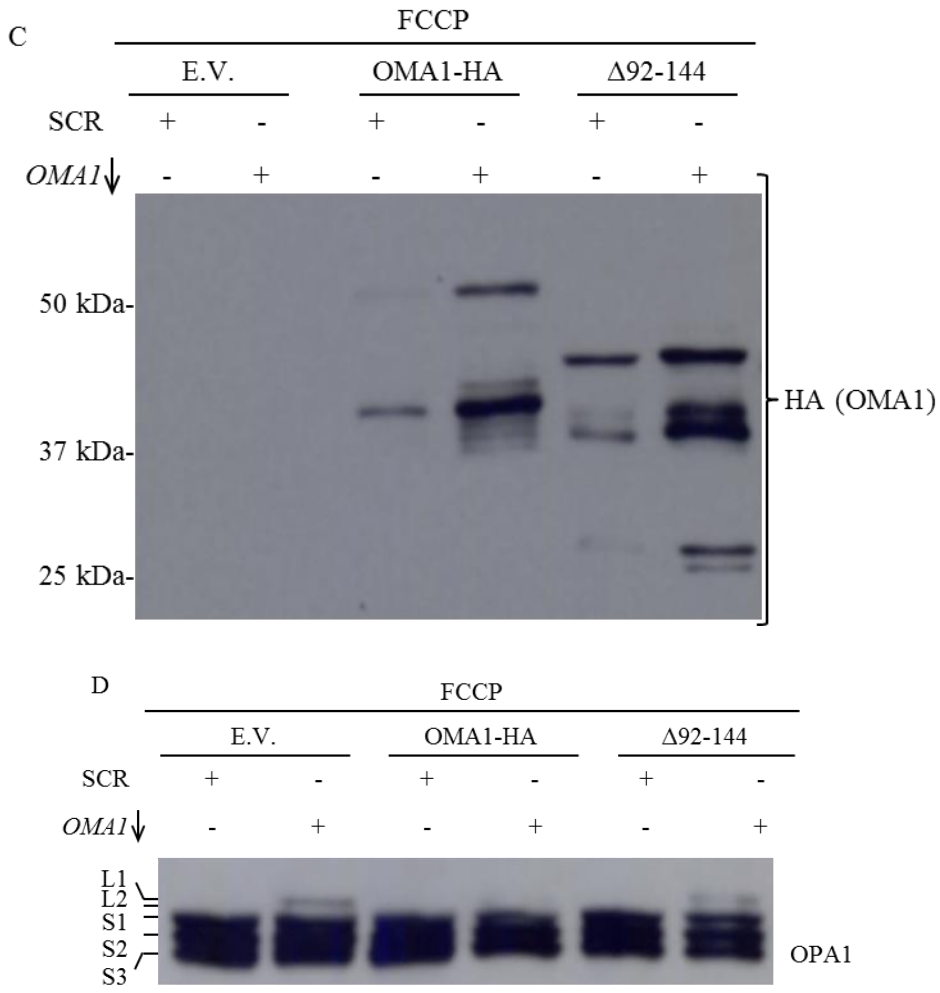

Figure 16: OMA1 60 kD is dispensable for OPA1 processing during physiologic condition.

(A-B)Immunoblot analysis of total extracts from HeLa cells silenced for OMA1 and then transfected with OMA1-HA, OMA1 Δ92-144-HA RNAi stealth insensitive or E.V and detected with the indicated antibodies. (C-D) Immunoblot analysis of total extracts from HeLa cells silenced for OMA1 and then transfected with OMA1-HA, OMA1 Δ92-144-HA RNAi stealth insensitive or E.V. HeLa cells were subsequently treated with FCCP 10 µM for 30 minutes and detected with the indicated antibodies..

OMA1 processing is dependent on mitochondrial membrane potential

The importance of $\Delta\Psi$ in the regulation of mitochondrial dynamics has been previously demonstrated (Song et al., 2007). In fact it was verified that the alteration of $\Delta\varphi$ can induce mitochondrial fragmentation through OMA1-mediated OPA1 processing (Ehses et al., 2009; Head et al., 2009). For this reason we investigated OMA1 processing upon the addition of an uncoupler drug (FCCP) at different time points. After 5' minutes of FCCP treatment, the amount of the 40kD band is decreased by 95%, with the complete disappearing at 15'; the 60 kD form remains stable during all the time course. As expected, OMA1 proteolytic inactive mutant didn't show any decrease in 40 kD amount since this mutant is not able to induce the auto-catalytic cleavage (Fig. 17A). On the other hand, the presence of the endogenous OMA1 allowed OPA1 processing after FCCP treatment (Fig 17A). OPA1 processing happens within the first 5 minutes of treatment, window of time in which the 95% of OMA1 is already activated (Fig. 17B).

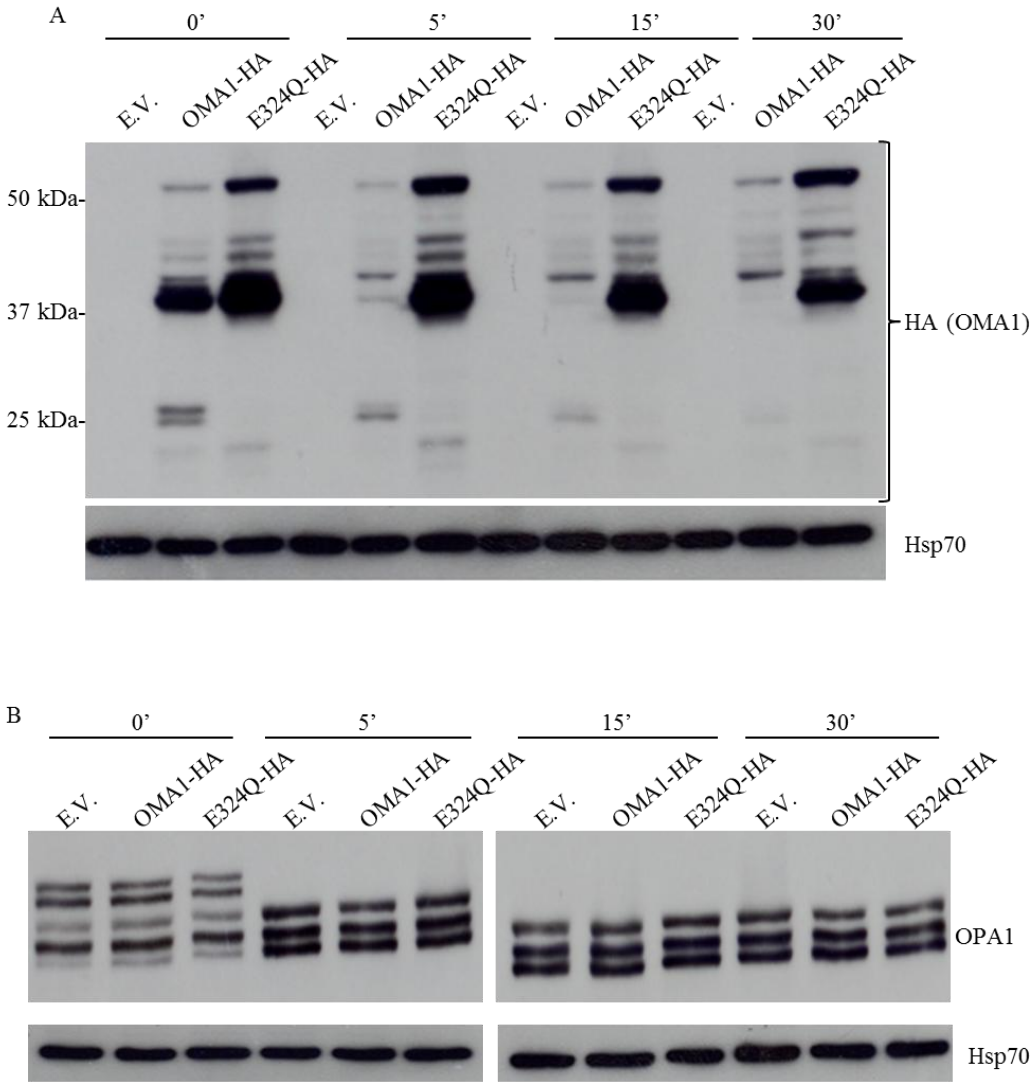

Figure 17: OMA1 activity is related to OMA1 40 kD disappearing.

(A-B) Immunoblot analysis of total extracts from HeLa cells transfected with OMA1-HA, OMA1 E324Q-HA or E.V and treated for the indicated time points with FCCP 10 µM. Membrane was immunodecorated with the indicated antibodies.

We then wanted to understand how OMA1 is regulated when the stress is removed. To this end, we performed FCCP washout and we evaluated the reappearing of OMA1 40 kD band and the OPA1 long forms (L1 and L2) at different time points. When FCCP is removed, the 40 kD band reappears after 10 minutes, while the OPA1 long isoform reappeared only after 6 hours (Fig. 18 A-B). This let us to conclude that OMA1 40 kD form is inactive and that OMA1 regulatory kinetic is extremely efficient with a very fast activation and deactivation mechanism.

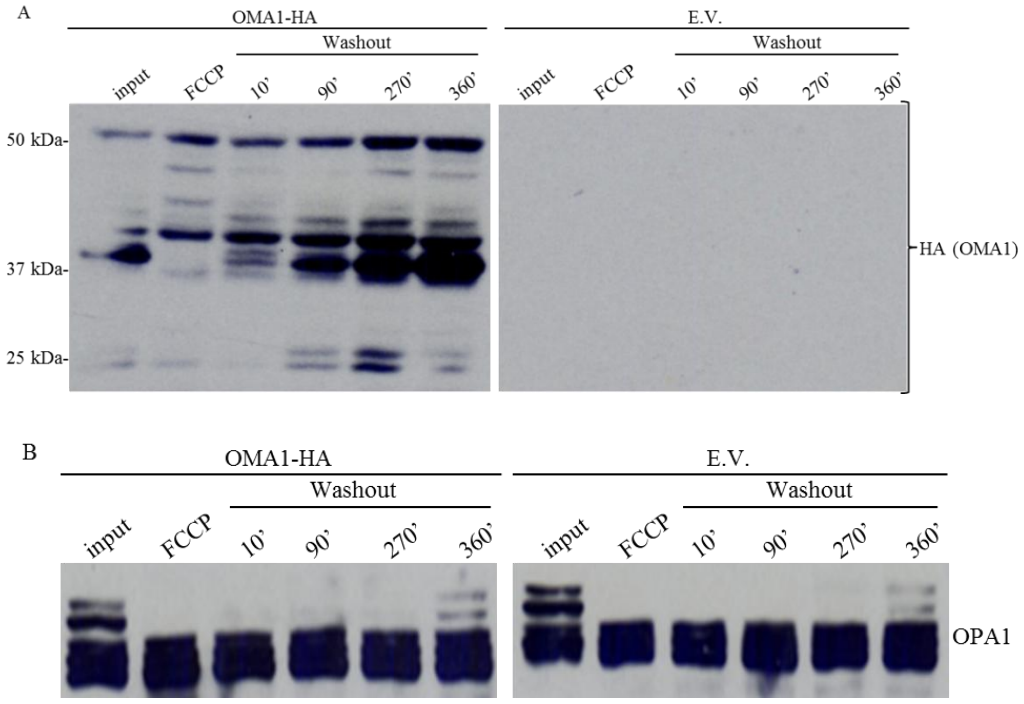

Figure 18: OMA1 40 kD band is stable in standard condition.

(A-B) Immunoblot analysis of total extracts from HeLa cells transfected with OMA1-HA, OMA1 E324Q-HA or E.V. Cells were treated with FCCP 10 μm for 30' ; then the stress was removed and harvested at the indicated time points. Membrane was immunodecorated with the indicated antibodies.

OMA1 40 kD is a substrate of YME1L1

Our data support the role of AFG3L2 in OMA1 processing. Nevertheless, the fact that OMA1 40 kD band remains visible in the absence of AFG3L2 suggests that another protease is involved in this mechanism. To test the hypothesis that YME1L1 could be this second protease we silenced it in HeLa cells. The knock down of *YME1L1* is not able to reduce the amount of the 40 kD band or to induce the 60 kD band accumulation while the double knock down didn't induce difference. These data exclude a direct involvement of YME1L1 in 40 kD OMA1 generation and support the idea that the residual amount of the 40 kDa in condition of AFG3L2 depletion could derive from incomplete silencing efficiency in HeLa cell experiments or from the presence of AFG3L1 in MEF experiments or additionally another protease could be involved in OMA1 40 kD generation. This alternative mechanism can be overactivated in dramatic conditions such as the double knock down, masking the expected OMA1 60 kD accumulation.

On the other hand, YME1L1 depletion is able to strongly increase the amount of OMA1 40 kD (Fig. 19A). The accumulation of the 40 kD band perfectly fits with the increased OMA1 activity on OPA1 in the absence of YME1L1; in fact it is known that the absence of YME1L1 induces mitochondrial network fragmentation through OPA1 processing in S1 mediated by OMA1 (Anand et al., 2014). This result highlights the role of YME1L1 in the regulation of OMA1 activity. To explain why

the absence of YME1L1 induces OMA1 40 kD accumulation we formulated four possible hypotheses:

1) YME1L1 deficiency is able to increase the amount of the *m*-AAA complexes;

2) YME1L1 overstimulates the *m*-AAA proteolytic activity;

3) The absence of YME1L1 compromises OMA1 autocatalytic process;

4) YME1L1 is directly involved in OMA1 40 kD degradation.

The silencing of YME1L1 doesn't increase AFG3L2 protein amount so we can exclude an increase in the *m*-AAA complex amount (Fig. 19A).

Then, we evaluated the possible over proteolytic activation of the *m*-AAA complexes by assaying MrpL32 processing in *YME1L1* KD condition. Nolden and colleagues demonstrated that MrpL32 is matured by the *m*-AAA protease and its absence induced the accumulation of Mrpl32 precursor form (Nolden et al., 2005). We silenced *YME1L1*, *AFG3L2* or both genes and then we transfected a HA-tagged version of MrpL32 in HeLa cells. The absence of AFG3L2 induces an accumulation of MrpL32 full length protein as previously demonstrated (Nolden et al., 2005), while the absence of YME1L1 doesn't increase the amount of MrpL32 mature product (Fig. 19B). This data demonstrate that the proteolytic activity of *m*-AAA complexes is not over-activated in the absence of YME1L1.

To test whether the absence of YME1L1 can affect the autocatalytic activation of OMA1 activity we evaluate the generation of OMA1 25 kD bands, to test the autocatalytic process, and the OMA1-mediated OPA1 processing to evaluate OMA1 activation. We found that in the absence of YME1L1, the OMA1 25 kD bands is

generated and the amount of OPA1 S1 band increased (Fig. 19A); excluding that the absence of YME1L1 could impair OMA1 autocatalytic process.

In order to verify if OMA1 40 kD band is a proteolytic substrate of YME1L1, we expressed wild-type YME1L1-MYC or YME1L-E543Q-Myc proteolytic inactive mutant in YME1L1 KD cells and valuated the amount of the 40kD band. Indeed, the overexpression of wild-type YME1L1-Myc in HeLa Cells silenced for YME1L1 led to a significant reduction in the levels of OMA1 40 kD, whereas transfection with YME1L-E543Q-Myc has no effect on the protein level (Fig. 19C). Putting together all these results we can assume that YME1L1 is directly involved in OMA1 degradation. It represents the catabolic mechanism that the mitochondrial quality control uses to rapidly remove OMA1 40 kD. In this way, OMA1 accumulation is avoided and the consequent mitochondrial network fragmentation caused by OPA1 over processing prevented.

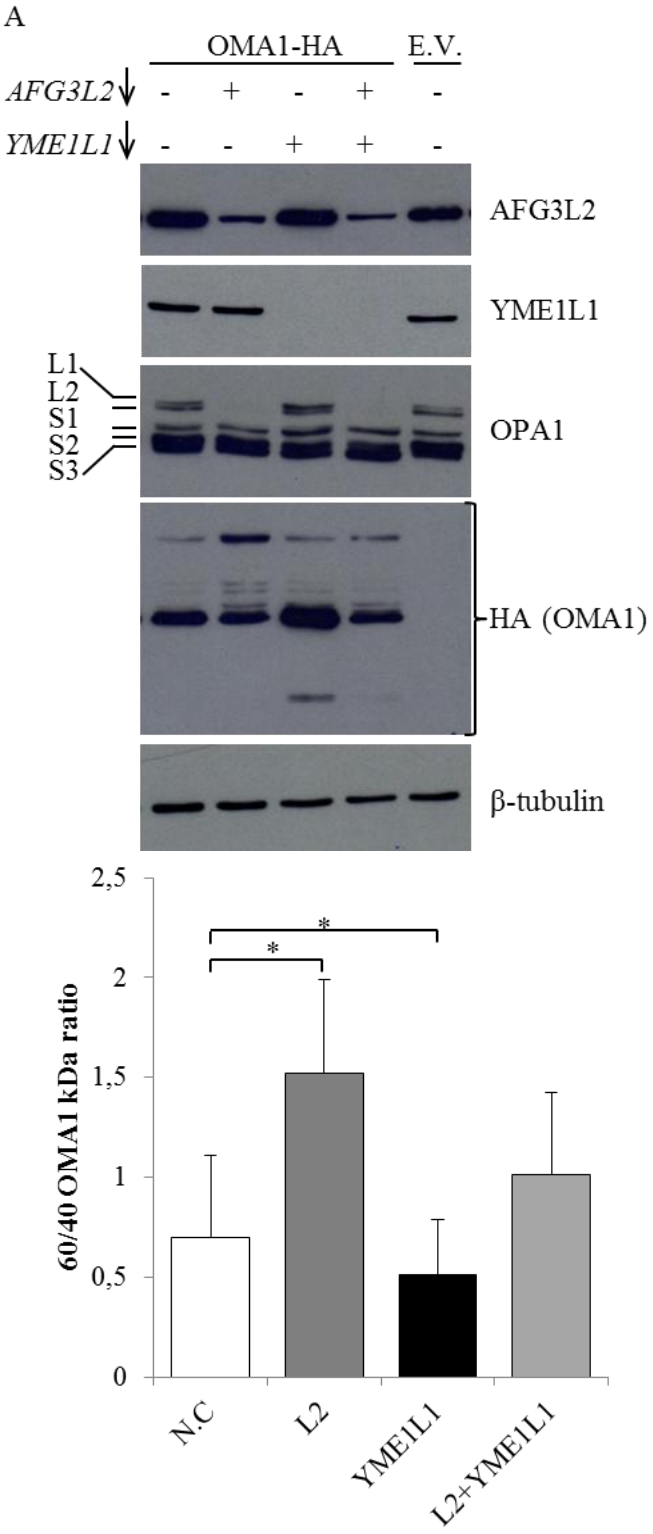
A
OMA1-HA
E.V.
AFG3L2 - + - + -
YME1L1 - - + + -
AFG3L2
YME1L1
L1
L2
S1
S2
S3
OPA1
HA (OMA1)
β-tubulin
60/40 OMA1 kDa ratio
2,5
2
1,5
1
0,5
0
*
*
N.C
L2
YME1L1
L2+YME1L1

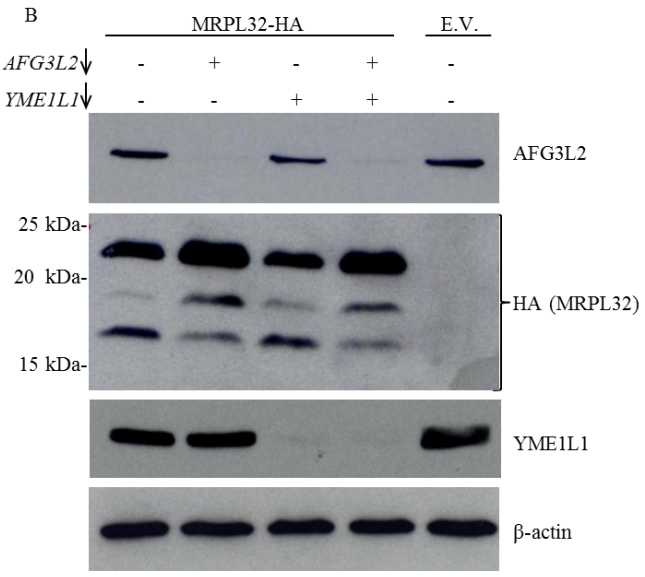
B
MRPL32-HA
E.V.
AFG3L2↓ - + - + -
YME1L1↓ - - + + -
AFG3L2
25 kDa-
20 kDa-
15 kDa-
HA (MRPL32)
YME1L1
β-actin

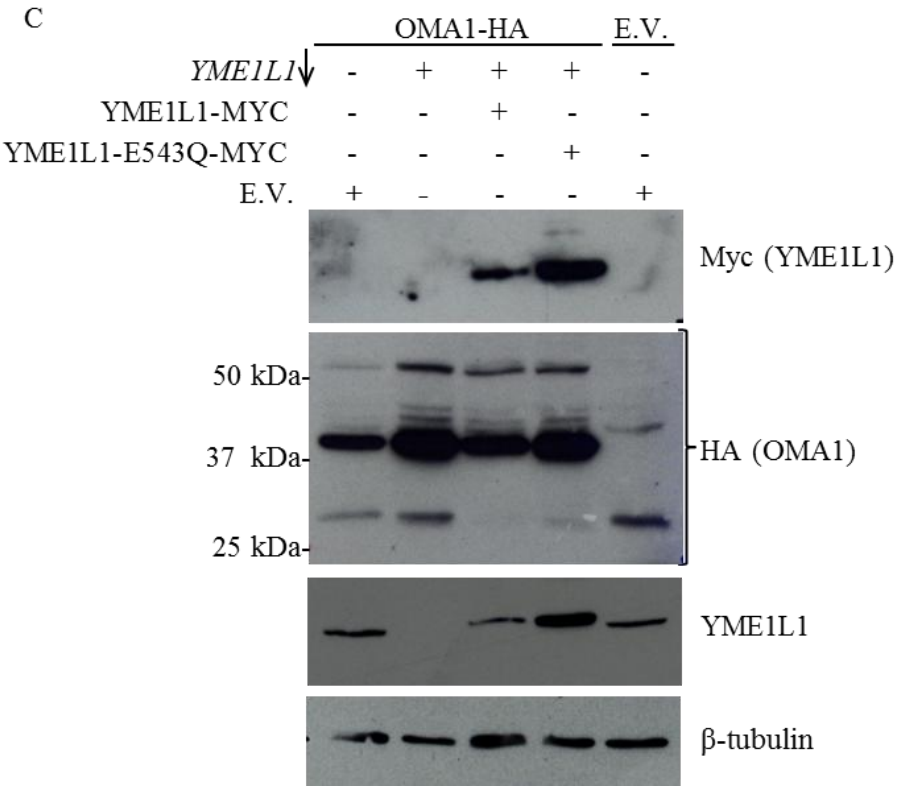
C
OMA1-HA
E.V.
YME1L1↓ - + + + -
YME1L1-MYC - - + - -
YME1L1-E543Q-MYC - - - + -
E.V. + - - - +
Myc (YME1L1)
50 kDa-
37 kDa-
25 kDa-
HA (OMA1)
YME1L1
β-tubulin

Figure 19: OMA1 402 kD band is a substrate of the *i*-AAA complexes.

(A): Immunoblot analysis of total extracts from HeLa cells silenced for AFG3L2, YME1L1 or both and then transfected with OMA1-HA or E.V and detected with the indicate antibodies. Quantification of the 60 and 40 kD band on β-tubulin after silencing of AFG3L2, YME1L1 or both the proteins. (B): Immunoblot analysis of total extracts from HeLa cells silenced for AFG3L2, YME1L1 or both and then transfected with MRPL32-HA or E.V and detected with the indicate antibodies.
(C):Immunoblot analysis of total extracts from HeLa cells silenced for YME1L1 and then co-transfected with OMA1-HA and YME1L1-MYC, YME1L1-E543Q-MYC or E.V and detected with the indicate antibodies.

DISCUSSION

SCA 28 is a novel form of autosomal dominant cerebellar ataxia, characterized by gait difficulties, nystagmus, ophtalmoparesis and hyperreflexia. Many SCA28-causing mutations were discovered in the last years in the *AFG3L2* gene. This gene codifies for a mitochondrial protease of the inner membrane belonging to the AAA-protein family that can assemble into homo-oligomers and hetero-oligomers with paraplegin forming the *m*-AAA complex. This complex is involved in protein quality control of the inner membrane and mediates chaperone-like activity on respiratory chain complexes and perform proteolytic maturation of substrates.

The animal model which recapitulates most features of SCA28 patients is an *Afg3l2* haploinsufficient mouse. It displays defects in motor coordination and balance due to PCs degeneration. Mutant PCs show increased electron density and condensed cytoplasm and nucleus but no signs of apoptotic bodies. These features are peculiar of dark cell degeneration (DCD) that is characteristic of excitotoxic injury. In the SCA28 model this type of degeneration originates for the first time from mitochondrial dysfunction. Indeed, histological studies on the cerebellum of mice *Afg3l2* heterozygous show dramatic defects in mitochondrial morphology and cristae organization and biochemical investigations revealed reduced activity of the respiratory chain. Mitochondrial phenotypes precede PC-DCD, demonstrating the mitochondrial origin of the degeneration.

We hypothesized that the pathological mechanism at the basis of PC-DCD in SCA28 mice involves defective Ca^{2+} internalization in mitochondria as a triggering event. This can in turn cause alteration of Ca^{2+} homeostasis and pathological accumulation of Ca^{2+} in *Afg3l2* mutant PCs in condition of normal glutamate stimulation, thus mimicking exitotoxic-mediated DCD. Indeed, it is well known that mitochondrial Ca^{2+} buffering has a key role in the regulation of cellular Ca^{2+} homeostasis, especially in neurons.

So, the aim of this thesis is focused on the clarification of the relationship between mitochondrial dysfunction and DCD. In particular I focused my research work on two aims: the analysis of mitochondrial morphology and mitochondrial Ca^{2+} buffering in the absence of AFG3L2 and the molecular mechanisms that cause mitochondrial fragmentation in the absence of AFG3L2.

SCA28 patients carry heterozygous mutations and haplo-insufficency is the mechanism of the disease; therefore *Afg3l2* heterozygous cells should represent the correct model to study SCA28. However, we couldn't find any alteration in mitochondrial Ca^{2+} buffering and morphology in *Afg3l2* heterozygous cells (MEFs and PCs) compared to wt. This could be explained by the fact that, the cell lines were derived from E15 embryo (MEFs) or P0 (PCs) mice while, the mitochondrial defects appear only at 4 months in SCA28 mice model, Indeed, up to 4 months *Afg3l2* heterozygous cells and wild type have the same behavior. In the light of these considerations and since it's very difficult to model neurodegeneration in vitro, we

decided to use *Afg3l2* ko cells to mimic in vitro the effect of the haploinsufficient in vivo.

The morphometric analysis of the mitochondrial network in MEFs disclosed that the absence of AFG3L2 induces an evident network fragmentation compared to *Afg3l2* wt and heterozygous MEFs, which maintained a tubular network organization.

We observed that mitochondrial fragmentation in *Afg3l2* ko cells reduces the volume of individual mitochondrial particles without changing the total volume of the organellar network. As a direct consequence, a fraction of mitochondria in *Afg3l2* ko cells lose their link to the ER and result positioned at a higher distance from the Ca^{2+} source, failing to match the MCU-activation needs (Rizzuto et al., 1998) and therefore remaining without substantial $[Ca^{2+}]_m$ rises. Moreover, studies have shown that Ca^{2+} entering mitochondria can spread and equilibrate rapidly within the matrix along large and tubular, but not fragmented organelles. In fact, the small size of mitochondrial particles in a fragmented network and the consequent lack of matrix connectivity limit the proper diffusion of the Ca^{2+} wave and increases the heterogeneity of mitochondrial Ca^{2+} responses (Frieden et al., 2004) (Szabadkai et al., 2004). These phenomena together account for the overall reduction in the mitochondrial Ca^{2+} load in *Afg3l2* ko cells.

Heterozygous and homozygous mutations in *AFG3L2* cause neurodegeneration that mostly involves PCs in the cerebellum and results in ataxia (Di Bella et al., 2010; Pierson et al., 2011). The fact that cerebellum is more sensitive to AFG3L2

dysfunction compared with other neuronal tissues can be explained by the high expression of this gene in PCs (Di Bella et al., 2010), but also with the special requirement of mitochondrial functionality by PCs. These are indeed unique neurons with very large and highly branched dendritic trees which receive only glutamate excitatory synaptic input from a single climbing fiber and from ~200.000 parallel fibers. They are therefore exposed to high Ca^{2+} influxes due to glutamatergic stimulation of both mGluR1 and AMPA receptors (Ito, 2002), moreover they need a more precise control of Ca^{2+} homeostasis compared to other neurons, implying a higher Ca^{2+} buffering power. For such reasons, mitochondria play a pivotal role in maintaining Ca^{2+} homeostasis in PCs by direct uptake of Ca^{2+} and, also, by providing ATP to pump Ca^{2+} across membranes. We therefore hypothesize that the inefficient buffering and shaping of the Ca^{2+} waves operated by mutant mitochondria provokes a local increase in $[Ca^{2+}]_c$ and that this, in chronic conditions like as in associated diseases, triggers PCs degeneration.

To verify this hypothesis, and considering the limitation represented by non-excitable and non-polarized cells such as fibroblasts, we cultured primary PCs and we tested in these cells if the proposed mechanism of pathogenesis for SCA28 was corrected.

EM analysis revealed dramatic alterations of organellar ultrastructure in mutant PCs, showing mitochondria with vesiculation of the inner membrane or completely swollen. In addition to these ultrastructural defects, *Afg3l2* ko PCs show increased

mitochondrial network fragmentation and faulty mitochondrial distribution in the dendritic tracks. In particular, we observed that the volume of mitochondria associated to dendrites is reduced in the absence of AFG3L2, indicating a skewed distribution of mitochondria toward the cell soma.

We directly measured $[Ca^{2+}]_m$ in primary PCs after KCl induction and we found it markedly reduced in *Afg3l2* PCs, in line with morphological alteration. Thus, such data allowed us to propose a pathogenetic mechanism in which loss and haploinsufficiency of *Afg3l2* causes fragmentation of mitochondria, which weakens the mitochondrial buffering of Ca^{2+} elevations in the soma. This scenario is worsened in mutant dendrites due to mitochondria underpopulation, too.

It's also conceivable that reduced ATP production by mutant mitochondria can locally slow down the kinetic of Ca^{2+} pumps, affecting the extrusion of Ca^{2+} from the cytosol into the ER and across the plasma membrane in dendrites.

All these data demonstrated that the alteration of mitochondrial dynamics is the cause of defective mitochondrial Ca^{2+} handling in *Afg3l2* mutant cell lines, providing a direct molecular link between mitochondrial defect and dark cell degeneration of Pcs (Model A).

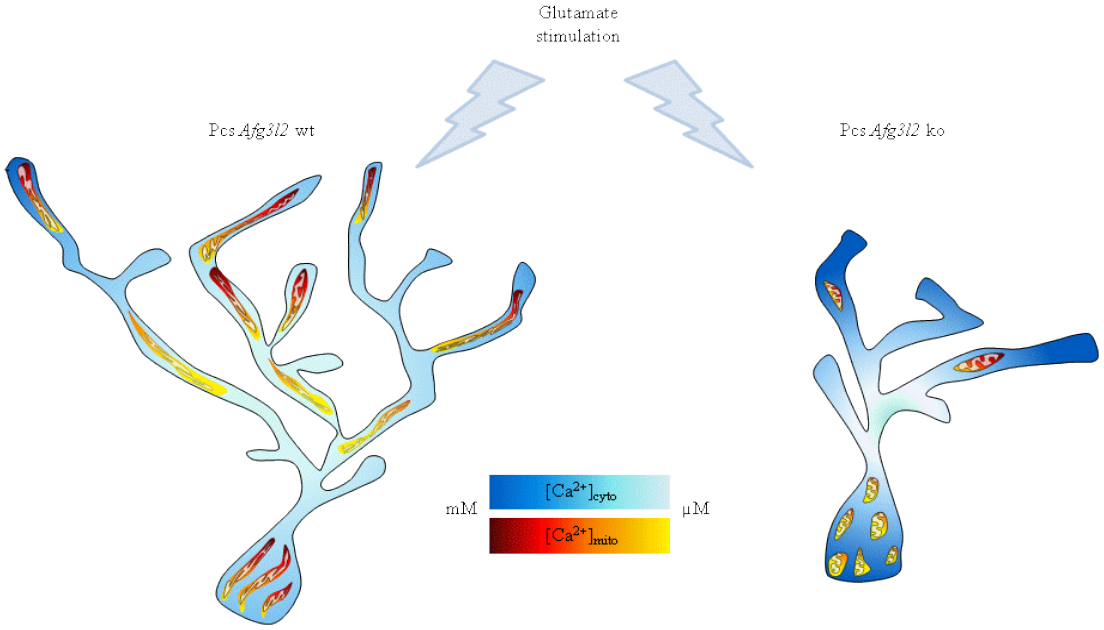

Model A

Mutation of *Afg3l2* causes fragmentation of mitochondria, which weakens the mitochondrial Ca^{2+} buffering increasing the $[Ca^{2+}]_{cyto}$ and finally inducing DCD. This scenario is worsened in mutant dendrites due to mitochondria underpopulation, too.

After demonstrating the mitochondrial network alteration, we focused on disclosing the molecular mechanism that causes mitochondrial fragmentation in the absence of *Afg3l2*.

Mitochondrial network fragmentation can be caused by an increase in the rate of fission events or a decrease in fusion. We excluded the first hypothesis since DRP1 didn't result relocalized on the mitochondrial surface in *Afg3l2* ko MEFs. This means that the mitochondrial fission machinery is not over-activated by the absence of AFG3L2 but there should be an alteration in the fusion mechanism. To test this hypothesis we evaluated OPA1 processing demonstrating that mutant *Afg3l2* MEFs and neuronal tissues shod an accumulation of the short OPA1 forms with the parallel decreased of OPA1 long forms.

These data demonstrate that *Afg3l2* ko cells have a strong defect in the inner membrane fusion machinery, by losing OPA1 long forms. OPA1 long forms are fundamental to maintain the correct cristae tightness and the consequent tubular structure of the network. How the lack of OPA1 long forms and the increase in OPA1 short forms could induce mitochondrial fragmentation is not known. We can speculate that short OPA1 isoforms may stimulate membrane fission and contribute to the coordination of mitochondrial fusion and fission. Indeed, it is conceivable that short OPA1 isoforms interact with the fission machinery at the OM or is involved in IM fission. A stimulatory role of short OPA1 isoforms in mitochondrial fission may be crucial under stress conditions or upon induction of apoptosis and/or mitophagy

and is therefore likely to be of particular importance for mitochondrial quality control.

The enhanced OPA1 cleavage in the absence of AFG3L2 was mediated by OMA1 as previously demonstrated (Ehses et al., 2009; Head et al., 2009). OMA1 full length proteins weight 60 kD but it was proposed that the active form is a shorter form around 40 kD. Up to date, nothing is known about the protease that mediates the 60/40 kD cleavage. Head and colleagues proposed YME1L, AFG3L2 and paraplegin as possible proteases involved in this mechanism and they tried to evaluate OMA1 60/40 kD processing after siRNA experiment. They failed to observe any difference in OMA1 processing after silencing of each of these genes, but at the same time declaimed that there may still be present residual proteases in their experiments as consequence of low silencing efficiency (Head et al., 2009). This limitation prevented them to give a definitive conclusion.

Moreover, in the same work the authors noticed that OMA1 60 kD form was detectable only after treatment with an uncoupler drug such as CCCP. Since this accumulation coincides with OPA1 processing, they proposed that the OMA1 60-kD form was the active species and that the 40-kD band was a breakdown product. These observations lead to a model in which OMA1 activity is normally attenuated by high rates of turnover. This turnover was slowed when mitochondria lose membrane potential or matrix ATP, making it possible to cleave OPA1 protein.

However, other groups rejected this idea giving to the 40 kD the role of the active form. In particular Baker and colleagues demonstrated that the OMA1 40 kD is the

active one on OPA1 and this is the one building OMA1 complex; nevertheless they never provide experiments that formally excluded OMA1 60 kD as the active form, even because they weren't able to detect the full length form by Western blot.

In both the papers authors were obliged to use an OMA1 tagged version since an antibody finely working in Western blot is not still available. The two groups used two different tags for OMA1; Head used HA-tag, while Eshes and Baker used a Myc tag. This difference could be a possible explanation to interpret the reason why Ehses and Baker didn't detected the 60 kD form. It is not known if the HA-tag could stabilize the half-life of OMA1 or otherwise if the Myc tag could increase its degradation, but in either the case the Myc or HA OMA1 versions maintain their pivotal role on OPA1 processing. Since OMA1-HA allows following the 60 kD and the 40 kD forms we decided to use this tag version of the protein for our study.

Starting from the information obtained in the first part of my thesis and from the above mentioned published works, we decided to investigate on OMA1 60/40 kD processing to understand whether OMA1 is directly regulated by AFG3L2 itself or indirectly by the respiratory deficiencies mediated by the loss of AFG3L2.

We clarified that the first step (60/40 kD) of OMA1 maturation occurs inside the mitochondria and not in the cytosol, since the mitochondrial import inhibition prevented OMA1 40 kD formation. These results indicate that the processing occurs inside the mitochondria, in line with previous paper (Head et al., 2009). These experiments allowed us to clarify that OMA1 doesn't have a canonical leader sequence cleaved by mitochondrial processing peptidase (MPP). OMA1

mitochondrial leader sequence was identified in different prediction software but we weren't able to discriminate between the precursor and the 60 kD form. We didn't observe OMA1 precursor form even combining the mitochondrial import inhibition to the proteasomal inhibition using MG132. This finding is even supported by experiments of Head and colleagues which demonstrated, with an in vitro system, that OMA1 is imported in the mitochondria also when the mitochondrial membrane potential is altered or when ATP is depleted. This could not be possible for proteins imported by classical TOM-TIM import machinery (Schmidt et al., 2010). In fact, it is known that alteration of the mitochondrial membrane potential or ATP depletion are sufficient to inhibit the mitochondrial import mechanism mediated by TOM-TIM complexes (Schmidt et al., 2010).

Moreover, OMA1 was not detected among the proteins identified in yeast TIM23-core complex interactome (Mehnert et al., 2014). Future studies will clarify if OMA1 is imported by an alternative known or unknown pathway.

By combining digitonin extractions with trypsin digestions we determined in which sub-mitochondrial compartment OMA1 40 kD is generated. OMA1 60 kD behaves like Mitofusin 2, an integrated outer membrane protein, and it is degraded by trypsin alone. This could be explained in two ways. In the first case OMA1 60 kD is only associated to the mitochondrial outer membrane as a pre-protein and so it is digested by trypsin; in the second case, trypsin digested the C-term tail of OMA1 60 kD that is still outside the mitochondria while the rest of the protein is going through the outer membrane during the import. Since the OMA1 60 kD form was detected as an

integral membrane protein (Head et al., 2009) it is reasonable to speculate that the right hypothesis is the second one. However, OMA1 40 kD was accessible to trypsin and disappeared only in the presence of digitonin. OMA1 40 kD showed the same trypsin sensibility of TIM23 indicating that OMA1 40 kD must have at least one transmembrane domain. The C-terminus of OMA1, and OMA1 M48 cleavage domain, must be exposed toward the IMM since OPA1 cleavage site is localized in this sub-mitochondrial localization. Considering our aim of disclosing the proteases involved in OMA1 60/40 kD processing, these results allowed us to focus our attention on the mitochondrial proteases localized in the inner mitochondrial membrane.

We observed OMA1 60 kD form accumulation using metallopeptidase inhibitors. We used this information and the sub-mitochondrial localization to screen several proteases databases, finally identifying 4 possible proteins involved in OMA1 60/40 kD processing: OMA1 - paraplegin - AFG3L2 and YME1L1.

Interestingly, these proteins are the same previously excluded by Head and colleagues (Head et al., 2009) but, since their data were not shown in the paper, we decided to investigate and verify if OMA1 60/40 kD processing is mediated by one of these proteins.

OMA1 itself was the first protein that we tested; in order to do it we used a proteolytic inactive mutant (OMA1-E324Q-HA). Transfection of this mutant in HeLa cells didn’t induce an accumulation of the 60 kD form, while we noticed the disappearing of the 25 kD bands. This experiment, even if performed in the presence

of the endogenous one, allowed us to conclude that OMA1 is able to digest itself from the N-term generating the 25 kD forms, but it is not involved in the generation of the 40 kD form. This result is supported by an experiment performed by Head and colleagues who transfected the proteolytic inactive mutant in OMA1 silenced cells. They performed this experiment with a different purpose but the Western blot showed the presence of the 40 kD band when the proteolytic inactive mutant was expressed (Head et al., 2009) thus confirming, our result. Interestingly, when we overexpressed OMA1-E324Q-HA in HeLa cells we didn't inhibit OMA1-mediated OPA1 processing. This result leads us to conclude that the proteolytic activity of OMA1 is extremely efficient since the endogenous OMA1 is able to perform OPA1 processing even when the proteolytic inactive form is overexpressed. In this condition, OMA1 complexes are theoretically formed by a high percentage of proteolytic inactive subunits and, therefore, the proteolytic activity should be impaired. On the contrary, OMA1 mediated OPA1 processing wasn't affected indicating that the endogenous form is sufficient to perform correctly all its proteolytic activity.

We also excluded paraplegin in the generation of OMA1 40 kD form. In fact, transfecting OMA1-HA in *SPG7*$^{-/-}$ human immortalized fibroblasts we didn't find any alteration in OMA1 processing. This is in line with unaltered OPA1 processing in the absence of paraplegin (Ehses et al., 2009).

A possible explanation for this result is that paraplegin only exists in hetero-oligomeric complexes together with AFG3L2, whose alterations in fibroblasts don't

affect mitochondrial dynamics. The possible involvement of paraplegin in OMA1 processing should be studied in cells where paraplegin mutations induce mitochondrial defects as spinal and peripheral axons (Ferreirinha et al., 2004).

Testing OMA1 processing in *Afg3l2* ko fibroblasts led us to observe an accumulation of OMA1 60 kD form compared to wild type MEFs and a decreased of the 40 kD form. This result was also observed in HeLa cells silenced for AFG3L2. In both the conditions we also detected an increased OMA1 mediated OPA1 processing and the consequent mitochondrial network fragmentation that we previously reported.

To explain how the absence of AFG3L2 induces OMA1 60 kD accumulation, we formulated four hypothesis:

- AFG3L2 is the protease that cleaves OMA1 60 kD. Thus generating the 40 kD form.
- AFG3L2 regulates another protease that exerts the above mentioned function.
- AFG3L2 impairment produces the mitochondrial stress that drives to OMA1 60/40 kD processing
- The absence of AFG3L2 causes a defect in the import of OMA1.

Our experiments support the first hypothesis showing that AFG3L2 is the protease that mediates OMA1 60/40 kD cleavage. After demonstrating a physical interaction between AFG3L2 and OMA1, we performed by co-immunoprecipitation between OMA1-HA and the proteolytic inactive mutant AFG3L2-E575Q-MYC. To achieve the results, given the fast kinetic of a proteolytic event, we needed to optimize the

interaction between AFG3L2 and OMA1. Moreover, the unavailability of a specific antibody against OMA1 working in Western blot, prevented us to perform the Co-Ip experiment in endogenous conditions. We confirmed the direct proteolytic role of AFG3L2 in OMA1 processing by a complementary approach: in fact, the overexpression of AFG3L2-Myc was able to restore OMA1 60/40 kD processing and partially OPA1 processing, while the overexpression of the proteolytic inactive mutant (AFG3L2-E575Q-Myc) wasn't able to do it. This result demonstrates that AFG3L2 is the protease involved in OMA1 40 kD generation. The clarification of the relationship between AFG3L2 and OMA1 is important because introduces a new pathway in the regulation of mitochondrial dynamics. In fact, it is conceivable that OMA1 interacts with AFG3L2 immediately after its import in an unfolded conformation. At this point the interaction should generate the OMA1 40 kD form that will be OMA1 oligomeric unit of OMA1 complexes.

However, the increased OPA1 processing and the decreased amount of OMA1 40 kD band that we found in the absence of AFG3L2 are difficult to reconcile with the model that indicates the 40 kD band as the active OMA1 form. A possible explanation could be that the real active OMA1 form is not the 40 kD, but one of its cleavage products. Indeed, in a previous paper, a second form of OMA1 slightly smaller than OMA1 40 kD form was detected using OMA1-specific antibodies (Baker et al., 2014). This smaller form is generated by an autocatalytic processing that involves the last C-term amino acids of the protein, causing the disappearing of the HA tag and therefore making it not visible by Western blot. It's conceivable that

the absence of AFG3L2 impairs the kinetic of OMA1 60kD to 40 kD conversion leading to the accumulation of the 60 kD, but at the same time the environmental stress caused by the absence of AFG3L2 (ATP depletion, increased ROS production), can activate OMA1 auto-catalytic cleavage, leading to a reduction of the 40 kD OMA1 and, possibly, to increased amount of the smaller form of OMA1, which is the one really acting on OPA1. In support to this, reintroduction of AFG3L2 in *Afg3l2* ko cells is able to reduce the stress and to restore the physiological condition, stopping OMA1 C-term auto-cleavage activation resulting in OMA1 40 kD band increase. In addition to the clarification of OMA1 60/40 kD mechanism, these data have an additional value because they identify a new mammalian substrate of AFG3L2. Up to date only MrpL32 was demonstrated to be matured by the *m*-AAA complexes (Nolden et al., 2005). Our data reinforce the idea that the *m*-AAA complexes can be involved in the maturation of several other proteins with different activity inside the mitochondria.

The N-Term of MrpL32 and OMA1 didn't show a high sequence homology, leading us to exclude the presence of a conserved consensus sequence recognized by the *m*-AAA, but they showed the same peculiar maturation system. In fact, these two proteins are processed by a proteolytic trimming. This mechanism was demonstrated in yeast by Bonn and colleagues (Bonn et al., 2011) for MrpL32; they discovered that the processing of the ribosomal subunit MrpL32 by the *m*-AAA protease depends on the folding of MrpL32 rather than on the specific recognition of the cleavage site. The *m*-AAA protease binds to N-term regions of newly imported MrpL32 and initiates

proteolysis, which is halted by a tightly folded, cysteine-containing domain of MrpL32. This sequence is not present in OMA1, but the trimming mechanism is conserved for OMA1 maturation. We observed the presence of degradative intermediates bands between the 60 kD and the 40 kD forms particularly when we silenced *AFG3L2* in HeLa cells. These bands were degraded when AFG3L2 was expressed in silenced cells, while they remained stable when the proteolytic inactive mutants were expressed. To confirm this mechanism we generated 10 mutants with deletion of 3 or 4 amino acids in different OMA1 regions identified as *m*-AAA possible target sequences by bioinformatics prediction tools; but in any case the *m*-AAA complexes were able to process OMA1. To have a further confirmation we generated a mutant with a deletion of 53 amino acids upon the N-term amino acid mapped in position 140 (OMA1-Δ92-144-HA) and even this mutant was processed by a trimming mechanism. Our experiment demonstrated that the N-term of OMA1 interacts with the *m*-AAA complexes and it is processed until the hydrophobic domain around the amino acid in position 140. It is reasonable to hypothesize that the *m*-AAA complexes halt OMA1 degradation in this position because this area contains 6 leucines. In fact, it was previously demonstrated that *m*-AAA proteases were not able to dislocate intermembrane protein from the inner mitochondrial membrane when the transmembrane domain of this protein had at least 5 leucines (Botelho et al., 2013).

Although all these mutants failed to show a common consensus sequence, OMA1 Δ173-176-HA mutant displayed an interesting behaviour. In fact, the deletion of these

4 amino acids induced the inhibition of the auto-catalytic processing identifying this area as a key regulatory domain for the proteolytic activity of OMA1 itself. This result is in line with what was proved by Baker and colleagues which individuated the lysines 176-177-181-185-186-188 as sensor domain, that induces conformational changes in OMA1 upon membrane depolarisation leading to its activation and autocatalytic turnover (Baker et al., 2014).

Future studies will be able to tell whether all the lysine containing sequence is fundamental for OMA1 activity or only the lysine in position 176. Clarification of this point could give a new strategy to modulate OMA1 activity and could be important to design therapeutic strategies in disorder as SCA28, caused by OMA1-mediated mitochondrial network fragmentation.

Another important point to be clarified is the role of OMA1 60 kD. As reported before in this discussion, recent papers demonstrated that the OMA1 active form is the 40 kD clipped off the last 30 amino acids (Baker et al., (Zhang et al., 2014); but once again a possible role of OMA1 60 kD on OPA1 processing, especially during stress condition when it accumulates (Head et al., 2009), was never demonstrated.

Transfecting OMA1 mutant Δ92-144 in *OMA1* silenced HeLa cells we observed that OPA1 processing was rescued demonstrating for the first time that the 60 kD form is dispensable during physiological conditions. The situation was less clear in the presence of a mitochondrial stress condition, such as Δφ depletion. In this situation OPA1 is processed but with a lower efficiency compared to the sample expressing OMA1- wt. This indicates that the deletion of the amino acids sequence 92-144 could

alter the structure of OMA1 complexes making it less responsive to the OMA1 activation. This result was unexpected since the mutant OMA1 Δ92-144-HA has all the theoretical amino acid sequence of OMA1 40 kD. This result could be the base of future studies in order to better clarify which are OMA1 monomers that will build the active complexes.

However, coming back to the initial role of OMA1 60 kD, the impossibility to generate an uncleavable form keep this question unsolved; and this should be taken in account especially when the role of OMA1 is studied in diseases that could induce OMA1 activation.

OMA1 regulatory activator mechanism has been widely described in previous paper (Baker et al., 2014) indicating the autocatalytic process at the C-term as a pivotal step for the activation of the proteolytic activity, describing the fundamental domain at OMA1 N-term. However, few information were showed about the time of activation or inactivation of the proteins. We demonstrated that OMA1 is immediately activated after few minutes of stress induction, since OPA1 long forms are quickly processed and OMA1 40 kD band disappeared in Western blot since the autocatalytic activation removes the HA tag as previously argued. Interestingly, also the inactivation kinetic of OMA1 is extremely fast, in fact, we could observe the reappearing of the inactive 40 kD form when the physiological condition is restored. This behavior underlines the importance of OMA1 in mitochondrial dynamics and in particular it showed a very efficient regulatory system which is able to active or to inactive OMA1 depending on the cellular needs.

We demonstrated that the *i*-AAA complexes are not involved in OMA1 60/40 kD processing but, interestingly we observed that the absence of the *i*-AAA induced an accumulation of OMA1 40 kD. This indicates that the *i*-AAA proteases mediates OMA1 40 kD degradation. This accumulation could be explained by two different hypothesis: in the first case the *i*-AAA protease degrades OMA1 40 kD form, before its oligomerization in OMA1 complexes; in the second hypothesis *i*-AAA is involved in the turnover of OMA1-complexes. Our data are in contrast with Baker and colleagues (Baker et al., 2014) recently published data, which didn't observe alteration in OMA1 40 kD amount after YME1L1 silencing. Our rescuing experiment excludes that our data could derive from a technical bias and we thought that Baker and colleagues failed to detect OMA1 40 kD accumulation for a matter of tag. As discussed before, the Myc tag, used in their experiment, could decrease the stability of the protein with a consequent increase in its degradation. This could finally mask the effect mediated by the absence of *i*-AAA since OMA1-Myc has already degraded with a fast kinetic.

These results demonstrated for the first time that the *m*-AAA and the *i*-AAA complexes work coordinately in the regulation of OMA1. These data suggest that the two AAA complexes could work together in the regulation of other proteins (Model B). In previous papers, it has been demonstrated that the absence of *AFG3L2* (Hornig-Do et al., 2012) or the absence of *YME1L1* (Stiburek et al., 2012) induces an accumulation of proteins belonging to respiratory complex I. To clarify whether *m*-AAA and *i*-AAA complexes specifically exert their chaperone like activity towards

complex I protein, acting through a coordinated action, would give a new perspective in the comprehension of diseases related to complex I defects (Fassone and Rahman, 2012).

Model B

Physiological condition

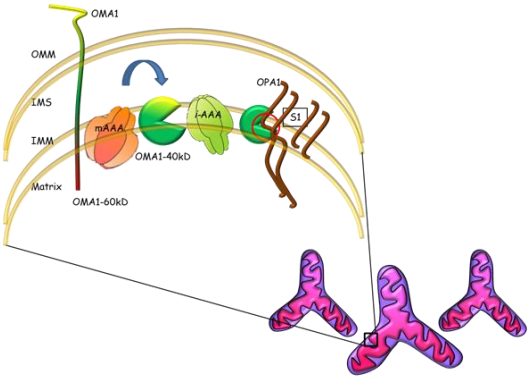

Absence of YME1L1

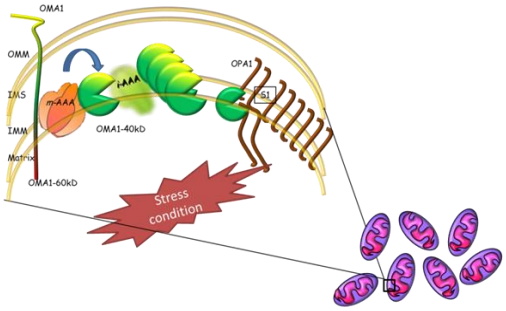

Absence of AFG3L2

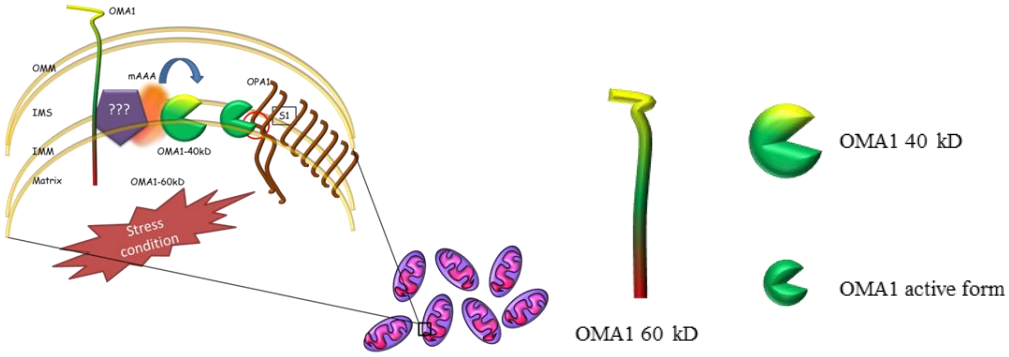

In physiological condition OMA1 full length interacts with AFG3L2 after mitochondrial import. This interaction will generate the pre-protein OMA1 40 kD. OMA1 40 kD is a substrate of the *i*-AAA protease avoiding its accumulation.
When necessary, OMA1 40 kD is activated by auto-catalytic processing and this smaller form can cleave OPA1 in S1 producing OPA1 short forms indispensable for the mitochondrial fission.

When YME1L1 is absent OMA1 40 kD accumulates. This accumulation together with the stress caused by the absence of the *i*-AAA complexes induces OMA1 activation. OMA1 40 kD undergoes auto proteolytic activation, OPA1 is processed and the mitochondrial network fragments.

When AFG3L2 is absent or mutated an unknown compensatory mechanism works to generate OMA1 40 kD. The absence of *m*-AAA complex induces several stress events that are able to activate OMA1.OMA1 40 kD form undergoes auto proteolytic activation, OPA1 is processed and the mitochondrial network fragments

CONCLUSION AND PERSPECTIVES

We studied the role of AFG3L2 in mitochondrial dynamics and mitochondrial Ca^{2+} buffering in SCA28 pathogenesis. Our studies demonstrated that PCs degeneration in *SCA28* model mice occurs as a consequence of defective Ca^{2+} buffering caused by mitochondrial network alterations. We found that *Afg3l2* ko mitochondrial network is fragmented as result of OMA1-mediated OPA1 processing. OMA1 processing in *Afg3l2* depleted cells is impaired: OMA1 60 kD accumulates, indicating that AFG3L2 processes OMA1 by trimming the N-terminus tail of the protein. Moreover, we provided evidence that another unknown protease is involved in OMA1 processing when the *m*-AAA complex is absent or altered. In addition to the role of the *m*-AAA in OMA1 maturation, we found that the *i*-AAA complex also has a pivotal role in the OMA1 regulatory mechanism, disclosing for the first time a co-operative mechanism between the *m*-AAA and the *i*-AAA.

The clarification of the relationship between mitochondrial dysfunction and Ca^{2+}buffering alteration gives new important perspectives from a translational point of view. In fact, we have already demonstrated that when we recovered the mitochondrial morphology of *Afg3l2* ko MEFs we also rescue the mitochondrial Ca^{2+} buffering defect (Maltecca et al., 2012). The data presented in this thesis on the causal link between mitochondrial morphology and the mitochondrial Ca^{2+} buffering in *Afg3l2* ko PCs allowed us to hypothesize that rescuing mitochondrial morphology could prevent neurodegeneration in SCA28. Since pharmacological treatments able to

rescue mitochondrial morphology are not available yet, it was more reasonable to act through the glutamatergic system, thus helping the poor mitochondrial Ca^{2+} buffering capacity.

According to this mechanism, our lab demonstrated that the SCA28 mice phenotype is fully rescued by halving the amount of metabotropic glutamate receptors (mGluR1). PCs express high levels of mGluR1 in the soma and in dendritic spines, and this receptor is essential for synapse plasticity and for motor coordination. The *Afg3l2* heterozygous *Grm1* heterozygous double mutants mice display motor function and coordination in the normal range and degenerating PCs are remarkably reduced compared to *Afg3l2* haploinsufficient mice. In parallel, our lab demonstrated that *Afg3l2* haploinsufficient mice treated with a drug able to consistently increase the transcription levels of the astrocyte glutamate transporter EAAT2 (Rothstein et al., 2005), showed a significant amelioration in motor function, coordination and PCs degeneration consequent to the reduced glutamatergic stimulation of PCs in *Afg3l2* heterozygous mice. (Maltecca et al., in press).

An obvious perspective will be to test rescuing other cerebellar ataxia characterized by PC-DCD. Indeed, PC-DCD has been described in SCA2 (Kasumu and Bezprozvanny, 2012), SCA3 (Boy et al., 2010), SCA5 (Ikeda et al., 2006) and SCA7(Custer et al., 2006). SCA2 is caused by mutations in ataxin 2, SCA3 by mutations in ataxin 3, SCA5 by mutations in β-III-spectrin (*SPTBN2*) and SCA7 by mutations in ataxin 7. These are not mitochondrial proteins and the molecular mechanism inducing excitotoxicity doesn't involve mitochondria. It has been

published that mutations in ataxin 5 and 7 induce increased glutamatergic stimulation with the consequent increment in the $[Ca^{2+}]_c$. The genetic and pharmacological rescue demonstrated in our lab for SCA28 could be successful also for the treatment of these other forms of SCA.

Furthermore, it has been published that high level of $[Ca^{2+}]_c$ impacts on the mitochondrial network organization inducing fragmentation (Cribbs and Strack, 2007). So, it will be striking to screen for new drugs able to induce mitochondrial fusion and to increase the Ca^{2+} buffering capability, and finally decrease $[Ca^{2+}]_c$. We have demonstrated that restoring the mitochondrial fusion is sufficient to rescue the mitochondrial Ca^{2+} alteration of a mitochondrial fragmented network (Maltecca et al., 2012)

From this point of view, this thesis can give another important starting point. In fact, we have disclosed the proteins involved in the regulation of OMA1 that directly impact on OPA1, the only protein actually involved in fusion and fission. Exogenously regulating OMA1 activity or modulating AFG3L2 or YME1L1 can deeply impact on diseases caused by mitochondrial dynamics alteration (Chen et al., 2014).

For this reason, future studies will be focused on the identification of possible post translational modifications (PTM) that could impact on the activity of these three proteins. In fact, in the last years, several works have demonstrated that several mitochondrial proteins undergo post translational modification inside the mitochondria. For example, it was recently demonstrated that OPA1activity is

regulated by acetylation/deacetylation processes mediated by SIRT3 (Samant et al., 2014). Moreover, it was reported that paraplegin processing is regulated by AFG3L2 tyrosine phosphorylation, although up to date it is still unknown which is the tyrosine kinase active in the intermembrane space (Almontashiri et al., 2014).Therefore the same OMA1 or YME1L1 activity can be modulated by post translational modifications and the clarification of this point could give new perspectives for the treatment of diseases affected by mitochondrial dynamics alteration.

As described in result and discussion, in the absence of the *m*-AAA proteases, OMA1 60/40 kD processing occurred through an alternative pathway uncharacterized. So, parallel to the identification of possible PTM it will be very important to clarify which is (are) the alternative protease(s) involved in OMA1 generation when AFG3L2 is absent. The complete clarification of the pathway will provide new strategies to treat mitochondrial related diseases. From this point of view, it is very interesting to observe that mutations involving mitochondrial dynamics are often associated to neurodegeneration. This is explained by the pivotal roles of mitochondria in neurons. Neurons rely their energetic demand principally on mitochondrial ATP, so it is evident that alterations in mitochondria can immediately impact on neuron health.

Moreover, the right localization of the mitochondria and the ATP production is fundamental to avoid neurodegeneration. In fact, it is particularly important that mitochondria are being transported to the peripheral dendrites to perform Ca^{2+} buffering, but it is equally important to provide the sufficient ATP amount to fuel ion

pumps (Ca^{2+} + Na^{+}/K^{+}) on the plasma membrane and ER. This explains why even proteins involved in mitochondrial transport can induce neurological diseases (Nguyen et al., 2014).

In the last years, the relationship between mitochondrial motility and dynamics, aimed several works demonstrating that the size of a mitochondrion have a direct impact on its mobility(Sheng and Cai, 2012). Indeed, interconnected mitochondrial tubules found in fission-deficient neurons are less efficiently transported to distal synapses, while it was demonstrated that DRP1 is required for delivering mitochondria to neuromuscular junctions (Verstreken et al., 2005). Conversely, mutation of a mitochondrial motor adaptor protein (Miro 1) results in mitochondrial fragmentation in addition to impaired motility. Moreover, neurons defective in Mfn2 display reduced mitochondrial motility and altered mitochondrial distribution (Chen et al., 2007). Therefore, regulating mitochondrial trafficking directly affects their morphology. At the same time, changing mitochondrial fusion–fission dynamics impacts transport and distribution. This complex balance could be a partial explanation of the high sensitivity of PCs, compared to other neurons, towards mitochondrial defects. In fact, it has been shown that mutations in other fission/fusion mitochondrial proteins, as Drp1 or Mitofusin, induce PCs degeneration (Ranieri et al., 2013). The high sensitivity of PCs to neurodegeneration when a mitochondrial dynamics protein is mutated is a matter of study. A possible explanation focuses the attention to the PCs unique architecture. In fact these cells have a very large dendritic tree and this implicates a continuous and massive post synaptic stimulation. As said

before, PCs are principally stimulated by climbing fibers which provide very powerful glutamatergic input to the proximal dendrites and cell soma. This implicates that the $[Ca^{2+}]_c$ at the dendritic sites can reach even 1mM concentration and so, to avoid excitotoxicity, the Ca^{2+} buffering machinery must be perfectly working. When mutations in mitochondrial "fusion/fission" proteins occur, there is the consequent alteration in the mitochondrial shape, ATP production and localization that finally impact on the Ca^{2+} buffering. All these evidence explain why PCs are particularly sensitive compare to the other neurons to mitochondrial defects. The case of autosomal dominant optic atrophy (ADOA) caused by mutation in OPA1 is also interesting. In this disease the neurodegeneration involves the optic nerve, in particular the retinal ganglion cell whose architecture is very similar to the PCs and even in this case the neurodegeneration is associated to glutamate excitotoxicity. This further evidence suggests that mutations in mitochondrial dynamics proteins could preferentially affect branched neurons finally inducing excitotoxicity.

ACKNOWLEDGEMENTS

Four years ago I was writing my under-graduated thesis and those acknowledgements finished with these words:

"Tutto è possibile per chi non si arrende e difende il sogno che ha…"

(Gente che spera-Articolo31)

My dream it is always the same: "to do something that could be useful even also for a single person". For this reason I started studding Biotechnology and I decided to work in this field. Four years and a PhD programme later I'm always more convinced that this is my way. I love to investigate, to snoop and to disclose the molecular mechanisms that rule our life and I'm sure that following this personal passion I will reach my final goal: "I will became a good scientist, I will combine something good". Today I have done a little step forward in this direction and this thesis is the first clue; but to prove this is a fact, we need at least two more evidences (statistic never lies)

The second one it is the most important but it is not inside in this manuscript. In fact, here it is resumed only the works of these years, but all the fantastic moments that I have spent with several special people are hidden. Realizing that 4 years are already passed without regrets is the second clue that I'm moving in the right way. I spent these beautiful years with people that have taught me, supported and reproached when necessary; and for this reason I want to thank them for everything.

So, I want to thank my boss, Professor Giorgio Casari, who bet on me, entrusted me with this compelling project and introduced me to the mitochondrial amazing world.

The second person that I want to acknowledge is Francesca Maltecca. She wasn't only my supervisor, she followed me every day in all this long period; she not only taught me the techniques but, she has taught me to use the brain and not only the

hands, to do the experiments putting all the controls and to keep always in mind what is the biological question that I want to investigate. In few words, she has taught me to be a good scientist. Thank you very much Francesca, these few words are a modest way to show all the gratitude to you.

I want to thank all my Labmates especially, papà Mau and La Eli ; Papà Mau for all his lab life suggestions and even for all the others (Keep always in mind: a puppy and a baby is the winner combination. (cit)). La Eli because she is not normal and she is my female alter ego. Thank you very much Eli.

I'm grateful to Mimma for the helpful scientific discussions and I'm thankful to our students Susanna and Sofia (Nana & Smilza) for all the laughter and the 8:00 pm happy hours in the lab.

Thank you very much to everybody for everything.

Ps. Are you wondering what is the third clue that make the evidence that I'm working in the right direction????

Well, I won a cup. ;-) #fuckingbrilliant

La seconda parte dei ringraziamenti la voglio scrivere in italiano perché è dedicata alle persone che tengo nel cuore e quindi voglio lasciare da parte il "tecnico inglese" a favore della mia lingua madre per trasmettere al meglio i sentimenti che voglio comunicare.

Le persone che più di tutte ci tengo a ringraziare sono i miei genitori. Ormai ho finito le parole per dirgli quanto siano speciali, per ringraziarli di tutto quello che fanno per me ancora oggi e per esprimergli la mia infinita gratitudine. Grazie di tutto mamma, grazie di tutto papà. Siete e sarete per sempre nel mio cuore.

Voglio rivolgere un pensiero anche a chi dall'alto mi protegge e veglia su di me. Mi mancate nonnini.

Un grazie di cuore a tutti i miei amici che dopo 15 anni sono ancora tutti li. Dalla prima superiore sempre assieme; sapere che c'è sempre qualcuno con cui poter uscire e passare dei momenti piacevoli per staccare la spina nei momenti più duri è uno dei doni più preziosi che mi sia mai stato fatto. Un grazie speciale va però alla GiuliaGiuliana che si è presa la briga di leggersi tutta la tesi per scovare tutti gli errori che ci avevo infilato.

The last but not the least special thank, va ad una persona speciale che ho al mio fianco e mi sostiene più di tutti. Grazie grazie bestiola.

"Tutto è possibile per chi non si arrende e difende il sogno che ha…"

BIBLIOGRAPHY

Abutbul-Ionita, I., J. Rujiviphat, I. Nir, G.A. McQuibban, and D. Danino. 2012. Membrane tethering and nucleotide-dependent conformational changes drive mitochondrial genome maintenance (Mgm1) protein-mediated membrane fusion. *The Journal of biological chemistry*. 287:36634-36638.

Akepati, V.R., E.C. Muller, A. Otto, H.M. Strauss, M. Portwich, and C. Alexander. 2008. Characterization of OPA1 isoforms isolated from mouse tissues. *J Neurochem*. 106:372-383.

Almontashiri, N.A., H.H. Chen, R.J. Mailloux, T. Tatsuta, A.C. Teng, A.B. Mahmoud, T. Ho, N.A. Stewart, P. Rippstein, M.E. Harper, R. Roberts, C. Willenborg, J. Erdmann, A. Pastore, H.M. McBride, T. Langer, and A.F. Stewart. 2014. SPG7 variant escapes phosphorylation-regulated processing by AFG3L2, elevates mitochondrial ROS, and is associated with multiple clinical phenotypes. *Cell Rep*. 7:834-847.

Anand, R., T. Wai, M.J. Baker, N. Kladt, A.C. Schauss, E. Rugarli, and T. Langer. 2014. The i-AAA protease YME1L and OMA1 cleave OPA1 to balance mitochondrial fusion and fission. *The Journal of cell biology*. 204:919-929.

Ankarcrona, M., J.M. Dypbukt, E. Bonfoco, B. Zhivotovsky, S. Orrenius, S.A. Lipton, and P. Nicotera. 1995. Glutamate-induced neuronal death: a succession of necrosis or apoptosis depending on mitochondrial function. *Neuron*. 15:961-973.

Anton, F., G. Dittmar, T. Langer, and M. Escobar-Henriques. 2013. Two deubiquitylases act on mitofusin and regulate mitochondrial fusion along independent pathways. *Molecular cell*. 49:487-498.

Arlt, H., G. Steglich, R. Perryman, B. Guiard, W. Neupert, and T. Langer. 1998. The formation of respiratory chain complexes in mitochondria is under the proteolytic control of the m-AAA protease. *The EMBO journal*. 17:4837-4847.

Ashburner, M., C.A. Ball, J.A. Blake, D. Botstein, H. Butler, J.M. Cherry, A.P. Davis, K. Dolinski, S.S. Dwight, J.T. Eppig, M.A. Harris, D.P. Hill, L. Issel-Tarver, A. Kasarskis, S. Lewis, J.C. Matese, J.E. Richardson, M. Ringwald, G.M. Rubin, and G. Sherlock. 2000. Gene ontology: tool for the unification of biology. The Gene Ontology Consortium. *Nat Genet*. 25:25-29.

Atorino, L., L. Silvestri, M. Koppen, L. Cassina, A. Ballabio, R. Marconi, T. Langer, and G. Casari. 2003. Loss of m-AAA protease in mitochondria causes complex I deficiency and increased sensitivity to oxidative stress in hereditary spastic paraplegia. *The Journal of cell biology*. 163:777-787.

Attwell, D., and S.B. Laughlin. 2001. An energy budget for signaling in the grey matter of the brain. *J Cereb Blood Flow Metab*. 21:1133-1145.

Baker, M.J., P.A. Lampe, D. Stojanovski, A. Korwitz, R. Anand, T. Tatsuta, and T. Langer. 2014. Stress-induced OMA1 activation and autocatalytic turnover regulate OPA1-dependent mitochondrial dynamics. *The EMBO journal*. 33:578-593.

Baloh, R.H., R.E. Schmidt, A. Pestronk, and J. Milbrandt. 2007. Altered axonal mitochondrial transport in the pathogenesis of Charcot-Marie-Tooth disease from mitofusin 2 mutations. *The Journal of neuroscience : the official journal of the Society for Neuroscience*. 27:422-430.

Bieniossek, C., T. Schalch, M. Bumann, M. Meister, R. Meier, and U. Baumann. 2006. The molecular architecture of the metalloprotease FtsH. *Proc Natl Acad Sci U S A*.

103:3066-3071.

Bonior, J., J. Jaworek, S.J. Konturek, and W.W. Pawlik. 2006. Leptin is the modulator of HSP60 gene expression in AR42J cells. *J Physiol Pharmacol*. 57 Suppl 7:135-143.

Bonn, F., T. Tatsuta, C. Petrungaro, J. Riemer, and T. Langer. 2011. Presequence-dependent folding ensures MrpL32 processing by the m-AAA protease in mitochondria. *The EMBO journal*. 30:2545-2556.

Botelho, S.C., T. Tatsuta, G. von Heijne, and H. Kim. 2013. Dislocation by the m-AAA protease increases the threshold hydrophobicity for retention of transmembrane helices in the inner membrane of yeast mitochondria. *The Journal of biological chemistry*. 288:4792-4798.

Boy, J., T. Schmidt, U. Schumann, U. Grasshoff, S. Unser, C. Holzmann, I. Schmitt, T. Karl, F. Laccone, H. Wolburg, S. Ibrahim, and O. Riess. 2010. A transgenic mouse model of spinocerebellar ataxia type 3 resembling late disease onset and gender-specific instability of CAG repeats. *Neurobiol Dis*. 37:284-293.

Bristow, E.A., P.G. Griffiths, R.M. Andrews, M.A. Johnson, and D.M. Turnbull. 2002. The distribution of mitochondrial activity in relation to optic nerve structure. *Arch Ophthalmol*. 120:791-796.

Cagnoli, C., C. Mariotti, F. Taroni, M. Seri, A. Brussino, C. Michielotto, M. Grisoli, D. Di Bella, N. Migone, C. Gellera, S. Di Donato, and A. Brusco. 2006. SCA28, a novel form of autosomal dominant cerebellar ataxia on chromosome 18p11.22-q11.2. *Brain*. 129:235-242.

Cagnoli, C., G. Stevanin, A. Brussino, M. Barberis, C. Mancini, R.L. Margolis, S.E. Holmes, M. Nobili, S. Forlani, S. Padovan, P. Pappi, C. Zaros, I. Leber, P. Ribai, L. Pugliese, C. Assalto, A. Brice, N. Migone, A. Durr, and A. Brusco. 2010. Missense mutations in the AFG3L2 proteolytic domain account for approximately 1.5% of European autosomal dominant cerebellar ataxias. *Hum Mutat*. 31:1117-1124.

Cai, Q., H.M. Zakaria, A. Simone, and Z.H. Sheng. 2012. Spatial parkin translocation and degradation of damaged mitochondria via mitophagy in live cortical neurons. *Curr Biol*. 22:545-552.

Chang, D.T., and I.J. Reynolds. 2006. Mitochondrial trafficking and morphology in healthy and injured neurons. *Prog Neurobiol*. 80:241-268.

Chen, H., and D.C. Chan. 2010. Physiological functions of mitochondrial fusion. *Ann N Y Acad Sci*. 1201:21-25.

Chen, H., S.A. Detmer, A.J. Ewald, E.E. Griffin, S.E. Fraser, and D.C. Chan. 2003. Mitofusins Mfn1 and Mfn2 coordinately regulate mitochondrial fusion and are essential for embryonic development. *The Journal of cell biology*. 160:189-200.

Chen, H., J.M. McCaffery, and D.C. Chan. 2007. Mitochondrial fusion protects against neurodegeneration in the cerebellum. *Cell*. 130:548-562.

Chen, L., A.J. Winger, and A.A. Knowlton. 2014. Mitochondrial dynamic changes in health and genetic diseases. *Mol Biol Rep*. 41:7053-7062.

Chiesa, A., E. Rapizzi, V. Tosello, P. Pinton, M. de Virgilio, K.E. Fogarty, and R. Rizzuto. 2001. Recombinant aequorin and green fluorescent protein as valuable tools in the study of cell signalling. *The Biochemical journal*. 355:1-12.

Choquette, A.C., S. Lemieux, A. Tremblay, Y.C. Chagnon, C. Bouchard, M.C. Vohl, and L. Perusse. 2008. Evidence of a quantitative trait locus for energy and macronutrient intakes on chromosome 3q27.3: the Quebec Family Study. *Am J Clin Nutr*. 88:1142-

1148.

Cipolat, S., O. Martins de Brito, B. Dal Zilio, and L. Scorrano. 2004. OPA1 requires mitofusin 1 to promote mitochondrial fusion. *Proc Natl Acad Sci U S A*. 101:15927-15932.

Cipolat, S., T. Rudka, D. Hartmann, V. Costa, L. Serneels, K. Craessaerts, K. Metzger, C. Frezza, W. Annaert, L. D'Adamio, C. Derks, T. Dejaegere, L. Pellegrini, R. D'Hooge, L. Scorrano, and B. De Strooper. 2006. Mitochondrial rhomboid PARL regulates cytochrome c release during apoptosis via OPA1-dependent cristae remodeling. *Cell*. 126:163-175.

Codazzi, F., A. Di Cesare, N. Chiulli, A. Albanese, T. Meyer, D. Zacchetti, and F. Grohovaz. 2006. Synergistic control of protein kinase Cgamma activity by ionotropic and metabotropic glutamate receptor inputs in hippocampal neurons. *J Neurosci*. 26:3404-3411.

Colegrove, S.L., M.A. Albrecht, and D.D. Friel. 2000. Dissection of mitochondrial Ca2+ uptake and release fluxes in situ after depolarization-evoked [Ca2+](i) elevations in sympathetic neurons. *J Gen Physiol*. 115:351-370.

Cribbs, J.T., and S. Strack. 2007. Reversible phosphorylation of Drp1 by cyclic AMP-dependent protein kinase and calcineurin regulates mitochondrial fission and cell death. *EMBO reports*. 8:939-944.

Csordas, G., P. Varnai, T. Golenar, S. Roy, G. Purkins, T.G. Schneider, T. Balla, and G. Hajnoczky. 2010. Imaging interorganelle contacts and local calcium dynamics at the ER-mitochondrial interface. *Mol Cell*. 39:121-132.

Custer, S.K., G.A. Garden, N. Gill, U. Rueb, R.T. Libby, C. Schultz, S.J. Guyenet, T. Deller, L.E. Westrum, B.L. Sopher, and A.R. La Spada. 2006. Bergmann glia expression of polyglutamine-expanded ataxin-7 produces neurodegeneration by impairing glutamate transport. *Nat Neurosci*. 9:1302-1311.

David, G., and E.F. Barrett. 2000. Stimulation-evoked increases in cytosolic [Ca(2+)] in mouse motor nerve terminals are limited by mitochondrial uptake and are temperature-dependent. *The Journal of neuroscience : the official journal of the Society for Neuroscience*. 20:7290-7296.

David, G., and E.F. Barrett. 2003. Mitochondrial Ca2+ uptake prevents desynchronization of quantal release and minimizes depletion during repetitive stimulation of mouse motor nerve terminals. *J Physiol*. 548:425-438.

De Brito, O.M., and L. Scorrano. 2008. Mitofusin 2 tethers endoplasmic reticulum to mitochondria. *Nature*. 456:605-610.

De Michele, G., M. De Fusco, F. Cavalcanti, A. Filla, R. Marconi, G. Volpe, A. Monticelli, A. Ballabio, G. Casari, and S. Cocozza. 1998. A new locus for autosomal recessive hereditary spastic paraplegia maps to chromosome 16q24.3. *Am J Hum Genet*. 63:135-139.

DeVay, R.M., L. Dominguez-Ramirez, L.L. Lackner, S. Hoppins, H. Stahlberg, and J. Nunnari. 2009. Coassembly of Mgm1 isoforms requires cardiolipin and mediates mitochondrial inner membrane fusion. *The Journal of cell biology*. 186:793-803.

Di Bella, D., F. Lazzaro, A. Brusco, M. Plumari, G. Battaglia, A. Pastore, A. Finardi, C. Cagnoli, F. Tempia, M. Frontali, L. Veneziano, T. Sacco, E. Boda, A. Brussino, F. Bonn, B. Castellotti, S. Baratta, C. Mariotti, C. Gellera, V. Fracasso, S. Magri, T. Langer, P. Plevani, S. Di Donato, M. Muzi-Falconi, and F. Taroni. 2010. Mutations in

the mitochondrial protease gene AFG3L2 cause dominant hereditary ataxia SCA28. *Nat Genet*. 42:313-321.

Dorn, G.W., 2nd, C.F. Clark, W.H. Eschenbacher, M.Y. Kang, J.T. Engelhard, S.J. Warner, S.J. Matkovich, and C.C. Jowdy. 2011. MARF and Opa1 control mitochondrial and cardiac function in Drosophila. *Circ Res*. 108:12-17.

Duchen, M.R. 2012. Mitochondria, calcium-dependent neuronal death and neurodegenerative disease. *Pflugers Archiv : European journal of physiology*. 464:111-121.

Duvezin-Caubet, S., M. Koppen, J. Wagener, M. Zick, L. Israel, A. Bernacchia, R. Jagasia, E.I. Rugarli, A. Imhof, W. Neupert, T. Langer, and A.S. Reichert. 2007. OPA1 processing reconstituted in yeast depends on the subunit composition of the m-AAA protease in mitochondria. *Mol Biol Cell*. 18:3582-3590.

Edener, U., J. Wollner, U. Hehr, Z. Kohl, S. Schilling, F. Kreuz, P. Bauer, V. Bernard, G. Gillessen-Kaesbach, and C. Zuhlke. 2010. Early onset and slow progression of SCA28, a rare dominant ataxia in a large four-generation family with a novel AFG3L2 mutation. *Eur J Hum Genet*. 18:965-968.

Ehses, S., I. Raschke, G. Mancuso, A. Bernacchia, S. Geimer, D. Tondera, J.C. Martinou, B. Westermann, E.I. Rugarli, and T. Langer. 2009. Regulation of OPA1 processing and mitochondrial fusion by m-AAA protease isoenzymes and OMA1. *The Journal of cell biology*. 187:1023-1036.

Faelber, K., S. Gao, M. Held, Y. Posor, V. Haucke, F. Noe, and O. Daumke. 2013. Oligomerization of dynamin superfamily proteins in health and disease. *Prog Mol Biol Transl Sci*. 117:411-443.

Fassone, E., and S. Rahman. 2012. Complex I deficiency: clinical features, biochemistry and molecular genetics. *J Med Genet*. 49:578-590.

Feldmann, H.M., V. Golozoubova, B. Cannon, and J. Nedergaard. 2009. UCP1 ablation induces obesity and abolishes diet-induced thermogenesis in mice exempt from thermal stress by living at thermoneutrality. *Cell Metab*. 9:203-209.

Frieden, M., D. James, C. Castelbou, A. Danckaert, J.C. Martinou, and N. Demaurex. 2004. Ca(2+) homeostasis during mitochondrial fragmentation and perinuclear clustering induced by hFis1. *The Journal of biological chemistry*. 279:22704-22714.

Friedman, J.R., L.L. Lackner, M. West, J.R. DiBenedetto, J. Nunnari, and G.K. Voeltz. 2011. ER tubules mark sites of mitochondrial division. *Science*. 334:358-362.

Frohlich, C., S. Grabiger, D. Schwefel, K. Faelber, E. Rosenbaum, J. Mears, O. Rocks, and O. Daumke. 2013. Structural insights into oligomerization and mitochondrial remodelling of dynamin 1-like protein. *The EMBO journal*. 32:1280-1292.

Gomes, L.C., G. Di Benedetto, and L. Scorrano. 2012. During autophagy mitochondria elongate, are spared from degradation and sustain cell viability. *Nat Cell Biol*. 13:589-598.

Griparic, L., T. Kanazawa, and A.M. van der Bliek. 2007. Regulation of the mitochondrial dynamin-like protein Opa1 by proteolytic cleavage. *The Journal of cell biology*. 178:757-764.

Gruol, D., M. Manto, and D. Haines. 2012. Ca2+ signaling in cerebellar Purkinje neurons--editorial. *Cerebellum*. 11:605-608.

Gunter, T.E., D.I. Yule, K.K. Gunter, R.A. Eliseev, and J.D. Salter. 2004. Calcium and mitochondria. *FEBS Lett*. 567:96-102.

Hales, K.G., and M.T. Fuller. 1997. Developmentally regulated mitochondrial fusion

mediated by a conserved, novel, predicted GTPase. *Cell*. 90:121-129.
Hanson, P.I., and S.W. Whiteheart. 2005. AAA+ proteins: have engine, will work. *Nature reviews. Molecular cell biology*. 6:519-529.
Head, B., L. Griparic, M. Amiri, S. Gandre-Babbe, and A.M. van der Bliek. 2009. Inducible proteolytic inactivation of OPA1 mediated by the OMA1 protease in mammalian cells. *The Journal of cell biology*. 187:959-966.
Herlan, M., C. Bornhovd, K. Hell, W. Neupert, and A.S. Reichert. 2004. Alternative topogenesis of Mgm1 and mitochondrial morphology depend on ATP and a functional import motor. *The Journal of cell biology*. 165:167-173.
Hermann, G.J., J.W. Thatcher, J.P. Mills, K.G. Hales, M.T. Fuller, J. Nunnari, and J.M. Shaw. 1998. Mitochondrial fusion in yeast requires the transmembrane GTPase Fzo1p. *The Journal of cell biology*. 143:359-373.
Hollenbeck, P.J. 1996. The pattern and mechanism of mitochondrial transport in axons. *Front Biosci*. 1:d91-102.
Hoppins, S., L. Lackner, and J. Nunnari. 2007. The machines that divide and fuse mitochondria. *Annu Rev Biochem*. 76:751-780.
Hornig-Do, H.T., T. Tatsuta, A. Buckermann, M. Bust, G. Kollberg, A. Rotig, M. Hellmich, L. Nijtmans, and R.J. Wiesner. 2012. Nonsense mutations in the COX1 subunit impair the stability of respiratory chain complexes rather than their assembly. *The EMBO journal*. 31:1293-1307.
Ikeda, Y., K.A. Dick, M.R. Weatherspoon, D. Gincel, K.R. Armbrust, J.C. Dalton, G. Stevanin, A. Durr, C. Zuhlke, K. Burk, H.B. Clark, A. Brice, J.D. Rothstein, L.J. Schut, J.W. Day, and L.P. Ranum. 2006. Spectrin mutations cause spinocerebellar ataxia type 5. *Nat Genet*. 38:184-190.
Ingerman, E., E.M. Perkins, M. Marino, J.A. Mears, J.M. McCaffery, J.E. Hinshaw, and J. Nunnari. 2005. Dnm1 forms spirals that are structurally tailored to fit mitochondria. *The Journal of cell biology*. 170:1021-1027.
Ishihara, N., Y. Fujita, T. Oka, and K. Mihara. 2006. Regulation of mitochondrial morphology through proteolytic cleavage of OPA1. *The EMBO journal*. 25:2966-2977.
Ito, M. 2002. The molecular organization of cerebellar long-term depression. *Nat Rev Neurosci*. 3:896-902.
Iyer, L.M., D.D. Leipe, E.V. Koonin, and L. Aravind. 2004. Evolutionary history and higher order classification of AAA+ ATPases. *J Struct Biol*. 146:11-31.
Kang, J.S., J.H. Tian, P.Y. Pan, P. Zald, C. Li, C. Deng, and Z.H. Sheng. 2008. Docking of axonal mitochondria by syntaphilin controls their mobility and affects short-term facilitation. *Cell*. 132:137-148.
Kasahara, A., and L. Scorrano. 2014. Mitochondria: from cell death executioners to regulators of cell differentiation. *Trends Cell Biol*.
Kaser, M., M. Kambacheld, B. Kisters-Woike, and T. Langer. 2003. Oma1, a novel membrane-bound metallopeptidase in mitochondria with activities overlapping with the m-AAA protease. *The Journal of biological chemistry*. 278:46414-46423.
Kasumu, A., and I. Bezprozvanny. 2012. Deranged calcium signaling in Purkinje cells and pathogenesis in spinocerebellar ataxia 2 (SCA2) and other ataxias. *Cerebellum*. 11:630-639.
Koirala, S., Q. Guo, R. Kalia, H.T. Bui, D.M. Eckert, A. Frost, and J.M. Shaw. 2013. Interchangeable adaptors regulate mitochondrial dynamin assembly for membrane

scission. *Proc Natl Acad Sci U S A*. 110:E1342-1351.
Koppen, M., and T. Langer. 2007. Protein degradation within mitochondria: versatile activities of AAA proteases and other peptidases. *Critical reviews in biochemistry and molecular biology*. 42:221-242.
Koppen, M., M.D. Metodiev, G. Casari, E.I. Rugarli, and T. Langer. 2007. Variable and tissue-specific subunit composition of mitochondrial m-AAA protease complexes linked to hereditary spastic paraplegia. *Mol Cell Biol*. 27:758-767.
Korobova, F., T.J. Gauvin, and H.N. Higgs. 2014. A role for myosin II in mammalian mitochondrial fission. *Curr Biol*. 24:409-414.
Korobova, F., V. Ramabhadran, and H.N. Higgs. 2013. An actin-dependent step in mitochondrial fission mediated by the ER-associated formin INF2. *Science*. 339:464-467.
Kwong, J.Q., M.F. Beal, and G. Manfredi. 2006. The role of mitochondria in inherited neurodegenerative diseases. *J Neurochem*. 97:1659-1675.
Lackner, L.L., and J.M. Nunnari. 2009. The molecular mechanism and cellular functions of mitochondrial division. *Biochimica et biophysica acta*. 1792:1138-1144.
Leboucher, G.P., Y.C. Tsai, M. Yang, K.C. Shaw, M. Zhou, T.D. Veenstra, M.H. Glickman, and A.M. Weissman. 2012. Stress-induced phosphorylation and proteasomal degradation of mitofusin 2 facilitates mitochondrial fragmentation and apoptosis. *Molecular cell*. 47:547-557.
Lee, C.W., and H.B. Peng. 2008. The function of mitochondria in presynaptic development at the neuromuscular junction. *Molecular biology of the cell*. 19:150-158.
Lee, S., S. Augustin, T. Tatsuta, F. Gerdes, T. Langer, and F.T. Tsai. 2011. Electron cryomicroscopy structure of a membrane-anchored mitochondrial AAA protease. *The Journal of biological chemistry*. 286:4404-4411.
Leist, M., and M. Jaattela. 2001. Four deaths and a funeral: from caspases to alternative mechanisms. *Nature reviews. Molecular cell biology*. 2:589-598.
Lin, M.T., and M.F. Beal. 2006. Mitochondrial dysfunction and oxidative stress in neurodegenerative diseases. *Nature*. 443:787-795.
Lopez-Pelegrin, M., N. Cerda-Costa, F. Martinez-Jimenez, A. Cintas-Pedrola, A. Canals, J.R. Peinado, M.A. Marti-Renom, C. Lopez-Otin, J.L. Arolas, and F.X. Gomis-Ruth. 2013. A novel family of soluble minimal scaffolds provides structural insight into the catalytic domains of integral membrane metallopeptidases. *The Journal of biological chemistry*. 288:21279-21294.
Lowell, B.B., S.S. V, A. Hamann, J.A. Lawitts, J. Himms-Hagen, B.B. Boyer, L.P. Kozak, and J.S. Flier. 1993. Development of obesity in transgenic mice after genetic ablation of brown adipose tissue. *Nature*. 366:740-742.
Ma, H., Q. Cai, W. Lu, Z.H. Sheng, and S. Mochida. 2009. KIF5B motor adaptor syntabulin maintains synaptic transmission in sympathetic neurons. *The Journal of neuroscience : the official journal of the Society for Neuroscience*. 29:13019-13029.
Maltecca, F., A. Aghaie, D.G. Schroeder, L. Cassina, B.A. Taylor, S.J. Phillips, M. Malaguti, S. Previtali, J.L. Guenet, A. Quattrini, G.A. Cox, and G. Casari. 2008. The mitochondrial protease AFG3L2 is essential for axonal development. *J Neurosci*. 28:2827-2836.
Maltecca, F., D. De Stefani, L. Cassina, F. Consolato, M. Wasilewski, L. Scorrano, R. Rizzuto, and G. Casari. 2012. Respiratory dysfunction by AFG3L2 deficiency causes

decreased mitochondrial calcium uptake via organellar network fragmentation. *Hum Mol Genet*. 21:3858-3870.

Maltecca, F., R. Magnoni, F. Cerri, G.A. Cox, A. Quattrini, and G. Casari. 2009. Haploinsufficiency of AFG3L2, the gene responsible for spinocerebellar ataxia type 28, causes mitochondria-mediated Purkinje cell dark degeneration. *The Journal of neuroscience : the official journal of the Society for Neuroscience*. 29:9244-9254.

Manders, E.M., Verbeek, F.J. and Aten, A. 1993. Measurement of colocalization of objects in dual color confocal images. . *Journal of Microscopy* 169, :375–382.

McQuibban, G.A., S. Saurya, and M. Freeman. 2003. Mitochondrial membrane remodelling regulated by a conserved rhomboid protease. *Nature*. 423:537-541.

Mears, J.A., L.L. Lackner, S. Fang, E. Ingerman, J. Nunnari, and J.E. Hinshaw. 2011. Conformational changes in Dnm1 support a contractile mechanism for mitochondrial fission. *Nat Struct Mol Biol*. 18:20-26.

Medler, K., and E.L. Gleason. 2002. Mitochondrial Ca(2+) buffering regulates synaptic transmission between retinal amacrine cells. *J Neurophysiol*. 87:1426-1439.

Mehnert, C.S., H. Rampelt, M. Gebert, S. Oeljeklaus, S.G. Schrempp, L. Kochbeck, B. Guiard, B. Warscheid, and M. van der Laan. 2014. The Mitochondrial ADP/ATP Carrier Associates with the Inner Membrane Presequence Translocase in a Stoichiometric Manner. *The Journal of biological chemistry*. 289:27352-27362.

Miller, K.E., and M.P. Sheetz. 2004. Axonal mitochondrial transport and potential are correlated. *J Cell Sci*. 117:2791-2804.

Mishra, P., V. Carelli, G. Manfredi, and D.C. Chan. 2014. Proteolytic cleavage of Opa1 stimulates mitochondrial inner membrane fusion and couples fusion to oxidative phosphorylation. *Cell Metab*. 19:630-641.

Montero, M., M.T. Alonso, A. Albillos, I. Cuchillo-Ibanez, R. Olivares, G.G. A, J. Garcia-Sancho, and J. Alvarez. 2001. Control of secretion by mitochondria depends on the size of the local [Ca2+] after chromaffin cell stimulation. *Eur J Neurosci*. 13:2247-2254.

Montesinos, M.S., Z. Chen, and S.M. Young, Jr. 2011. pUNISHER: a high-level expression cassette for use with recombinant viral vectors for rapid and long term in vivo neuronal expression in the CNS. *J Neurophysiol*. 106:3230-3244.

Morris, R.L., and P.J. Hollenbeck. 1993. The regulation of bidirectional mitochondrial transport is coordinated with axonal outgrowth. *J Cell Sci*. 104 (Pt 3):917-927.

Murphy, M.P. 2009. How mitochondria produce reactive oxygen species. *Biochem J*. 417:1-13.

Ng, P., and F.L. Graham. 2002. Construction of first-generation adenoviral vectors. *Methods Mol Med*. 69:389-414.

Nguyen, T.T., S.S. Oh, D. Weaver, A. Lewandowska, D. Maxfield, M.H. Schuler, N.K. Smith, J. Macfarlane, G. Saunders, C.A. Palmer, V. Debattisti, T. Koshiba, S. Pulst, E.L. Feldman, G. Hajnoczky, and J.M. Shaw. 2014. Loss of Miro1-directed mitochondrial movement results in a novel murine model for neuron disease. *Proc Natl Acad Sci U S A*. 111:E3631-3640.

Nicholls, D.G. 1974. The influence of respiration and ATP hydrolysis on the proton-electrochemical gradient across the inner membrane of rat-liver mitochondria as determined by ion distribution. *Eur J Biochem*. 50:305-315.

Nicholls, D.G., and S.L. Budd. 2000. Mitochondria and neuronal survival. *Physiol Rev*.

80:315-360.

Nolden, M., S. Ehses, M. Koppen, A. Bernacchia, E.I. Rugarli, and T. Langer. 2005. The m-AAA protease defective in hereditary spastic paraplegia controls ribosome assembly in mitochondria. *Cell*. 123:277-289.

Nystrom, T. 2005. Role of oxidative carbonylation in protein quality control and senescence. *The EMBO journal*. 24:1311-1317.

Olichon, A., L. Baricault, N. Gas, E. Guillou, A. Valette, P. Belenguer, and G. Lenaers. 2003. Loss of OPA1 perturbates the mitochondrial inner membrane structure and integrity, leading to cytochrome c release and apoptosis. *The Journal of biological chemistry*. 278:7743-7746.

Pagliarini, D.J., S.E. Calvo, B. Chang, S.A. Sheth, S.B. Vafai, S.E. Ong, G.A. Walford, C. Sugiana, A. Boneh, W.K. Chen, D.E. Hill, M. Vidal, J.G. Evans, D.R. Thorburn, S.A. Carr, and V.K. Mootha. 2008. A mitochondrial protein compendium elucidates complex I disease biology. *Cell*. 134:112-123.

Palmer, A.E., M. Giacomello, T. Kortemme, S.A. Hires, V. Lev-Ram, D. Baker, and R.Y. Tsien. 2006. Ca2+ indicators based on computationally redesigned calmodulin-peptide pairs. *Chem Biol*. 13:521-530.

Park, Y.Y., O.T. Nguyen, H. Kang, and H. Cho. 2014. MARCH5-mediated quality control on acetylated Mfn1 facilitates mitochondrial homeostasis and cell survival. *Cell death & disease*. 5:e1172.

Pierson, T.M., D. Adams, F. Bonn, P. Martinelli, P.F. Cherukuri, J.K. Teer, N.F. Hansen, P. Cruz, J.C. Mullikin For The Nisc Comparative Sequencing Program, R.W. Blakesley, G. Golas, J. Kwan, A. Sandler, K. Fuentes Fajardo, T. Markello, C. Tifft, C. Blackstone, E.I. Rugarli, T. Langer, W.A. Gahl, and C. Toro. 2011. Whole-exome sequencing identifies homozygous AFG3L2 mutations in a spastic ataxia-neuropathy syndrome linked to mitochondrial m-AAA proteases. *PLoS Genet*. 7:e1002325.

Pizzo, P., I. Drago, R. Filadi, and T. Pozzan. 2012. Mitochondrial Ca(2)(+) homeostasis: mechanism, role, and tissue specificities. *Pflugers Archiv : European journal of physiology*. 464:3-17.

Pozzan, T., and R. Rizzuto. 2000. High tide of calcium in mitochondria. *Nature cell biology*. 2:E25-27.

Praefcke, G.J., and H.T. McMahon. 2004. The dynamin superfamily: universal membrane tubulation and fission molecules? *Nature reviews. Molecular cell biology*. 5:133-147.

Quiros, P.M., A.J. Ramsay, D. Sala, E. Fernandez-Vizarra, F. Rodriguez, J.R. Peinado, M.S. Fernandez-Garcia, J.A. Vega, J.A. Enriquez, A. Zorzano, and C. Lopez-Otin. 2012. Loss of mitochondrial protease OMA1 alters processing of the GTPase OPA1 and causes obesity and defective thermogenesis in mice. *The EMBO journal*. 31:2117-2133.

Ranieri, M., S. Brajkovic, G. Riboldi, D. Ronchi, F. Rizzo, N. Bresolin, S. Corti, and G.P. Comi. 2013. Mitochondrial fusion proteins and human diseases. *Neurology research international*. 2013:293893.

Rapaport, D., M. Brunner, W. Neupert, and B. Westermann. 1998. Fzo1p is a mitochondrial outer membrane protein essential for the biogenesis of functional mitochondria in Saccharomyces cerevisiae. *The Journal of biological chemistry*. 273:20150-20155.

Rawlings, N.D., M. Waller, A.J. Barrett, and A. Bateman. 2013. MEROPS: the database of proteolytic enzymes, their substrates and inhibitors. *Nucleic acids research*. 42:D503-

509.

Rizzuto, R., P. Pinton, W. Carrington, F.S. Fay, K.E. Fogarty, L.M. Lifshitz, R.A. Tuft, and T. Pozzan. 1998. Close contacts with the endoplasmic reticulum as determinants of mitochondrial Ca2+ responses. *Science*. 280:1763-1766.

Rothstein, J.D., S. Patel, M.R. Regan, C. Haenggeli, Y.H. Huang, D.E. Bergles, L. Jin, M. Dykes Hoberg, S. Vidensky, D.S. Chung, S.V. Toan, L.I. Bruijn, Z.Z. Su, P. Gupta, and P.B. Fisher. 2005. Beta-lactam antibiotics offer neuroprotection by increasing glutamate transporter expression. *Nature*. 433:73-77.

Roy, A., J. Yang, and Y. Zhang. 2012. COFACTOR: an accurate comparative algorithm for structure-based protein function annotation. *Nucleic acids research*. 40:8.

Ruthel, G., and P.J. Hollenbeck. 2003. Response of mitochondrial traffic to axon determination and differential branch growth. *The Journal of neuroscience : the official journal of the Society for Neuroscience*. 23:8618-8624.

Saar, K., F. Geller, F. Ruschendorf, A. Reis, S. Friedel, N. Schauble, P. Nurnberg, W. Siegfried, H.P. Goldschmidt, H. Schafer, A. Ziegler, H. Remschmidt, A. Hinney, and J. Hebebrand. 2003. Genome scan for childhood and adolescent obesity in German families. *Pediatrics*. 111:321-327.

Samant, S.A., H.J. Zhang, Z. Hong, V.B. Pillai, N.R. Sundaresan, D. Wolfgeher, S.L. Archer, D.C. Chan, and M.P. Gupta. 2014. SIRT3 deacetylates and activates OPA1 to regulate mitochondrial dynamics during stress. *Mol Cell Biol*. 34:807-819.

Santel, A., and M.T. Fuller. 2001. Control of mitochondrial morphology by a human mitofusin. *J Cell Sci*. 114:867-874.

Saris, N.E., and E. Carafoli. 2005. A historical review of cellular calcium handling, with emphasis on mitochondria. *Biochemistry (Mosc)*. 70:187-194.

Saxton, W.M., and P.J. Hollenbeck. 2012. The axonal transport of mitochondria. *J Cell Sci*. 125:2095-2104.

Schmidt, O., N. Pfanner, and C. Meisinger. 2010. Mitochondrial protein import: from proteomics to functional mechanisms. *Nature reviews. Molecular cell biology*. 11:655-667.

Schuermann, M. 1990. An expression vector system for stable expression of oncogenes. *Nucleic acids research*. 18:4945-4946.

Sesaki, H., S.M. Southard, A.E. Hobbs, and R.E. Jensen. 2003. Cells lacking Pcp1p/Ugo2p, a rhomboid-like protease required for Mgm1p processing, lose mtDNA and mitochondrial structure in a Dnm1p-dependent manner, but remain competent for mitochondrial fusion. *Biochem Biophys Res Commun*. 308:276-283.

Sheng, Z.H., and Q. Cai. 2012. Mitochondrial transport in neurons: impact on synaptic homeostasis and neurodegeneration. *Nature reviews. Neuroscience*. 13:77-93.

Shimohata, N., S. Chiba, N. Saikawa, K. Ito, and Y. Akiyama. 2002. The Cpx stress response system of Escherichia coli senses plasma membrane proteins and controls HtpX, a membrane protease with a cytosolic active site. *Genes Cells*. 7:653-662.

Shutt, T., M. Geoffrion, R. Milne, and H.M. McBride. 2012. The intracellular redox state is a core determinant of mitochondrial fusion. *EMBO reports*. 13:909-915.

Smets, K., T. Deconinck, J. Baets, A. Sieben, J.J. Martin, I. Smouts, S. Wang, F. Taroni, D. Di Bella, W. Van Hecke, P.M. Parizel, C. Jadoul, R. De Potter, F. Couvreur, E. Rugarli, and P. De Jonghe. 2014. Partial deletion of AFG3L2 causing spinocerebellar ataxia type 28. *Neurology*. 82:2092-2100.

Smirnova, E., L. Griparic, D.L. Shurland, and A.M. van der Bliek. 2001. Dynamin-related protein Drp1 is required for mitochondrial division in mammalian cells. *Molecular biology of the cell*. 12:2245-2256.

Smith, A.C., and A.J. Robinson. 2009. MitoMiner, an integrated database for the storage and analysis of mitochondrial proteomics data. *Mol Cell Proteomics*. 8:1324-1337.

Song, Z., H. Chen, M. Fiket, C. Alexander, and D.C. Chan. 2007. OPA1 processing controls mitochondrial fusion and is regulated by mRNA splicing, membrane potential, and Yme1L. *The Journal of cell biology*. 178:749-755.

Song, Z., M. Ghochani, J.M. McCaffery, T.G. Frey, and D.C. Chan. 2009. Mitofusins and OPA1 mediate sequential steps in mitochondrial membrane fusion. *Molecular biology of the cell*. 20:3525-3532.

Stiburek, L., J. Cesnekova, O. Kostkova, D. Fornuskova, K. Vinsova, L. Wenchich, J. Houstek, and J. Zeman. 2012. YME1L controls the accumulation of respiratory chain subunits and is required for apoptotic resistance, cristae morphogenesis, and cell proliferation. *Mol Biol Cell*. 23:1010-1023.

Stowers, R.S., L.J. Megeath, J. Gorska-Andrzejak, I.A. Meinertzhagen, and T.L. Schwarz. 2002. Axonal transport of mitochondria to synapses depends on milton, a novel Drosophila protein. *Neuron*. 36:1063-1077.

Strack, S., T.J. Wilson, and J.T. Cribbs. 2013. Cyclin-dependent kinases regulate splice-specific targeting of dynamin-related protein 1 to microtubules. *The Journal of cell biology*. 201:1037-1051.

Suno, R., H. Niwa, D. Tsuchiya, X. Zhang, M. Yoshida, and K. Morikawa. 2006. Structure of the whole cytosolic region of ATP-dependent protease FtsH. *Molecular cell*. 22:575-585.

Szabadkai, G., A.M. Simoni, M. Chami, M.R. Wieckowski, R.J. Youle, and R. Rizzuto. 2004. Drp-1-dependent division of the mitochondrial network blocks intraorganellar Ca2+ waves and protects against Ca2+-mediated apoptosis. *Molecular cell*. 16:59-68.

Tabata, T., S. Sawada, K. Araki, Y. Bono, S. Furuya, and M. Kano. 2000. A reliable method for culture of dissociated mouse cerebellar cells enriched for Purkinje neurons. *J Neurosci Methods*. 104:45-53.

Taguchi, N., N. Ishihara, A. Jofuku, T. Oka, and K. Mihara. 2007. Mitotic phosphorylation of dynamin-related GTPase Drp1 participates in mitochondrial fission. *The Journal of biological chemistry*. 282:11521-11529.

Tatsuta, T., and T. Langer. 2009. AAA proteases in mitochondria: diverse functions of membrane-bound proteolytic machines. *Res Microbiol*. 160:711-717.

UniProtConsortium. 2013. Activities at the Universal Protein Resource (UniProt). *Nucleic acids research*. 42:7486.

Verstreken, P., C.V. Ly, K.J. Venken, T.W. Koh, Y. Zhou, and H.J. Bellen. 2005. Synaptic mitochondria are critical for mobilization of reserve pool vesicles at Drosophila neuromuscular junctions. *Neuron*. 47:365-378.

Yachdav, G., E. Kloppmann, L. Kajan, M. Hecht, T. Goldberg, T. Hamp, P. Honigschmid, A. Schafferhans, M. Roos, M. Bernhofer, L. Richter, H. Ashkenazy, M. Punta, A. Schlessinger, Y. Bromberg, R. Schneider, G. Vriend, C. Sander, N. Ben-Tal, and B. Rost. 2014. PredictProtein--an open resource for online prediction of protein structural and functional features. *Nucleic acids research*. 42:5.

Zhan, M., C. Brooks, F. Liu, L. Sun, and Z. Dong. 2013. Mitochondrial dynamics: regulatory

mechanisms and emerging role in renal pathophysiology. *Kidney Int*. 83:568-581.

Zhang, K., H. Li, and Z. Song. 2014. Membrane depolarization activates the mitochondrial protease OMA1 by stimulating self-cleavage. *EMBO reports*. 15:576-585.

Zhao, J., T. Liu, S. Jin, X. Wang, M. Qu, P. Uhlen, N. Tomilin, O. Shupliakov, U. Lendahl, and M. Nister. 2011. Human MIEF1 recruits Drp1 to mitochondrial outer membranes and promotes mitochondrial fusion rather than fission. *The EMBO journal*. 30:2762-2778.

Zhou, H., and A.L. Beaudet. 2000. A new vector system with inducible E2a cell line for production of higher titer and safer adenoviral vectors. *Virology*. 275:348-357.

Zhu, X.H., H. Qiao, F. Du, Q. Xiong, X. Liu, X. Zhang, K. Ugurbil, and W. Chen. 2012. Quantitative imaging of energy expenditure in human brain. *Neuroimage*. 60:2107-2117.